THERMO-PHYSICAL PROPERTIES AND STRUCTURAL ASPECTS OF SOME PHOSPHATE AND SILICATE GLASSES/GLASS-CERAMICS

By

BABITA TIWARI

(Enroll. No. PHYS01200704024)

Bhabha Atomic Research Centre, Mumbai, India

A thesis submitted to the

Board of Studies in Physical Sciences

In partial fulfillment of requirements

For the Degree of

DOCTOR OF PHILOSOPHY

of

HOMI BHABHA NATIONAL INSTITUTE

October 2012

Homi Bhabha National Institute

Recommendations of the Viva Voce Board

As members of the Viva Voce Board, we certify that we have read the dissertation prepared by Babita Tiwari entitled "Thermo-physical properties and structural aspects of some phosphate and silicate glasses/glass-ceramics" and recommend that it may be accepted as fulfilling the dissertation requirement for the Degree of Doctor of Philosophy.

Chairman: Prof. G.K. Dey Gautam Kumar Dey Date: 5/4/2013

Guide: Prof. G.P. Kothiyal Date: 5\4\2013

Member-1: Prof. S.K. Kulshreshtha Date: 5/4/2013

Member-2: Prof. A.R. Kulkarni ARKulkarni Date: 5/4/13

Member-3: Prof. S. Basu Date: 5/4/13

Final approval and acceptance of this dissertation is contingent upon the candidate's submission of the final copies of the dissertation to HBNI. I hereby certify that I have read this dissertation prepared under my direction and recommend that it may be accepted as fulfilling the dissertation requirement.

Date: 5-4-2013

Place: Mumbai

Guide: Prof. G.P. Kothiyal

STATEMENT BY AUTHOR

This dissertation has been submitted in partial fulfillment of requirements for an advanced degree at Homi Bhabha National Institute (HBNI) and is deposited in the Library to be made available to borrowers under rules of the HBNI.

Brief quotations from this dissertation are allowable without special permission, provided that accurate acknowledgement of source is made. Requests for permission for extended quotation from or reproduction of this manuscript in whole or in part may be granted by the Competent Authority of HBNI when in his or her judgment the proposed use of the material is in the interests of scholarship. In all other instances, however, permission must be obtained from the author.

Babita Tiwari

DECLARATION

I, hereby declare that the investigation presented in the thesis has been carried out by me. The work is original and has not been submitted earlier as a whole or in part for a degree/diploma at this or any other Institution/University.

Babita Tiwari

DEDICATED TO MY FAMILY

ACKNOWLEDGEMENTS

First and foremost I would like to express my sincere gratitude to my research guide **Prof. G. P. Kothiyal**, Head, Glass and Advanced Ceramics Division, BARC for his valuable guidance, constant encouragement and support that he has provided during the course of this dissertation. I would like to extend my heartfelt gratitude to **Prof. S. C. Gadkari,** Head, Crystal Technology Section**,** who made this thesis possible and has made available his vital and unflinching support in a number of ways. I would like to thank **Prof. S. K. Gupta,** Head, Technical Physics Division, for allowing me to carry out this work and encouraging me throughout this work.

I am deeply indebted to **Dr. V. Sudarsan** Head, Structural Chemistry Section, for technical discussions and suggestions and providing his invaluable time and for shaping the work in final written form.

I greatly acknowledge the contributions of my doctoral committee members **Prof. G. K. Dey, Prof. S. K. Kulshreshtha, Prof. A. R. Kulkarni** and **Prof. S. Basu** who spared their valuable time for periodical critical assessment of my work. Incorporation of their constructive suggestions has greatly enhanced the technical level of my research work.

I am thankful to **Dr. C. G. S. Pillai, Dr. M. Pandey, Dr. S. Bhattacharya and Dr. A. Ananthanarayanan** for carrying out different experiments and valuable discussion during the course of the work.

I wish to thank **Mr. A. Dixit** and **Mr. A. Sarkar** for assisting in my experimental works all throughout the studies and **Mrs. A. Patil, Mrs. S. Singaravelan, Mr. J. Nuwad, Mr. R. Kumar, Mr. S. Radhakrishnan, Mr. P. V. Gaikwad, Mr. K. M. Bandal and Mr. K. V. Apparao** for carrying out different experiments and technical assistance. I am also thankful to the all other staff members of GCTL and CTL for technical support. I thank

with apology all those people whose contributions to this work have escaped my attention and, thus, have gone unnoticed.

Words alone cannot express what I owe to **my Parents** who always encouraged and supported me to come over the stressed situations. Their blessings made this thesis possible. Thanks are due to my other family members for their true blessings.

I would like to show my gratitude from the depth of my heart to my **husband Kamal**, who has always supported me and made me relaxed in the burdensome situations. His true love, continuous encouragement and support in all aspects, played a vital role in completion of this dissertation. I specially thank to my loving **son Pratyush** who sacrificed many times his desire to spend time with me. His innocent love and cute smile inspired me to complete this dissertation.

Babita Tiwari

Contents

Synopsis

Glass is an amorphous (non-crystalline) solid material, which has random structure of the liquid from which it is derived by cooling below freezing point without crystallization. Glass is also defined as configurationally frozen liquid which exhibits glass transition behaviour [1]. The glass transition is a phenomenon in which a solid amorphous phase shows a more or less abrupt change in derivative thermodynamic properties from crystal like to liquid like values with change of temperature [1]. Thermodynamically 'glassy' state is a meta-stable state which depends upon the thermal history of the melt and slowly relaxes to a more stable state [2]. In addition to scientific interest, glass as a substance plays an essential role in technology and industry. Physical, chemical and optical properties of glasses make them suitable for various technological applications like hermetic sealing, radioactive waste immobilization, bio-engineering, optics and optoelectronics material etc. Many industries such as automobiles, architecture, display technology etc. greatly depend upon glasses due to their functionality, cost and ease of manufacturing [3].

Crystallization in glasses is usually deleterious to various properties, however; controlled crystallization of glasses can result in a new kind of polycrystalline material known as glass-ceramics with improved thermo-physical, electrical, mechanical and chemical properties [4]. Glass-ceramics by definition are the products of controlled crystallization of glasses in which crystalline phases embedded in a glassy matrix. As a result of improved thermo-physical and chemical properties, they find application in a number of areas such as dielectrics, cookware, sealants etc [4]. Glass-ceramics generally result in higher strength compared to glass and allow fine control over properties such as thermal expansion coefficient (TEC) through control of the amount, nature and morphology of the phases crystallized.

Even though glasses lack extended periodic arrangement of atoms, most of them possess considerable extent of short range order (up to a few atomic spacing) and in some cases even medium range order (ten to thirty angstroms) [5]. For crystalline materials, which consist of regular repetition of basic unit cells, solving the structure within a unit cell is sufficient to understand the structural features of crystalline materials. This approach fails in the case of glasses as they can't be represented as a regular repetition of such basic structural units. In 1932 Zachariasen made first attempt to understand the structure of glassy materials, who suggested the existence of a continuous random network (CRN) in glasses [6]. However, the structure for many glasses known today could not be explained by CRN model alone and a number of other models have been suggested to understand the structural arrangements of atoms in these glassy materials [5]. With the discovery of newer structure sensitive material characterization techniques like high resolution nuclear magnetic resonance (NMR), extended X-ray absorption fine structure (EXAFS) and high resolution transmission electron microscope (TEM) etc., better understanding of the structure of glassy phase has been achieved [5]. Based on the extensive studies of various oxide glasses, it has been observed that, the thermo-physical properties of these glasses like TEC, micro-hardness, onset of optical absorption, moisture sensitiveness etc. depend on the nature of different structural units, present in the glass network [5]. Good understanding of the structure-property relationship in glasses and glass-ceramics is very essential to improve their properties by suitable substitution as well as to design new compositions for novel applications i.e. hermetic sealing.

In this dissertation thermo-physical properties and structural aspects of some technologically important phosphate and silicate glasses/glass-ceramics have been investigated. And an attempt has been made to correlate the thermo-physical properties of these materials with their structural features. Thesis covers work carried out on the thermo-physical, optical, microstructural and structural properties of sodium aluminium titano-phosphate glasses (NATP), strontium zinc silicate (SZS) and barium zinc silicate (BZS) based glasses and glass-ceramics. The sodium alumino-phosphate glasses are useful for low temperature sealing [7] and certain optical applications, while the barium and strontium based silicate glass-ceramics find application in high temperature sealing like sealant material for solid oxide fuel cell (SOFC) [8,9]. Precise knowledge of the crystallization temperature is required for glass-ceramic formation, which is obtained by differential thermal analysis (DTA). The TEC of the parent glasses and glass-ceramics are measured using thermo-mechanical analyzer (TMA). In order to assess the hardness of the glasses and glass-ceramics, Vickers micro-hardness measurement is employed. Since the properties of glass-ceramics are strongly affected by the nature and morphology of phases, X-ray diffraction (XRD) and SEM are used for the characterization of glass-ceramics. Structural information of glasses and glass-ceramics has been obtained from Raman, Fourier transformed infrared (FTIR) and magic angle spinning nuclear magnetic resonance (MAS-NMR) spectroscopic techniques. Sealing studies with promising compositions of SZS/BZS glasses were also carried out to ensure that these glasses have adequate adhesion/bonding properties with other SOFC components such as Crofer-22-APU and YSZ.

This thesis comprises of six chapters and the content of each chapter is briefly described in the following sections.

Chapter 1: Introduction

This chapter gives briefly an introduction to glasses and glass-ceramics and their important characteristics. Glasses are defined as non-crystalline materials that lack long range periodic order and exhibit glass transition behaviour [1,5]. An overview of the glass transition phenomenon is provided and various theories/models proposed have been mentioned, although the present understanding is not sufficient to fully explain the phenomenon of glass transition. Various types of glasses including phosphate and silicate based oxide glasses are described along with their advantages and disadvantages. Further, the nature of various structural units present in the representative phosphate and silicate glasses, and the changes brought about in these structural configuration by addition of different additives have been described. The different methods of preparing amorphous and glassy materials are also discussed. Subsequently, crystallization of glasses is discussed in brief along with theoretical perspective relevant to homogenous and heterogeneous nucleation and crystal growth. The advantages of glass-ceramics with respect to certain important properties are discussed. The importance of the present work and various studies carried out on actual glass/glass-ceramics systems investigated in this thesis are brought out in brief.

Chapter 2: Experimental Techniques

In this chapter details of the preparation and characterization techniques used in the present work are given along with basic principles, their merits/demerits etc. In starting the melt quench method employed for synthesis of bulk and frit glasses is described. In order to prepare glass-ceramics, the crystallization behaviour of the glasses is studied using DTA. Based on the DTA data, glasses are crystallized and the phases formed identified by XRD.

The density of the prepared glasses and glass-ceramics were measured using the Archimedes principle, with distilled water or toluene as the immersion fluid. TEC, glass transition temperature (T_g) and softening temperature (T_{ds}) of the glass and glass-ceramic samples were measured using a Setaram 92-12 thermo-mechanical analyzer. Mechanical strength/hardness of glasses was measured using a Vickers micro-hardness tester (VMHT-30M Leica/Austria). Micro-hardness (MH) is an indicator of the connectivity of the network and changes with composition and crystallization. The absorption edge and optical gap also depend on the composition as well as the nature of glass network therefore optical absorption studies were carried out using UV-Vis spectrophotometer (Jasco V-670 Japan). Non-bridging oxygen atoms can also lead to the creation of localized centers in the glasses and some of them can give luminescence on optical excitation. Luminescence spectra of a few glasses were also recorded using an Edinburgh fluorescence FLSP 920 instrument.

Raman and FTIR spectroscopic techniques are capable of probing both short range and medium range order and give valuable information regarding the structural aspects of the glasses and glass-ceramics. In order to further understand the short range order in glasses and glass-ceramics, MAS-NMR spectroscopy was employed. This technique allows probing of the immediate environment of the atoms in the material and enables the characterization of the glasses. Scanning electron microscopy (SEM) was employed to examine the morphology of the crystalline phases formed in the glass-ceramics and the energy dispersive spectroscopy of X-ray (EDS) was used to probe the chemical composition of the phases. To show the efficacy of a few promising glasses for high temperature sealing application seals were prepared and tested for vacuum integrity. Therefore, at the end of this chapter seal fabrication and leak testing at elevated temperature are also discussed.

Chapter 3: Studies on sodium aluminium titano-phosphate (NATP) glasses

In this chapter synthesis, thermo-physical and optical properties along with structural aspect of sodium aluminium titano-phosphate glasses have been discussed. Studies carried out to investigate the role of TiO_2 on thermo-physical and optical properties of the sodium alumino-phosphate (NAP) glass with substitution of TiO_2 for P_2O_5. Sodium alumino-phosphate glasses with different amounts of TiO_2 (0, 2, 5, 10, 15 and 20 mol%) incorporated at the expense of P_2O_5, were prepared by melt quench method. In these glasses density, T_g and MH increased while TEC and molar volume decreased with increasing TiO_2 concentration up to 10 mol% and beyond that these properties show reverse trends. The variation in thermo-physical properties was explained on the basis of structural changes in the glass with the addition of TiO_2. Structural studies using ^{31}P MAS-NMR spectroscopy revealed the existence of both Q^1 and Q^2 structural units of phosphorus (where Q^n represents the P structural units having ‘n’ number of bridging oxygen atoms). With the increase of TiO_2 up to 10 mol%, the concentration of Q^1 structural units increase at the expense of Q^2 structural units due to the depolymerization of polyphosphate chains as TiO_2 replaces the P_2O_5. An increase in the chemical shift of the Q^2 structural units has been attributed to the decrease in the chain length as well as the formation of $P\text{-}O^-\text{-}Ti^{4+}$ linkages at the expense of P-O-P linkages [10,11]. Incorporation of TiO_2 at the expense of P_2O_5 in the glass can also lead to a change in the coordination of Al^{3+} ions in the glass. ^{27}Al MAS-NMR studies revealed the change in the coordination of Al^{3+} ions from octahedral to tetrahedral with incorporation of TiO_2 more than10 mol%. It is inferred that Al^{3+} ions extend the glass network by forming P-O-Al type linkages, with tetrahedral configuration of Al^{3+} ions in the glass [10]. Raman and FTIR studies of these glasses also reflected the significant structural changes in the glass. Raman spectroscopy revealed that Ti^{4+} exits in these glasses in the form of TiO_4 and TiO_6 units. At lower concentration of TiO_2, TiO_6 units are more favourable and at higher concentration (more than 10 mol%) TiO_4 units are more favourable [10]. Based on these studies it is concluded that TiO_2 behaves as a network modifier up to 10 mol% and above that TiO_2 acts as network former and a Ti-O-Ti/Al based network connected with discrete PO_4 structural units that exist in the glass. The $E_{optical}$ values (value of the optical gap) were found to decrease with an increase in TiO_2. $E_{optical}$ values decreased significantly up to 5 mol% and marginally beyond that. This has been attributed to the conversion of bridging oxygen to non-bridging oxygen atoms, which facilitates the excitation of electrons attached to the oxygen atom [11]. Thus the observed variation in thermo-physical and optical properties are consistent with the structural changes in the NATP glass by TiO_2 incorporation. The degradation behaviour of the glass surface in humid atmosphere is a crucial parameter in determining the success of the glass in its final application. Weathering (degradation) studies of prepared NATP glasses revealed that glasses containing more than 5 mol% TiO_2 are more durable than the NAP glass.

Chapter 4: Studies on strontium zinc silicate (SZS) glass/glass-ceramics

In this chapter strontium zinc silicate based glasses and glass-ceramics were investigated as potential sealants for high temperature applications such as solid oxide fuel cells (SOFC). Recently glasses in this system have also been reported as prospective bone graft materials [12]. In the present study glasses having composition (in wt.%) $51SrO$-$9ZnO$-$(40-x)SiO_2$ (SZS), where x represents the different additives like B_2O_3, Al_2O_3, Cr_2O_3, Y_2O_3, TiO_2 and V_2O_5 have been synthesized and converted into glass-ceramics through a controlled crystallization process. Thermo-physical, microstructural and structural properties of these glasses and glass-ceramics have been presented here. Adhesion/bonding characteristics of a few selected glasses with Crofer-22-APU (commonly used interconnect in SOFC) and YSZ (an electrolyte material for SOFC) were also investigated using SEM and EDS.

It is observed that investigated glasses and glass-ceramics have desired range of TEC (90-120×10^{-7}/°C) and sufficiently high softening temperature (T_{ds}), as required for SOFC sealant materials [13]. These glasses have densities in the range of 3.66-3.78 (10^3 kg/m^3) and MH in the range of 6.26-7.17 GPa. MH of all these glasses is quite high, reflecting higher bond strength thereby may withstand higher load [13]. Prolonged use of glasses at high temperature will results the crystallization of glasses. Therefore, crystallization kinetics of SZS glasses has been studied by DTA using the Ozawa [14], Kissinger and Matusita-Sakka equations [15]. Study revealed the diffusion controlled bulk crystallization of base SZS glass with two and three dimensional growth. Further, we obtained quite high activation energy for crystallization of base glass, indicating the highly thermal activated kinetics, which makes poor control over the crystallization during the sealing process [16]. Effect of additives on crystallization of SZS glass has also been investigated. It is observed that, with the addition of B_2O_3, V_2O_5 and Cr_2O_3 constituents in the glass, the surface crystallization mechanism starts dominating over bulk crystallization and the activation energy decreases. A composition, having B_2O_3 and V_2O_5 shows lower activation energy thereby better control over the crystallization. Microstructural evolution of SZS glass, having composition 51SrO-9ZnO-40SiO_2 (wt.%), during heating suggests that the glass undergoes a phase separation apparently by spinodal decomposition mechanism prior to crystallization and resulted in a highly interconnected microstructure of two crystalline phases [16]. Structural modifications in the glass with the additives and also with the temperature are studied using Raman, FTIR and NMR spectroscopic techniques. An attempt has been made to correlate these structural changes with the thermo-physical and crystallization properties. Studies revealed that mainly Q^1 and Q^2 silicate structural units are present in the network of the SZS glass. With addition of B_2O_3 and other additives glass network depolymerizes and concentration of Q^1 units increases at the expense of Q^2 units. Formation of crystalline phases during heat treatment is related to the presence of different silicate structural unites in the glass network. B_2O_3 goes into the glass network as triangular (BO_3) borate structural units [13]. X-ray diffraction studies revealed that $Sr_2ZnSi_2O_7$ and $Sr_3Si_3O_9$ phases crystallize in SZS Glass-ceramics and $Sr_2ZnSi_2O_7$ solid-solution phase formed in compositions having B_2O_3 and/or Al_2O_3. The $Sr_2ZnSi_2O_7$ (Sr-hardystonite) is one of the members of melilite group of minerals having a general formula $X_2Y(T_2O_7)$. Al/B may occupy the position of Y and T sites in tetrahedral coordination. ^{27}Al and ^{11}B MAS-NMR spectra show the crystallization of B and Al in tetrahedral coordination. MAS-NMR studies along with XRD suggest the formation of $Sr_2ZnSi_2O_7$ solid-solution by incorporation of B and Al atoms in the $Sr_2ZnSi_2O_7$ crystalline phase. Raman and NMR studies indicate that $Sr_2ZnSi_2O_7$ phase crystallizes first at a lower temperature and later $Sr_3Si_3O_9$ phase. Raman spectra depict a 3 membered ring structure for the $Sr_3Si_3O_9$ crystalline phase.

A few glass compositions showed good bonding with YSZ and Crofer-22-APU reflected from the inter-diffusion of elements across the interface. On the basis of thermo-physical and bonding properties, a glass having B_2O_3 and V_2O_5 seems to be more suitable for SOFC sealant applications [13]. As a demonstration of suitability of material for high temperature sealing, seals have been prepared and tested for vacuum integrity up to 950°C [13].

Chapter 5: Studies on barium zinc silicate (BZS) glasses and glass-ceramics

This chapter has been devoted to the studies carried out on barium zinc silicate based glasses and glass-ceramics. Glasses having composition (in wt.%) 51BaO-9ZnO-(40-x)SiO_2 (BZS), where x represents the additives like B_2O_3, Nd_2O_3, V_2O_5, and TiO_2 were prepared by melt-quench method and transformed into glass-ceramics by controlled crystallization. Based on thermo-physical properties it is found that these materials have the requisite thermal properties for making suitable seals to different cell components of the SOFC. These glasses were characterized using dilatometry, DTA, X-ray diffraction and micro-hardness measurements. These have shown glass transition temperatures higher than 670°C and crystallization temperatures more than 830°C, which are advantageous for the high temperature sealant. All these glasses and glass-ceramics have TEC in the range 93-150 x 10^{-7}/°C (30-600°C), which is desirable for making seals with the SOFC components. It is found that Nd_2O_3 increases T_g and T_{ds} and reduces the TEC. It is also observed that B_2O_3 increase the flow property (reduces viscosity) but its higher amount suppresses the crystallization tendency. The crystallization studies have revealed that the weight ratio of B_2O_3 to SiO_2 decides the crystallization of different barium silicate phases. Crystallization kinetics of the BZS glass has been determined by DTA using the Ozawa, Kissinger and Matusita-Sakka equations. Kinetic parameters suggest the bulk crystallization with two and three dimensional growth of crystals by diffusion controlled growth mechanism.

As a demonstration of suitability of material for high temperature sealing, seals have been prepared and tested for vacuum integrity up to 800°C for 500 h. Studies revealed that B_2O_3 containing BZS glasses are more suitable for making the seal with Crofer-22-APU.

Chapter 6: Summary and conclusions

This chapter summarizes the work carried out in the thesis and presents important findings along with future scope of the work. In the present study we have investigated some technologically important phosphate and silicate based glasses and glass-ceramics. Effect of different additives on thermo-physical and crystallization properties has been explored through a comprehensive structure-property correlation. In the case of NATP glasses an attempt has been made to demonstrate that, the thermo-physical properties are sensitive function of the different structural configurations present in these glasses and can be modified by incorporating suitable additives. It is found that up to 10 mol% TiO_2 acts as a modifier and beyond that as a glass former. Decrease in the degradation of glass surface in humid environment was observed with the TiO_2 incorporation in NAP glasses, which reflect the higher chemical durability of NATP glasses. Development of a phosphate glass composition with higher chemical durability is beneficial to use unique properties of phosphate glasses in various fields of technology. NATP glasses with ~10 mol% TiO_2 have TEC around $168 \times 10^{-7}/°C$ which is closely matched with the thermal expansion of Cu and Cu-Be alloy, therefore suitable for making matched type glass-to-metal seals with these metals and alloys. For SZS and BZS glasses studies demonstrate the utility of structural and thermo-physical characterization in optimization of composition of glasses/glass-ceramics for novel applications. Studied compositions of SZS and BZS glasses fulfill the most important criteria (TEC and T_g) of thermo-physical properties for making suitable sealant for high temperature applications. Adherence/bonding behaviour of investigated SZS and BZS glass compositions reveled that B_2O_3 and V_2O_5 are useful constituents for increasing the flow of glass at the sealing temperatures. Structural studies of SZS glasses and glass-ceramics indicate the depolymerization of silicate network with the incorporation of different additives. This is associated with the modification of thermo-physical properties of glasses. Raman and FTIR studies show the decisive role of structural units on the formation of crystalline phases during heat treatment. XRD studies revealed the formation of solid-solution of $Sr_2ZnSi_2O_7$ phase in SZS compositions containing B_2O_3 and/or Al_2O_3, but it is difficult to identify the nature and composition of the solid-solution. It is also difficult to distinguish crystallization of $Sr_2B_2SiO_7$ and $Sr_2Al_2SiO_7$ phases from the crystalline $Sr_2ZnSi_2O_7$ phase in XRD due to close proximity in their Bragg peaks; however, the use of MAS-NMR throws some light on it. ^{27}Al and ^{11}B MAS-NMR spectra confirm the crystallization of B and Al in tetrahedral coordination, although it is difficult to say that B/Al making a solid-solution in the $Sr_2ZnSi_2O_7$ phase or separate phases. Here on the basis of NMR and XRD studies we attribute that B and Al make a solid-solution in the $Sr_2Al_2SiO_7$ phase. Information about crystallization kinetics and mechanism is important to develop suitable glass-ceramic sealants and sealing procedure. Crystallization kinetics studies indicate that, with the incorporation of additives in the glass, surface crystallization mechanism starts dominating over bulk crystallization and activation energy decreases. A composition, having B_2O_3 and V_2O_5 shows lower activation energy thereby better control over the crystallization during sealing process. Liquid in liquid phase separation by spinodal decomposition mechanism has been observed prior to the crystallization in the SZS glass. Studies carried out so far demonstrate the potentiality of SZS and BZS glass-ceramics for high temperature sealant application.

In the thesis an effort has been made to show that the thermo-physical properties of the investigated glasses are sensitive function of structural configurations present in these glasses and can be modified by incorporation of suitable additives. However, there is a need to augment this information about the structure of glasses with a variety of other structure sensitive techniques like high resolution EXAFS, XPS, as well as small angle X-ray and neutron scattering. It is proposed to carry out these studied in near future. MAS-NMR experiments like spin echo double resonance (SEDOR) and rotational echo double resonance (REDOR) are being proposed to investigate the structure and environment around the next nearest neighbour of Si atom. Further such experiments can also give information regarding cation distribution in the glass. ^{17}O MQMAS is planned to understand the environment around the oxygen atom as well as to estimate the different types of oxygen atoms in the glass and glass-ceramics. ^{51}V MAS-NMR is also proposed to investigate the effect of V_2O_5 on the structure and therefore on properties of the glass. ZnO can behave as a glass modifier or glass former depending on the composition of the glass. It will be interesting to study the structural surrounding of Zn atom in investigated SZS/BZS glasses by means of EXAFS. To show the insulating properties of studied glasses and glass-ceramics, the measurement of electrical conductivity with temperature is planned in the near future. Effect of two intermediate oxides (mixed intermediate effect) can be investigated as a function of the $TiO_2/(Al_2O_3+TiO_2)$ ratio with fixed amounts of Na_2O and P_2O_5. The phase quantification may be initiated for these systems using MAS-NMR and XRD. The chemical durability of prepared glasses in different media (acidic, alkaline and neutral) and at different temperature is also worth to investigate. Other studies include long term phase stability by a combination of XRD and MAS-NMR in wet oxidizing and reducing environments that mimic the operational conditions of fuel cells. Further scope also exists in terms of reaction studies with other fuel cell components, especially over the long-term use. It has been reported that incorporation of ZnO reduces the formation of detrimental $SrCrO_4$ phase [17]. Therefore, effect of ZnO and other additives on the formation of $SrCrO_4/BaCrO_4$ needs to be investigated.

Bibliography

1. S. R. Elliot, Physics of Amorphous Materials, Longman Inc., New York (1990).
2. M. Arbab, L. J. Shelestak and C. S. Harris, Am. Ceram. Soc. Bull., 84 (2005) 30-35.
3. J. E. Shelby, Introduction to glass science and technology, 2nd Edition, CRC Press (2005).

4. W. Holland and G. H. Beall, Glass-Ceramic Technology, The American Ceramic Society, Westerville, Ohio (2002).
5. J. Zarzycki, in: R. W. Cahn, P.Haasen, E. J. Kramer (Eds), Material Science and Technology, Vol.9, VCH, Weinheim, (1991).
6. W. H. Zachariasen, J. Am. Chem. Soc., 54 (1932) 3841-51.
7. J.Y. Wei, Y. Hu, L.G. Hwa, J. Non-Cryst. Solids 288 (2001) 140-7.
8. J. W. Fergus, J. Power Sources. 147 (2005) 46-57.
9. C. Lara, M.J. Pascual, A. Duran, J. Non-Cryst. Solids. 348 (2004) 149-55.
10. Babita Tiwari, M. Pandey, V. Sudarsan, S.K. Deb and G.P. Kothiyal, Physica-B Condensed Matter, 404 (2009) 47-51.
11. Babita Tiwari, V. Sudarsan, A. Dixit and G.P. Kothiyal, J. Am. Ceram. Soc. 94 (5), (2011) 1440-46.
12. D. Boyd, G. Carroll, M.R. Towler, C. Freeman, P. Farthing, I.M. Brook, J. Mater. Sci.: Mater. Med., 20 (2009) 413-20.
13. Babita Tiwari, A. Dixit and G.P. Kothiyal, Int. J. Hydrogen Energy 36 (2011) 15002-8.
14. T. Ozawa, J. Therm. Anal., 9[3] (1976) 369-73.
15. K. Matusita, S. Sakka, J. Non-Cryst. Solids, 38-39 (1980) 741-6.
16. Babita Tiwari, A. Dixit, C.G.S. Pillai, S.C. Gadkari and G.P. Kothiyal, J. Am. Ceram. Soc. 95 (4), (2012) 1290-96.
17. T. Zhang, H. Zhang, G. Li, H. Yung, J. Power Sources, 195 (2010) 6795-97.

Signature of Student: Babitatiwari

Date: 25|5|2012

Doctoral Committee:

S. No.	Name	Designation	Signature	Date
1.	Dr. G. K. Dey	Chairman	Gautam Kumar Dey	25/5/12
2.	Dr. G. P. Kothiyal	Convener		25-5-2012
3.	Dr. S. K. Kulshreshtha	Member		25/5/2012
4.	Dr. A. R. Kulkarni	Member	ARKulkarni	25/5/12
5.	Dr. S. Basu	Member		25-5-12

List of Publications

International Journals: 07 (published) + 2 (accepted) + 3 (to be communicated)

1. **Babita Tiwari**, and coworkers “Comparison of strontium zinc based and barium zinc based silicate glasses” under preparation.

2. **Babita Tiwari**, S.C. Gadkari and G.P. Kothiyal, “Studies on crystallization of SrO-ZnO-B_2O_3-SiO_2 based glasses”, under preparation.

3. **Babita Tiwari**, M. Pandey, V. Sudarsan, S.C. Gadkari and G.P. Kothiyal, “Thermo-physical, crystallization and structural studies of Strontium zinc silicate based glass-ceramics”, to be communicated.

4. **Babita Tiwari**, S.C. Gadkari and G.P. Kothiyal, “Investigation on Glasses in strontium zinc borosilicate system as sealants for solid oxide fuel cell”, *Adv. Mater. Res.* accepted.

5. **Babita Tiwari**, M. Pandey, S.C. Gadkari and G.P. Kothiyal, “Synthesis and Structural Studies of Multi-Component Strontium Zinc Silicate Glass-Ceramics”, *AIP Journal: Confer. Proc.* accepted.

6. G.P. Kothiyal, M. Goswami, **Babita Tiwari**, K. Sharma, A. Ananthanarayanan, Lionel Montagne, “Some recent studies on glass/glass-ceramics for use as sealants with special emphasis for high temperature applications”, *J. Adv. Ceram.* 1(2) (2012) 110-129.

7. **Babita Tiwari**, S. Bhattacharya, A. Dixit, S.C. Gadkari and G.P. Kothiyal, “Effect of V_2O_5 on SrO-ZnO-B_2O_3-SiO_2 Glass-Ceramics for High Temperature Sealant Application”, *AIP Journal: Confer. Proc.* 1447 (2012) 575-76.

8. **Babita Tiwari**, A. Dixit, C.G.S. Pillai, S.C. Gadkari and G.P. Kothiyal, "Crystallization kinetics and mechanism of Strontium zinc silicate glass", *J. Am. Ceram. Soc.* 95(4) (2012) 1290-96.

9. **Babita Tiwari**, V. Sudarsan, A. Dixit and G.P. Kothiyal, "Study of Glass/Glass-Ceramics in the SrO-ZnO-SiO_2 System as High Temperature Sealant for SOFC Applications", *Int. J. Hydrogen Energy* 36 (2011) 15002-8.

10. **Babita Tiwari**, V. Sudarsan, A. Dixit and G.P. Kothiyal, "Effect of TiO2 Addition on the Optical, Thermo-Physical, and Structural Aspects of Sodium Alumino-Phosphate Glasses", *J. Am. Ceram. Soc.* 94(5) (2011) 1440-46.

11. **Babita Tiwari**, M. Pandey, V. Sudarsan, S.K. Deb and G.P. Kothiyal, "Study of structural modification of sodium alumino-phosphate glasses with TiO_2 addition through Raman and NMR spectroscopy", *Physica-B* 404 (2009) 47-51.

12. G. P. Kothiyal, A. Ananthanarayanan, **Babita Tiwari,** M.Goswami and V. K. Shrikhande, "Studies on some Glasses and Glass-Ceramics for various Applications including Seals", *Mater. Sci. Forum*, 587-588 (2008) 162-166.

International/National Conferences: 10

13. **Babita Tiwari**, A. Sarkar, S. C. Gadkari and G. P. Kothiyal, "Crystallization Kinetics of BaO-ZnO-SiO_2 Glass", 22- AGM of MRSI- Bhopal, Feb-13-16, 2011.

14. **Babita Tiwari**, A. Dixit and G.P. Kothiyal, "Crystallization kinetics of SrO-ZnO-SiO_2", International conference on Materials chemistry (ICMC – 2010), BARC, Mumbai, Dec. 7-11, 2010.

15. **Babita Tiwari**, M. Pandey, A. Dixit, and G.P. Kothiyal, "Phase evaluation and Raman studies of SrO-ZnO-SiO_2 Glass-ceramics", International workshop & Symposium on the Synthesis and Characterization of Glass/Glass-Ceramics (IWSSCGGC-2010), YASHADA, Pune, July 7-10, 2010.

16. **Babita Tiwari**, A. Sarkar, A. Dixit and G.P. Kothiyal, "Thermo-physical and devitrification studies of alkaline-earth based silicate glasses as sealant for SOFC", International conference on Electroceramics (ICE – 2009), University of Delhi, New Delhi, Dec. 13-17, 2009.

17. **Babita Tiwari**, A. Dixit and G.P. Kothiyal, "Study of Glass-Ceramics in the SrO-ZnO-SiO_2 System as High Temperature Sealant for SOFC Applications", International Symposium & Exhibition on Fuel Cell Technologies (FUCETECH 2009), Nehru Centre, Mumbai, Nov. 11-13, 2009.

18. **Babita Tiwari**, A Sarkar, and G P Kothiyal, "Thermo-physical properties and crystallization behavior of BaO based silicate glasses for high temperature sealants", National Symposium on Science and Technology of Glass and Glass-ceramics (NSGC-2008), BARC, Mumbai, Oct. 15-17, 2008.

19. **Babita Tiwari**, A Dixit, V Sudarsan, and G P Kothiyal, "Optical and NMR studies of Na_2O-Al_2O_3-TiO_2-P_2O_5 glasses", National Symposium on Science and Technology of Glass and Glass-ceramics (NSGC-2008), BARC, Mumbai, Oct. 15-17, 2008.

20. G.P. Kothiyal, A. Ananthanarayanan, **Babita Tiwari**, M. Goswami, "Studies on some glass-ceramic sealant for different applications including SOFC", 3rd MRS-S Conference on Advanced Materials, Singapore, Feb. 25-27, 2008.

21. Aparna Patil, **Babita Tiwari**, M. Goswami, S. Manikandan, A. Dixit, A. Sarkar and G.P. Kothiyal,"Some observations on thermo-physical properties of BaO-ZnO/CaO-SiO_2 glasses",

National conference on Advanced Materials, Devices and Technologies (NCAMDT), Tirupati, Feb. 21-23, 2008.

22. **<u>Babita Tiwari</u>**, V. Sudarsan, M. Pandey, A. Dixit, S.K. Deb, and G.P. Kothiyal, "Structural characterization of Na_2O-Al_2O_3-TiO_2-P_2O_5 glass by MAS-NMR and vibrational spectroscopy", 10th Int. Conf. on Advanced Materials (IUMRS-ICAM-2007), Bangalore, India, Oct. 8-13, 2007.

List of Figures

List of Tables

Chapter 1

General Introduction

Glass, one of the most ancient materials, has fascinated and attracted enormous interest both scientifically and technologically. This age-old material plays a key role in numerous applications like electronics [1], photonics [2], biomedicine [3], radioactive waste storage [4] and many others, along with classical ones like windows, architecture, lenses, containers etc. Glass which was earlier considered mainly an optical, dielectric or passivating material can now be used to make active devices like switches, memories, sensors, solar cells, catalysts etc [5]. These widespread uses reflect an ever increasing role of glass in our modern technical society and industry.

1.1 Glass: A Historical Perspective

Glass is one of the most ancient materials known and used by the mankind. Before people learned to make glasses, they had found naturally formed glasses like obsidian, fulgurites, impactites and tektites and used these as arrow heads, knives and primitive jewelry [6]. The origin of first synthetic glass is lost in antiquity and legend. However, according to archeologists glass formation was discovered in ancient Egypt and Mesopotamia as far back as 3500 BC [7]. The invention of glass blowing around Ist century BC in the region of what is modern day Syria greatly expanded the application of glasses. From 1500 BC onwards, commerce helped spread glass making to Europe and Eastern Asia. Glasses also grew in importance from being merely decorative materials to materials with utility. By the 15th century, the use of glass in architecture was well established. In the next two centuries, Europe was a centre of glass related activity. By the end of the 17th century, glass making was industrialized in England. There, at the end of the 17th century, Ravenscroft invented lead glass: a combination of silica with potash and lead oxide. The development of lead glass allowed the construction of long range telescopes in the 18th century and nowadays still widely used due to its radiation shielding properties. Development of glass sheets with uniform thickness and very flat surface by float glass process (invented in 1959 by Pilkington Brothers) revolutionized architecture industry. Flat panel display glasses for television and computer screens are also produced by this process. Thus, glass-making process has evolved over centuries and most commercial glass production is now part of heavy industrial complexes.

1.2 Definition of Glass

A glass is defined in ASTM [8] as 'an inorganic product of fusion, which has been cooled to rigid condition without crystallization'. According to this definition, a glass is a non-crystalline solid material obtained by a melt-quenching process. Glass is also defined as an amorphous/non-crystalline solid completely lacking in long-range periodicity and exhibit glass transition behaviour [9,10]. The terms amorphous and non-crystalline are synonymous. The glass transition is a phenomenon in which a solid amorphous phase shows an abrupt change in the derivative thermodynamic properties from solid like to liquid like values with change of temperature [9]. Nowadays, non-crystalline materials that can't be distinguished from melt-quenched glasses of the same composition are obtainable by using various other techniques such as chemical vapor deposition, sol-gel process, etc. Therefore, most glass scientists regard the term 'glass' as covering 'all non-crystalline solids that show a glass transition' regardless of the preparation method. Glass is also defined as a configurationally frozen liquid which exhibits glass transition behaviour [10].

From a thermodynamic point of view, the 'glassy' state is a meta-stable state and unlike crystalline state it is not unique. The 'glassy' state depends upon the thermal history of the melt and represents a local minimum in the free energy. Given adequate time, the system will relax to a more stable state, of lower free energy, provided the energy barrier separating these states can be crossed [11]. For practical purpose however, the time taken for relaxation of most everyday glasses is so long that the question of metastability is purely academic.

1.3 Glass Transition Phenomenon

The glass transition is an essential attribute of any glassy material. The glass transition phenomenon is quite complex and many theories have been suggested based on various parameters/properties, which characterize the glasses. These theories have been successful only to a limited extent as the glass transition is a function of many parameters like heat capacity, thermal conductivity, melting temperature, cooling rate etc. Significant variation in the value of glass transition temperature (T_g) has also been observed depending on the method used for its measurement. This is because when a melt is quenched to form a glass, the different degrees of freedom get arrested and during heating these degrees of freedom start getting relaxed. These different degrees of freedom, corresponding to different properties, which are used to evaluate T_g, relax at different rates and result in different values of T_g being measured. When a liquid is cooled either crystallization may take place at the freezing point (or melting point 'T_m'), or else the liquid will become 'supercooled' for temperatures below T_m. This 'supercooled' liquid becomes more viscous with decreasing temperature, and ultimately attains the viscosity ($\eta = 10^{14.6}$ dPa s) characteristic of a solid [9]. Although glass has atomic arrangement akin to liquid state, in terms of all other properties such as rigidity etc., glass is unequivocally a solid. This phenomenon can be understood readily by monitoring the changes in enthalpy/volume as a function of temperature (Figure 1.1). The crystallization process is manifested by an abrupt change in extensive thermodynamic variables like enthalpy 'H' or volume 'V' at T_m, whereas glass formation is characterized by a gradual change in slope. The temperature range over which the change of slope occurs is called the 'glass-transformation range' [9,10]. As the transition of liquid to the glassy state is continuous, the T_g cannot be uniquely defined. However, for convenience the T_g is expressed as 'fictive' temperature 'T_f', the temperature obtained by intersection of the extrapolated liquid and glass curves (Figure 1.1). It depends on the rate of cooling of the supercooled liquid. The slower the rate of cooling, the larger is the region in which the liquid may retain supercooled state, implying lower T_f or T_g, as shown in Figure 1.1. Thus, the 'T_g' of a glass is not an intrinsic property but depends on its thermal history [10]. Dependence of T_g on the cooling rate q is given as:

$$q = q_0 e^{-\frac{1}{c}\left(\frac{1}{T_g} - \frac{1}{T_M}\right)} \tag{1.1}$$

where c and q_o are constants [10]. The experimentally measured value of T_g is not unique. The value of T_g depends on the time scale of the experiment used to observe it.

The relaxation process is another very important aspect of glass transition. The configurational changes, which are responsible for the relaxation process, become increasingly slow as the temperature decreases. At T_g the material shows a solid like behaviour for observation time 't_0' which is smaller than the structural relaxation time 't_r'. For $t_r < t_0$, the material behaves like a liquid. A transition is said have taken place when the parameters corresponding to liquid like behaviour differ significantly from solid like ones, as in the case for heat capacity. In other words, T_g should occur when t_0 is equal or comparable to t_r.

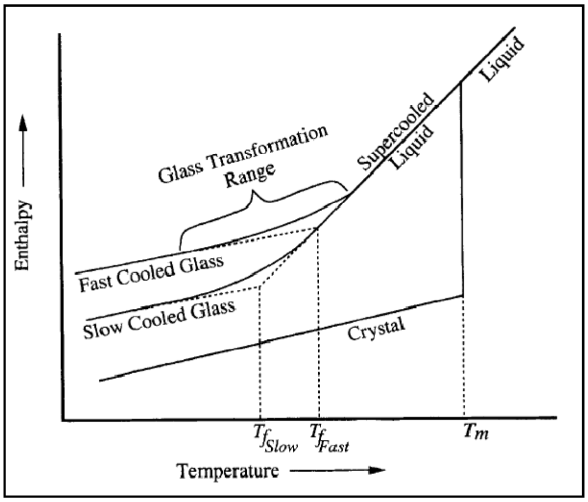

Figure 1.1: Variation in enthalpy or volume of a glass forming melt with the temperature [10].

The glass transition can also be expressed as a phenomenon in which a solid glassy phase shows abrupt change in the derivative thermodynamic properties such as heat capacity, thermal expansion coefficient (TEC) etc [10] at the transition temperature. The order of a phase transition in Ehrenfest scheme is defined as the order of the lowest derivative of Gibbs free energy (*G*), which shows a discontinuity at the transition point [10]. In liquid to crystal transition at freezing (or melting) temperature 'T_m' the volume 'V' and enthalpy 'H', which are the first derivative Gibbs free energy, are discontinuous. Hence, liquid to crystal transition is a first order transition. However, in liquid to glass transition, the thermodynamic variables such as volume, enthalpy and entropy are continuous and the quantities such as thermal expansion 'α_T' compressibility 'K_T' and heat capacity 'C_P', which are the second order derivative of Gibbs free energy, are discontinuous. Hence, the glass transition is a manifestation of a second order phase transition [10]. However, this simple model is unable to explain the change in T_g values, depending on the thermal history of the glass samples. Therefore, the glass transition is not a simple second-order phase transition. However, without involving a second-order thermodynamic transition, Prigogine and Defay [12] showed that the ratio R defined as follows:

$$R = \frac{\Delta K_T \Delta C_P}{TV(\Delta \alpha_T)^2} \tag{1.2}$$

is equal to unity if a single ordering parameter determines the position of equilibrium in a relaxing system, but if more than one ordering parameter is responsible, then R > 1; the latter case seems to describe most glasses. Nevertheless, there is a thermodynamic aspect in addition to the relaxation character of the transition evinced by Kauzmann's paradox [13]. Although the glass transition appears superficially to be a second-order thermodynamic phase transition, it is not ideally second order.

Tendency of a material to form a glass has been described by Hruby [14] by defining a parameter 'K_g', which involves the T_g, T_m and the crystallization temperature (T_c) as follows:

$$K_g = \frac{T_c - T_g}{T_M - T_c} \tag{1.3}$$

If (T_c-T_g) is large and (T_m-T_c) is small, the inhibition to the process of nucleation and crystallization is strong and consequently the glass-forming tendency of the system is high. T_g is also defined in terms of the experimental time scale as that temperature at which the liquid attains viscosity of a solid (~$10^{14.6}$ dPa.s). In this kinetic approach, glass can be considered as a 'frozen in liquid'. It is well known that the viscosity, or equivalently the relaxation time of glasses increase very rapidly on cooling the liquid to the vicinity of the glass transition. The point at which the viscosity, or relaxation time, are so large that equilibrium no longer exists between the thermal state of the glass-forming system and the surrounding heat bath, is the thermodynamic T_g. This commonly occurs at about two thirds of the melting temperature in silica based glasses. There are two typical phenomenological behaviors of the viscosity as a function of the temperature. The first one is the Arrhenius relaxation law as given in Eq. (1.4), according to which viscosity (as well as relaxation time) grows exponentially at low temperature [15].

$$\eta = \eta_0 exp\left(\frac{A}{T}\right) \tag{1.4}$$

Here, η_0 is a constant while A is the activation energy for viscous flow. The second one is the Vogel-Fulcher-Tammann equation, which is expressed as [16]

$$\eta = \eta_0 exp\left(\frac{B}{T - T_0}\right) \tag{1.5}$$

where η_0, B and T_0 are constants. This equation describes the viscosity $\eta(T)$ of glass at any temperature T more successfully and diverges even faster than Arrhenius equation. Glasses have been distinguished in two categories; strong and fragile, according to the temperature dependence of viscosity around the glass transition. The distinction is based on the flow behaviour of glasses in the molten state. The glasses for which viscosity obeys Arrhenius behaviour are designated as strong glasses, whereas; glasses whose viscosity follows the Vogel-Fulcher-Tammann law, come in the category of fragile glasses.

Glass transition phenomenon has also been explained by invoking the free volume theory [17]. In this model a glass is assumed to consist of hard spheres. The total volume of the glass is divided into two parts namely the one occupied by molecule or spheres, V_{oc} and another part, V_f, in which molecules are free to move. For a glassy material free volume is independent of temperature and gets frozen at certain locations when glass is formed. For liquids, with decrease in the temperature both free and occupied volumes decrease and there occurs a redistribution of free volume. According to free volume theory, the glass transition occurs when the free volume of a liquid is decreased below a critical value. The fractional free volume is given by the expression,

$$V_{ff} = \frac{V_{fg}}{V_g} = T_g \times \Delta\alpha_T \tag{1.6}$$

where V_{fg} is the free volume of the glass and V_g is the volume of glass and $\Delta\alpha_T = \alpha_{T_L} - \alpha_{T_g}$, where α_{T_L} and α_{T_g} represent volume thermal expansion of liquid and glass respectively. It has been demonstrated that for several glasses, 10% of the total volume is free at T_g [15]. Free volume theory has been modified for wider applicability by incorporating percolation theory [18,19], which accounts for the exchange of free volumes between the nearest neighbour liquid like cells without any simultaneous change in the volumes of any solid like cells. In conclusion it may be mentioned that no single theory can explain all aspects of glass transition phenomenon completely. However, these theories are qualitatively successful in explaining glass transition phenomenon for a variety of systems. Any complete theory describing the formation of a glass from the liquid state must therefore combine both relaxation and thermodynamic aspects in a natural way; the recent developments of free-volume theory using percolation arguments perhaps point the way to this goal.

1.4 Structural Aspects of Glasses

Good understanding of the structural arrangements of atoms in any material is a key factor to a detailed understanding of its physical and chemical properties. The structure of crystalline materials is well established and is classified according to structure of the unit cell. However, the lack of symmetry and periodicity in amorphous materials make such approach inapplicable for them. Even though there is lack of long range periodic order, these materials often possess considerable structural order over length scale of many Ǻ [20]. Therefore, a length scale may be arbitrarily defined, which separates microscopic structure from macroscopic structure in amorphous solids [21]. Understanding of the structure of amorphous solids has advanced with the development of experimental techniques like nuclear magnetic resonance (NMR), extended X-ray absorption fine structure (EXAFS) spectroscopies and small angle X-ray/neutron scattering (SAXS/SANS) [22]. Diffraction methods (X-ray, neutron or electron) can be used to get information about the first and second co-ordination spheres around an atom and the interconnection of the regions of short-range order [23]. Raman and infrared (IR) vibrational spectroscopies are also extremely valuable for structural exploration in heteronuclear glass forming systems [23].

Glass formation does not depend on the type of bonding. Besides the large class of inorganic glasses with mixed covalent ionic bonds there exist metallic glasses and organic glasses with van der waals bonds. Therefore, determination of structure for every class of glass is a wide scientific field with a number of different theories and experimental methods to confirm them. The most important structural model for oxide glasses was proposed by Zachariasen [24] in 1932 based on continuous random network hypothesis. Continuous Random Network (CRN) model was based on the existence of the polyhedra that are linked together to form an overall random network. He suggested that the crystalline and the glassy form of an oxide should have the same type of oxygen polyhedra joined in a similar way except that in the glassy phase there is range of bond angles and bond lengths. Further, the network should be sufficiently flexible to incorporate the disorder, which is characteristic of the glassy phase, and the internal energy of both the crystalline and glassy phase should be comparable. The X-ray diffraction (XRD) studies carried out by Warren [25] supported this theory. The difference in structure of crystalline and glassy forms of a hypothetical two-dimensional oxide, say, A_2O_3 is shown in Figures 1.2(a) and 1.2(b).

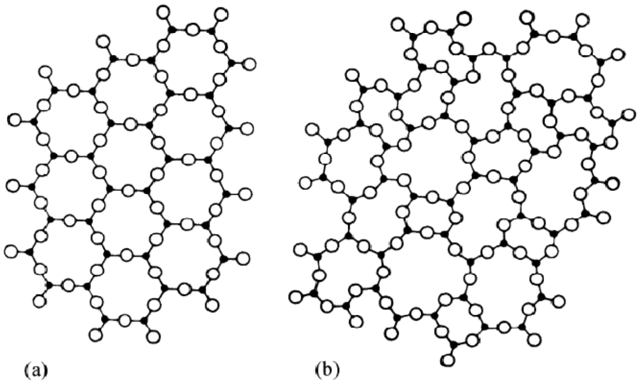

Figure 1.2: Atomic structural representation of a A_2O_3 crystal (a) and a A_2O_3 glass (b) (Filled circles are A = cations and open circles are O = oxygen).

Thus, both the crystalline and the glassy forms are composed of AO_3 triangles joined to each other at corners, except that the glassy form has disorder introduced by changes in the A–O–A bond angles and A–O bond length. The triangles or O–A–O angles themselves need not be deformed much. According to the Zachariasen's CRN theory, the following criteria are valid for glass formation in simple compounds like SiO_2, B_2O_3, P_2O_5, GeO_2, As_2S_3, As_2Se_3, BeF_2, $ZnCl_2$ etc:

1. An oxide or compound tends to form a glass if it easily forms polyhedral groups as the smallest building units.
2. The cation polyhedra share only corners not edges or faces.
3. Anions (like O^{2-}, S^{2-}, Se^{2-}, F^{1-}, Cl^{1-},…) should not bind more than two central atoms (in simple glasses anions form bridges between two adjacent polyhedral).
4. The number of vertices of polyhedron should be less than six.

5. At least three vertices of a polyhedron must be shared with neighbouring polyhedral in order to form a three-dimensional (3D) network.

Zachariasen classified the cations in a glass as follows:

1. Network-formers (NWF) e.g. Si, B, P etc. with the coordination number 3 or 4.
2. Network-modifiers (NWM) e.g. Li, Na, Sr, Ba etc. with coordination numbers generally greater or equal to 6.
3. Intermediates that may either reinforce the network by cross-linking (coordination number 3 or 4) or weaken the network by depolymerization (coordination number 6-8). Moreover the intermediate cations solely cannot form the single component glass.

NWM oxides (e.g. Na_2O) depolymerize the perfectly connected continuous random network of glass formers (e.g. SiO_2). The action of the modifier is to break up the continuous silica network by introducing "dangling or non-bridging oxygens (NBOs)". This process is shown in Figure 1.3 and is not limited to silica glass only, but can occur in other inorganic systems as well.

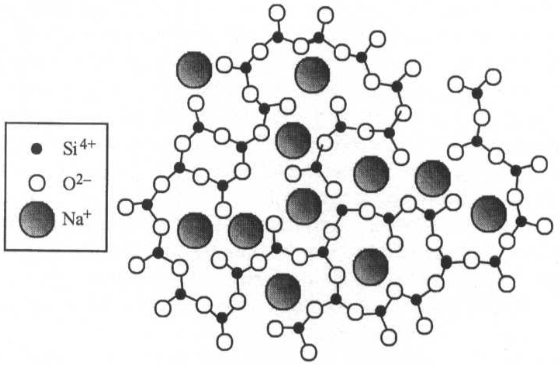

Figure 1.3: Two-dimensional schematic diagram of the silicate glass structure in the presence of modifier ions such as Na^+ and the formation of non-bridging oxygens.

The original CRN model of glass structure [24] can also be extended to describe the structure of strongly ionic or covalent non-oxide glasses such as halides and chalcogencides, respectively. A modified random network (MRN) model was given by Greaves to describe the structure of modified oxide glasses [26]. At the other extreme, the structure of organic glasses where molecular units are held by van der Waals forces requires a random-packing type of description, similar to the structure proposed for metallic glasses [27,28]. The lack of experimental information about the structure of glass and the difficulties in describing the polymerized structure in the long range extent can be partially solved by the concept of atom-specific structure elements (ASEs) developed by Sprenger [22,29].

1.5 Types of Glasses

Glasses have been broadly classified into two different ways. First one is based on the actual components present in them and second one, based on their end use. Glasses based on silicate, phosphate, borate, borosilicate etc, networks belong to the first category; whereas optical glasses, sealing glasses, laser glasses etc, correspond to the second category. Other types of glasses include metallic glasses, halide glasses, organic glasses, mixed anion glasses, ionic glasses and chalcogenide glasses. Brief description regarding the different structural aspects and properties of some of the glasses is presented in the following section.

1.5.1 Oxide glasses

Oxide glasses are historically the oldest and industrially the most exploited. Human uses of these range from the ancient and the mundane (containers, windows) to the leading edge of new technologies of data processing and transmission (lasers, optical fiber, semiconductor devices) and the long-term nuclear waste storage. Most of the present day industrial glasses are silicate or alumino-borosilicate glasses containing a variety of monovalent and divalent oxides [30]. Oxide glasses not containing silica are generally of limited volume in terms of consumption and used only in specialty applications.

1.5.1.1 Silicate glasses

Pure silica (SiO_2) glass is compositionally simplest and technologically one of the most important glasses. Pure silica glass is prepared by heating sand in a refractory metal or graphite crucible at around 2000°C. However, high purity silica glasses for optical applications have been prepared either from the hydrolysis or oxidation of $SiCl_4$ in flame. Silica is structurally an archetypal example of a CRN model made of corner-sharing SiO_4 tetrahedra. XRD studies of vitreous silica, carried out by various authors [31,32], revealed that each silicon is surrounded by four nearly equidistant oxygen atoms at an average distance of 1.608±0.004 Å. The O-O bond distance is 2.626 Å with a mean bond angle of 109.7±0.6°. The Si-O-Si angle distribution in silica glass was obtained by ^{29}Si magic angle spinning (MAS) NMR studies [31] and this agrees quite well with the results obtained from XRD. Introduction of NWM oxides to silica results in the breakage of extended Si-O-Si network, creating non-bridging oxygen atoms. Thermo-physical properties like micro-hardness (MH), T_g etc, decrease with increase in non-bridging oxygen atoms as the more rigid and covalent Si-O-Si bonds are converted to less rigid $Si\text{-}O^{-}\text{-}M^{+}$ linkages (M is NWM metal ion). The different silicon structural units present in modified silicate glasses have been designated as Q^n units, where n represents the number of bridging oxygen atoms attached to silicon as shown in Figure 1.4. ^{29}Si MAS-NMR studies of $Na_2O\text{-}SiO_2$ glasses [33,34], revealed that glasses containing 33.3 mol% Na_2O exhibit only Q^3 structural units of Si, with further increase in Na_2O, the progressive conversion of Q^3 units to Q^2 units of Si takes place and at

50 mol% of Na_2O mainly Q^2 structural units are present. Unlike alkali metal oxides, certain other metal oxides like PbO, ZnO etc [35,36] have been found to behave both as network former as well as network modifier depending on their concentration.

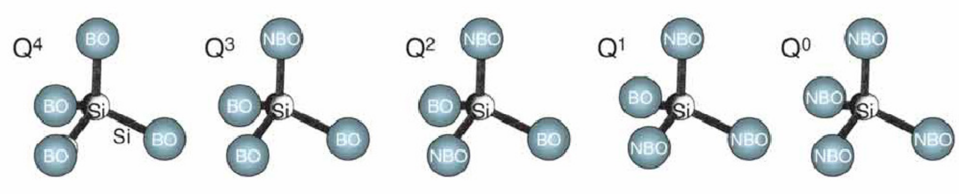

Figure 1.4: Silicate tetrahedral units that can exist in silicate glasses.

1.5.1.2 Phosphate glasses

Glasses having P_2O_5 as one of the major components are called phosphate glasses. Electronically phosphate glasses often have larger band gaps than silicates and, therefore, better ultraviolet (UV) transmission [37]. Phosphate glasses have comparatively low T_g making them easily processable and with high TEC well matched to those of metals, so are prime materials for hermetic seals especially with low melting and high expansion metals like Al, Cu etc [38]. Al and Al alloys are important materials for space applications because of lower weight and cost and desired mechanical properties. Certain phosphate glass compositions (e.g. aluminium phosphate) have large rare-earth stimulated emission cross-sections and low thermo optical coefficients (compared with silicate glasses) and are the materials of choice, particularly for high power laser applications [39-41]. Phosphate glasses also have low dispersion and relatively high refractive indices (compared with silicate-based optical glasses) and are developed for achromatic optical elements. Phosphate melts have high solubility factors for heavy cations and anions which lead to a range of fast ion conductors for solid state electrolytes. These glasses have high ionic conductivity as well as thermal and electrochemical stability. Therefore they are extensively studied for solid-state ionic devices [42]. In the recent years these glasses have particular interest due to the biocompatibility.

Pure P_2O_5 glasses are highly moisture sensitive as mentioned earlier and immediately react with water and hence are of less practical importance. Anhydrous P_2O_5 glasses are prepared in sealed silica ampoules in dry boxes from crystalline P_2O_5/P_4O_{10} which is purified by vacuum distillation. Like silicate glasses, the phosphate glasses are constructed from corner-sharing tetrahedra, with the important difference that these are three-fold rather than four-fold coordinated. Schematic diagram representing different Q^n structural units present in phosphate glasses is shown in Figure 1.5.

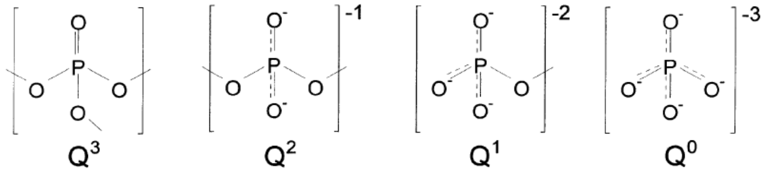

Figure 1.5: Phosphate tetrahedral units that can exist in phosphate glasses.

Recent neutron diffraction studies of these glasses revealed that vitreous P_2O_5 contains two types of P-O bonds, i.e. P-TO (TO = terminal oxygen bond) or P-NBO (NBO bond) and P-BO (BO = bridging oxygen bond). The former is slightly shorter than the latter. Infrared and Raman spectroscopic studies carried out on vitreous P_2O_5, also distinguish between bridging and terminal oxygen atoms [43,44]. Similar to binary silicate glasses, addition of modifying oxides to vitreous P_2O_5 results in the conversion of BO to NBO. Interpretation of structural aspects and physico-chemical properties of alkali phosphate glasses have to be made only after accounting for moisture contents in these glasses. Initially development and technological applications of phosphate glasses was limited by their poor chemical durability but eventually problem of durability solved by the inclusion of suitable intermediates like Al_2O_3, In_2O_3, Fe_2O_3 etc, [45-48]. Chemical durability of low melting iron phosphate glasses has lead to their development as nuclear waste hosts [48]. The moisture sensitiveness of phosphate glasses arises because of TO/NBO atoms present in it. These NBO atoms can be made to have strong covalent linkages with other metal ions like Al^{3+}, Sb^{3+}, Bi^{3+} etc, thereby reducing the hygroscopic nature of these samples.

1.5.1.3 Borate glasses

Pure Borate glasses are difficult to prepare under normal conditions without any moisture content. Water free Borate glasses are prepared by Poch [49] by melting orthoboric acid for several hours at a pressure of 1 mm of Hg.

Various structural studies carried out on pure borate glasses revealed that the structure of the glass agree well with the model proposed by Krogh-Moe [50]. According to this model B_2O_3 glasses mainly contain boroxol rings. The classic work of Krogh-Moe indicated the possible presence of 5 different types of borate species in the glass structure (Figure 1.6). Glass formation of B_2O_3 with various metal oxides has been extensively studied by various authors [51,52] and they have pointed out that some anomalous behaviour exists for these glasses. For example, in Na_2O-B_2O_3 system two separate regions of glass formation exists in the range of composition 28.5 to 33.5 mol% of B_2O_3 and 62 to 100 mol% of B_2O_3. The glass formation gap can however be removed by adding Al_2O_3 [53]. Structural aspects of binary borate glasses have been mainly investigated by ^{11}B, ^{10}B NQR (Nuclear Quadrupole

Resonance) and NMR techniques. Addition of Na_2O to B_2O_3 glass, up to 33 mol%, results in progressive conversion of trigonal boron structural units (BO_3) to tetrahedral boron structural units (BO_4). Above 33 mol% of Na_2O, relative concentration of BO_4 structural units started decreasing [54].

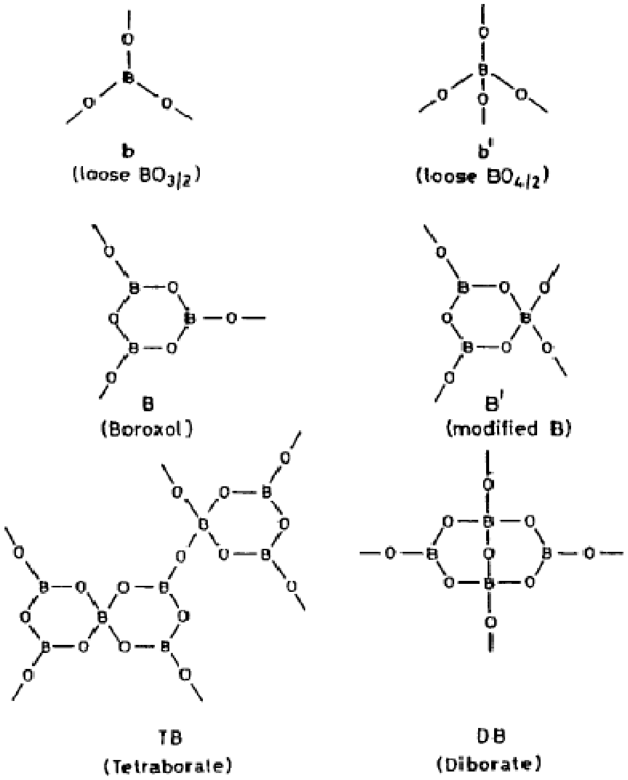

Figure 1.6: Possible borate species in the borate glass structure [54].

Borate glasses generally melt at lower temperatures and are frequently used as solder glasses. Primary requirement of solder glass is that, it needs to be a fluid at a temperature, which is well below the deformation temperature of the glass to be sealed. Borate glasses containing high concentration of rare earth oxides are used to manufacture lens systems with high numerical aperture and low spherical aberrations.

1.5.2 Halide glasses

Glasses having major anions form elements of the group VII-A (particularly F^- and/or Cl^-) are called halide glasses. BeF_2 and $ZnCl_2$ are the known examples of halide glasses [55-57]. These are obtained by simply quenching halides from their molten state. Structures of simple BeF_2 and $ZnCl_2$ glass characterized by 3D CRN model of corner-shared BeF_4 and $ZnCl_4$ tetrahedra, respectively, and bridging halogens [58,59]. BeF_2 glasses doped with lanthanide ions like Nd^{3+} has got potential application as high-power laser materials because BeF_2 has very low linear and non-linear refractive indices. $ZnCl_2$ and BeF_2 are hygroscopic, which limits there utility. $ZnCl_2$ glasses with $PbCl_2$, $CdCl_2$ and $CdBr_2$ have been found to be more resistant to water attack [60]. Chloride bridges are much weaker than the fluoride bridges and the glasses are inherently unstable towards devitrification. Its tendency towards devitrification, however, improves by the addition of other halides like KBr and $PbBr_2$. The metal-fluorine (M-F) bond is unstable towards oxidation as M-O bond is inherently stronger. Fluoride glasses are technologically important (laser window, optical waveguide, optical fibers etc.) due to optical transparency over a wide range of wavelengths from near-UV to mid-IR. Multi-component heavy metal fluoride glasses have been developed with such applications in view, although the devitrification tendencies of such glasses are still a limitation and the bowl size that can be realized limits the fiber length that can be drawn.

1.5.3 Chalcogenide glasses

Glasses formed by compounds containing elements of Group VI-B of the periodic table, viz, S, Se, Te are known as chalcogenide glasses. Methods like vapour-quenching technique produces amorphous materials in the form of thin films over a wide composition range whereas the melt-quench techniques have been used to make glasses in the bulk form over a limited composition range [52]. The band gap of chalcogenide glasses is of the order of 1-3 eV and hence these materials show semiconducting behaviour. These glasses are potential candidates for various technological applications, which include IR transmission, switching devices for computer memories etc. Crystalline and amorphous chalcogenide materials are extensively used as optical components in IR transmission. Compared to oxide materials, the chalcogenide materials have higher cut off wavelength in the IR region. The higher optical wavelength of these materials ensures lower value of Rayleigh scattering cross section and this property of chalcogenide glasses makes them as potential candidates for low loss optical waveguides. Chalcogenide glasses have relatively higher value of non-linear refractive index compared to oxide glasses and this property is used for making non-linear optical devices from such materials. In addition to these applications, chalcogenide glasses are also used for Xerography, lithography, solid-state threshold and memory switches etc [61].

1.5.4 Metallic glasses

Solid alloys with liquid like atomic structure are called metallic glasses. Discovery of metallic glasses was a byproduct of the development of rapid quenching (RQ) methods [62]. RQ method is employed to improve properties of alloys particularly by increasing solute concentrations in alloys. In general, metallic melts have a very high tendency to crystallize and therefore, very high rates of quenching (10^6 Ks^{-1}) are required to form the metallic glasses like AuSi glass.

More recently more complex alloys of 4 to 6 different elements have been produced at much lower cooling rates (1 Ks^{-1}) [63]. These low cooling rates offer the production of bulk metallic glasses (BMGs) [64,65]. These BMGs have more elevated elastic limit and corrosion resistant than crystalline metals. BMGs were found to have a new type of glassy structure with a high degree of dense randomly packed atomic configurations with much smaller excess volume and higher packing density than in oxide glasses. Inoue classified the BMGs into three types: metal-metal type, metal-metalloid type and Pd-metalloid type alloys.

Since metallic glasses are generally quenched at very high rates, they are characterized by high fictive temperatures. Therefore, annealing leads to significant increase in densities and improved properties. Several metallic glasses exhibit a tendency towards crystallization even during annealing, perhaps due to facile heterogeneous and surface nucleation. Glassy metals have been of importance particularly because of their special magnetic properties with low hysteresis and high values of magnetization. They are valuable in making transformer laminations [66].

1.5.5 Organic glasses

Organic glasses consist of carbon-carbon chains which are so entangled that rapid cooling of the melt prevents rearrangement into crystalline state. The simplest glass known as polyethylene is formed from long chains made of -CH_2- moieties. These are used to produce optical lenses, polyvinyl chloride (PVC) bottles and to protect glass articles [67]. Their structures closely resemble those of vitreous sulfur and selenium, which also consist of entangled chains. The chains in organic glasses can also be cross-linked, just as they are in chalcogenide glasses, with consequent changes in their properties. Increasing the degree of cross-linking, increases the viscosity of the melt and the T_g. In general, the properties of organic glasses closely parallel those of the inorganic glasses with chain-based structures, including the ability to produce materials with oriented properties by application of stress during forming. Small regions of oriented chains often exist in organic glasses, so that many of these materials actually resemble to less crystalline glass-ceramics.

1.6 Preparation of Glasses/Amorphous Solids

To obtain a glass or an amorphous solid, it is necessary either to retain at ambient temperature the disordered state of a liquid or gas, or alternatively, to destroy the periodic structure of crystal. Therefore, glasses or amorphous solid can be prepared by various physical and chemical methods as shown in the schematic diagram below (Figure 1.7).

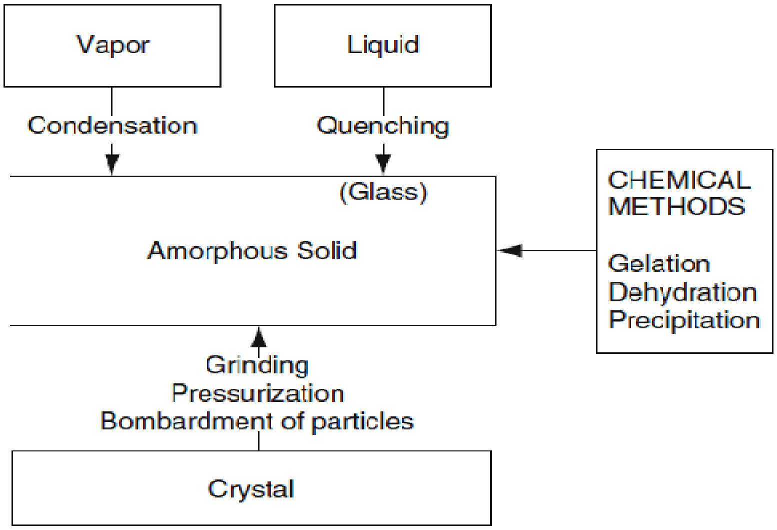

Figure 1.7: Various methods of preparation of amorphous solids.

1.6.1 Melt quenching

The oldest established and popular method of preparing an amorphous solid is to cool the molten form of a material sufficiently fast to preclude nucleation and crystal growth [68].

Amorphous materials produced in this manner have often in the past been termed 'glasses'. Nowadays, glasses are defined as those materials which exhibit glass-transition phenomena and hence are not necessarily formed only by melt quenching, although the great majority of melt-quenched amorphous solids do indeed show glass-transition behaviour. The distinguish feature of the melt-quench process is that the amorphous solid is formed by the continuous hardening (i.e. increase in viscosity) of the melt. In contrast, crystallization of the melt occurs as a discontinuous solidification. Rates of cooling, required for glassy phase formation are different for different materials. For example, certain easy glass formers such as SiO_2, P_2O_5, B_2O_3 etc, will form glassy phase even under conditions of slow cooling (1K/s) whereas to get metallic glasses cooling rates of the order of 10^4-10^6 K/s are required. This process include melting of material in suitable crucibles/pots made of alloy (Pt-Rh, alumina etc) followed by pouring of the melt. Effective cooling can be achieved by quenching the melt immediately after removing from the furnace and placing it in between conducting materials like copper or brass plates or pouring in graphite moulds. Glass in frit form is often obtained by quenching the melt directly in water or chilled water. A batch prepared by mixing predetermined amounts of pulverized raw materials to attain the desired property, is placed, in a tank furnace made of firebrick or into a crucible made of clay, platinum etc, to be fused into a liquid at high temperature. Generally the molten glass is kept at the temperature which corresponds to a viscosity of 10-10^2 dPa.s, i.e. 1400-1500°C for most commercial glasses for more than 10 h in order to remove tiny bubbles and to enhance the homogenization of the melt through convection and the inter-diffusion of the constituent atoms. The formation of a melt into a desired shape is carried out at a temperature corresponding to the viscosity of 10^3-10^4 dPa.s, i.e. 900-1100°C for most commercial glasses, by applying various forming methods such as casting into a mold, blowing, up-drawing, down-drawing, pressing, rolling out, floating, and various their combinations. In this way the high flexibility in the geometry of products, which is the most distinctive feature of the melt quenching technique, is possible.

Most of the formed glasses are usually annealed in a temperature range near the T_g to remove any thermal stresses which are developed during the forming and subsequent cooling due to the low thermal conductivity of a glass. Most of the oxide glasses based on conventional network formers like SiO_2, P_2O_5, B_2O_3 etc, can be prepared by this method. However, the preparation of metallic glasses requires special techniques like melt spinning, melt extraction etc. The advantage of the melt-quenching technique over other methods is the large flexibility of composition. The melt-quenching technique has limitation for the preparation of ultra-high pure glasses.

1.6.2 Vapor quenching

Vapor condensation techniques are used to prepare glasses that cannot be prepared by the melt quenching technique and generally used for the preparation of amorphous films. These techniques yield the highest apparent cooling rates and construct the “glass” one atom at a time from the vapor phase. It relies on the fact that atoms, once vaporized and propelled on a cold substrate, do not have time to reach a crystallographic order. Thermal evaporation, electron beam, Ion bombardment, plasma induced decomposition are used for this purpose. Depending on the method to vaporize the material to be amorphized, vapor quenching is termed as thermal evaporation [69], sputtering, glow discharge (GD), chemical vapour deposition (CVD).

Thermal evaporation is one of the most widely used methods for producing amorphous thin films. In this method the powdered material to be amorphized is placed inside an evacuated chamber, ($1\text{x}10^{-6}$ mbar), having a substrate material kept at a lower temperature and is heated either resistively (for low melting materials) or using electron beam (for high melting materials). Due to the lower temperature of the substrate, the mobility of the atoms that are reaching the surface of the substrate is significantly reduced and are randomly frozen resulting in the formation of amorphous thin film. Thin films of amorphous semiconductors like Si, Ge, GaAs, chalcogenides etc, are prepared by this method. The principal advantage of this method is that the composition and physical characteristics of the resulting films can be varied by changing various parameters like substrate temperature, substrate and source separation and orientation of base gas pressure in the chamber etc. The main disadvantage of this method is the compositional inhomogeneity in the film. Also in many cases, the composition of the material in the vapour phase is different from that of the source, for example, when the starting material is stoichiometric As_2S_3, the vapour phase is found to contain As_4S_4 molecules.

Sputtering method involves the bombardment of a target by energetic ions obtained from low-pressure plasma resulting in the removal of atoms or clusters of atom from the target material followed subsequently by their deposition as a thin film on the substrate. Sputtering method is more flexible compared to the thermal evaporation method and reasonably homogeneous and uniformly thick and stoichiometric deposits can be produced by this method. The main disadvantage of the method is that it requires close control of many parameters namely, the sputtering gas and its pressure, ratio of partial pressure of reactive gas to inert gas, radio frequency (RF) power applied to target, bias voltage of target or substrate etc.

Glow discharge (GD) method is similar to sputtering process, but instead of ions from the plasma ejecting the material from the target, chemical reaction is initiated in the gas phase by creating an RF glow discharge of the reactant gas, leading to the deposition of the solid form on a substrate placed inside a chamber. It is difficult to control parameters precisely in this method as compared to the former two methods.

Chemical vapour deposition (CVD) method, in principle, is similar to glow discharge method but the decomposition of the reactant gas is achieved by thermal energy (pyrolytically), for which temperatures of the order of 1000 K, are commonly used. Amorphous hydrogenated Si (a-Si: H) as well as B and P doped samples of amorphous Si etc., have been prepared by this technique.

1.6.3 Solid state method to amorphize crystalline material

Bombardment of crystalline materials with higher energy radiation of neutrons, charged particles etc, results in, transfer of kinetic energy from the particles to the interacting atoms, which produces temperatures of the order of thousands of degree centigrade for a short duration of 10^{-10}-10^{-11} s over a region of the order of ~10^4 atoms. This produces local melting followed by an ultrafast quenching. It has been demonstrated that quartz and cristobalite can be progressively amorphized by irradiation and their properties tend towards that of vitreous SiO_2 [70]. Also exposure of various ceramic materials to neutron beam (~$3x10^{20}$ n/cm^2) renders this material amorphous. The main advantage of this technique is the introduction of radioactivity in the sample. In addition to this, many other methods have been reported to produce amorphous materials which are specific for certain systems, such as high pressure shock waves, slow mechanical grinding, explosive compaction etc. It has also been observed that some intermetallic compounds can be made amorphous by hydrogen absorption [71-73].

1.6.4 Electrochemical method

Amorphous oxide layers of a metal can be grown on the surface of metal by using it as an anode in an electrolytic cell having a variety of aqueous electrolytes. When DC voltage is applied between the electrodes, the cations migrate towards the cathode and the anions, which include the O^{2-}, migrate towards the anode. At the anode, under sufficient over voltage, O^{2-} reacts with the metal producing the glassy layer of the oxide having thickness up to several thousands of angstroms. It has been demonstrated that glassy films of oxides of Al, Zr, Nb, Ta etc, can be easily prepared by this method [74].

1.6.5 Solution method: Sol-gel

Gel is an elastic solid matter produced abruptly from a viscous liquid by a process involving continuous polymerization. Gel, which is amorphous and homogeneous, is heated to remove volatile components and produce an initial densification, followed by a final process of sintering at appropriate temperatures to produce amorphous solid. For example amorphous SiO_2 can be prepared from alkoxy silanes, like $Si(OCH_3)_4$ or $Si(OC_2H_5)_n$. These alkoxides undergo polycondensation and hydrolysis, which on heating leads to progressive formation of metal oxides. The reaction can be schematically represented as:

$$M\,(OR)_n + nH_2O \rightarrow M\,(OH)_n + nR(OH) \tag{1.7}$$

$$pM\,(OH)_n \rightarrow pMO_{n/2} + pn/2\; H_2O \tag{1.8}$$

M can be elements like Si, Al, Ti, Zr etc. The resulting metal oxide produced is in the form of extremely small particles (~ 2 nm).

Advantage of sol-gel technique is that many refractory materials can be prepared homogeneously at a relatively lower temperature, especially below the melting point. Also the purity of the materials can be improved as the starting materials can be purified to the desired extent by various techniques [75]. Even though the process appears to be simple, the reactions are very sensitive to the external conditions like temperature, concentration of water, reaction time etc. The reaction conditions should be carefully controlled so that undesirable products having formula $(SiO)_x$ $(OH)_y$ $(OR)_z$ etc are avoided. Also it is difficult to get always the proper organic metallic precursors for more exotic cations. The processes of drying and sintering the gel are more complicated and the time consumed is relatively more than that for the other techniques.

Despite the wide diversity of techniques that can produce the amorphous/glassy state, melt quenching remains the most popular glass making technique. It is very important at the outset of a study of the amorphous state to notice that although many materials can be prepared in an amorphous form by more than one technique, the different forms need not, and often do not, have the same properties. As there is no unique structure for an amorphous solid (an infinite number of possible structures being in principle possible), and hence there is no reason that different preparative techniques produce materials with the same or similar structure. In addition, the various techniques differ in the degree to which their products depart from equilibrium, mainly as a result of the rate of (effective) cooling; vapour deposited material is therefore expected to be less near an equilibrium state than melt quenched material. This difference can be seen at two levels: macroscopic structural inhomogeneities (e.g. voids, density fluctuations) are more prevalent in vapour deposited material as compared to microscopic structural defects, such as broken bonds and vacancies. These can have dramatic effects on various properties, particularly electronic. A further important point to note about the preparation of amorphous solids is that, owing to non-reproducibility of the glass samples, even for the same preparative technique, there may be differences in the nature of the material produced unless great care and attention is paid to control the various experimental parameters.

1.7 Glass-Ceramics

Glass-ceramics are ceramic materials formed through the controlled crystallization of glass. In glass-ceramics, the crystalline phases are entirely produced by crystal growth from the homogeneous glass phase and this distinguishes these materials from traditional ceramics. As the name clearly indicates, glass-ceramics have combination of both glassy and crystalline phase. Processing of glass-ceramics is generally a simple regulated thermal process, where new exceptional characteristics are achieved by precipitating desired crystal phases in the base glass. In case of glass-ceramics, the nature and concentration of crystal phases can be varied and it is possible to tailor the properties of glass-ceramics to suits the end use in mind [76].

In general, glass-ceramics show favourable chemical, thermal, dielectric and biological properties superior to metals and various polymers [77]. These properties are listed in Table 1.1. Further, glass-ceramics are superior to normal glasses and conventional ceramics as well, especially with regard to tunable thermo-physical properties and microstructure.

Table 1.1: Favourable Properties of glass-ceramics.

Particularly Favourable Properties of Glass-Ceramics
Processing properties Rolling, casting, pressing, spin casting, press-and-blow method, drawing are possible Limited and controllable shrinkage No porosity in monolithic glass-ceramics
Thermal properties Expansion can be controlled as desired, depending on the temperature, with zero or even negative expansion being coefficients of thermal expansion possible High temperature stability
Optical properties Translucency or opacity Photo-induction is possible Pigmentation Opalescence, fluorescence
Chemical properties Restorability or high chemical durability
Biological properties Biocompatibility Bioactivity
Mechanical properties Machinability High strength and toughness
Electrical and Magnetic properties Isolation capabilities (low dielectric constant and loss, high resistivity and breakdown voltage) Ion conductivity and superconductivity Ferromagnetism

The first step toward realizing a glass-ceramic is the formation of the parent glass. A number of techniques for this such as melt quench, sol-gel, chemical vapor deposition etc, which have been discussed previously, may be employed for glass formation. Subsequently, the glass must be crystallized according to a carefully optimized heat treatment schedule. This critical phase in the production of glass-ceramics is optimized using a combination of differential thermal analysis (DTA)/differential scanning calorimetry (DSC) data and experimental heat treatments.

Glasses are melted, fabricated to shape, and thermally converted to a predominantly crystalline ceramic. The basis of controlled internal crystallization lies in efficient nucleation that allows the development of fine, randomly oriented grains generally without voids, micro-cracks, or other type of porosity. Glass-ceramics offer the possibility of combining the special properties of conventional sintered ceramics with the distinctive characteristics of glasses. It is, however, possible to develop modern glass-ceramic materials with features unknown thus far in either conventional ceramics or glasses or in other materials such as metals or organic polymers. Furthermore, developing glass-ceramics demonstrate the advantage of combining various remarkable properties in one material. Glass-ceramics demonstrating particularly favourable properties were developed on the basis of variation in the chemical composition and of the microstructure.

1.8 Crystallization of Glass

The suitability of a glass-ceramic to any particular application is decided by the nature and morphology of the crystalline phases formed. Transformation of a glass to a crystalline solid occurs by the formation of nuclei and their subsequent growth. Therefore, the processes of nucleation and crystallization in glasses are of particular importance. These two very critical steps in the formation of a glass-ceramics are dependent upon the composition of the base/parent glass, the nucleating agents added and the heat treatment schedule.

1.8.1 Nucleation

Nucleation is the process of the formation of stable nuclei (crystalline embryo of critical size) that may sustain further growth. Classically, a nucleus is an entity that belongs to a different phase but is in unstable equilibrium with respect to the supersaturated parent phase [78]. The two main mechanisms of nucleation are homogeneous and heterogeneous nucleation. In the process of homogeneous nucleation, a new phase develops in the absence of any foreign boundaries due to local fluctuations in the density and kinetic energy of the melt. Heterogeneous nucleation occurs at sites of low energy (heterogeneities) in the melt such as container walls, insoluble inclusions, and free surfaces. For the preparation of glass-ceramics, the most widely accepted mechanism is the heterogeneous nucleation, where nucleating agents are incorporated in the glass to initiate the growth of required phase.

1.8.1.1 Homogeneous nucleation

Theory of homogeneous nucleation in liquid is explained by Volmer and Maurer [79,80] and later on, the same has been reviewed by Jackson [81]. In the homogeneous nucleation there exist two barriers to the formation of a nucleus. First, the thermodynamic barrier involves the free energy change in a system when a nucleus is formed. The second, or kinetic, barrier is the result of the requirement that mass be moved or rearranged in space to allow the growth of an ordered particle (a crystal) from a disordered liquid. The overall process is described by the expression

$$I = Aexp[-(\Delta G^{*} + \Delta G_{D})/kT] \qquad (1.9)$$

where A is a constant, ΔG^{*} and ΔG_{D} are the thermodynamic and kinetic free energy barriers to nucleation, respectively, k is the Boltzmann constant, and T is the absolute temperature (K). In this case, ΔG^{*} is actually the work required to form a nucleus of critical size, i.e., one which will grow instead of redissolve into the melt. The pre-exponential constant A in Eq. (1.9) is given by

$$A = 2n_{v}V^{1/3}(kT/h)(\gamma/kT)^{1/2} \qquad (1.10)$$

where n_{v} is the number of formula units of the crystallizing component phase per unit volume of the melt, V is the volume per formula unit, γ the crystal-melt interfacial free energy per unit area, and h is Planck's constant. A is essentially constant over the temperature range of nucleation measurement and, to a good approximation, can be expressed by

$$A = n_{v}(kT/h) \qquad (1.11)$$

Assuming spherical nuclei of radius r with a solid-liquid interfacial energy, γ_{sl}, between the nucleus and the melt, the energy changes that accompany their formation are volume free energy and surface free energy given as follows:

$$\text{Volume free energy} = -\frac{4}{3}\pi r^{3}\Delta G_{v}$$

$$\text{Surface free energy} = 4\pi r^{2}\gamma_{sl}$$

The net free-energy change (denoted by ΔG) resulting from the formation of a nucleus is given by the sum of these terms as:

$$\Delta G = -\frac{4}{3}\,\pi r^2 \Delta G_v + \, 4\pi r^2 \gamma_{sl} \tag{1.12}$$

The functional dependence of ΔG on r is given in Figure 1.8. Since the energy needed for the creation of new surfaces has r^2 dependence whereas the volume energy term scales with r^3, this function clearly goes through a maximum at a critical radius r_c, which implies that the formation of small clusters with $r < r_c$ locally increases the free energy of the system. Differentiating Eq. (1.12), equating to zero, and solving for r_c gives

$$r_c = 2\gamma_{sl}/\Delta G_v \tag{1.13}$$

which yields the height of energy barrier ΔG_c(Figure 1.8)

$$\Delta G_c = \frac{16\,\pi\,\gamma_{sl}^3}{3\Delta\,G_v^2} \tag{1.14}$$

Small clusters with $r < r_c$, are called embryos and are more likely to redissolve than grow. Occasionally, however, an embryo becomes large enough ($r \approx r_c$) and is then called a nucleus with an equal probability of growing or decaying.

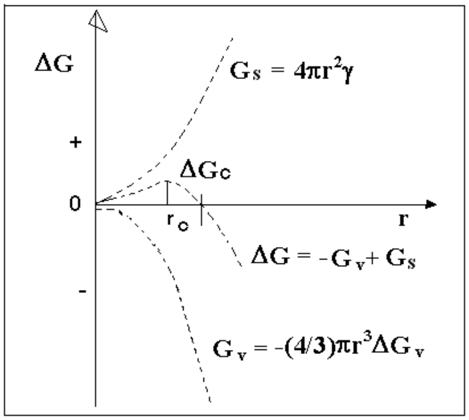

Figure 1.8: Free energy versus embryo radius for a given $T < T_m$. Note that ΔG_c goes through a maximum at $r = r_c$.

Kinetic barrier of nucleation, ΔG_D can be explained in terms of an effective diffusion coefficient, D, which is given

$$D = (kT\lambda^2/h)exp(-\Delta G_D/kT) \tag{1.15}$$

Where λ is the atomic jump distance, D is also related to the viscosity, η, of the melt *via* the Stokes-Einstein relation

$$D = \frac{kT}{3\pi\lambda\eta} \tag{1.16}$$

Using the relations given by Eq. (1.15) and (1.16), and substituting into our original expression, Eq. (1.9), we obtain the expression

$$I = (Ah/3\pi\lambda^3\eta)exp(\Delta G^*/kT) \tag{1.17}$$

If we further substitute the simplified expression for A, as given by Eq. (1.11), into Eq. (1.17), we can also write this expression as

$$I = (n_v kT/3\pi\lambda^3\eta)exp(\Delta G^*/kT) \tag{1.18}$$

1.8.1.2 Heterogeneous nucleation

Technologically, the vast majority of nucleation occurs heterogeneously at defects such as dislocations, interfaces, pores, grain boundaries, and especially free surfaces. These heterogeneities, present preferred nucleation sites for three reasons. First, they are regions of higher free energy, and that excess energy becomes available to the system upon nucleation. Second, and more importantly, the heterogeneities tend to reduce γ_{sl}, which allows nucleation to occur at relatively small supercoolings, where homogeneous nucleation is unlikely. Third, the presence of pores or free surfaces will reduce any strain energy contribution that may suppress the nucleation or growth process. According to James [82] the steady-state heterogeneous rate of nucleation of a supercooled liquid on a flat substrate can be given by

$$I_{het} = A_{het} exp[-(\Delta G_{het} + \Delta G_D)/kT] \tag{1.19}$$

where the subscript 'het' refers to values for heterogeneous nucleation. Activation energy of heterogeneous nucleation (ΔG^*_{het}) is a function of the angle of contact (θ) between the crystal nucleus [83,84] and the substrate and can be expressed as

$$\Delta G^*_{het} = \Delta G^* f(\theta) \tag{1.20}$$

The term $f(\theta)$ is given by

$$f(\theta) = \frac{(2 + \cos\theta)(1 - \cos\theta)^2}{4} \tag{1.21}$$

for any contact angle (θ) less than 180° as shown in Figure 1.9, the free energy barrier is less for nucleus formation on the surface of the heterogeneity than for homogenous nucleation. As a result, heterogeneous nucleation will occur wherever possible in preference to homogeneous nucleation.

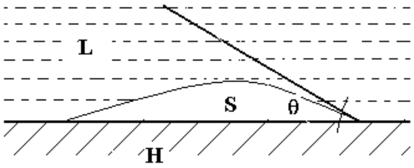

Figure 1.9: Model for heterogeneous nucleation.

(L: liquid phase, H: substrate/catalyst, S: nucleus, θ: contact angle)

1.8.2 Crystal growth

Once the nuclei are formed, they will tend to grow until they start to impinge upon each other. The growth of the crystals depends on the nature of the growing interface which has been related to the entropy of fusion. Surface tension is less important for growth because the surface energy barrier to form r_c is already overcome thus the rate of the crystal growth depends on the rate of arrival of the atoms at the surface of the nucleus. The growth is normal growth where all atoms arriving at the crystal-liquid interface form a part of the crystal. This process is feasible when the interface is rough on an atomic scale. If the interface is smooth on the atomic level then each layer has to be nucleated separately and this is called surface nucleation growth. In the normal growth model the rate of the crystal growth (u) can be derived as follows [85]:

Consider atoms jumping back and forth across the liquid/solid interface and ν, is the atomic jump frequency, then, energy needed to jump from liquid (l) to solid (s) can be given as,

$$\nu_{ls} = \nu \exp\left(-\frac{\Delta \mathrm{G_d}}{kT}\right) \tag{1.22}$$

where $\Delta \mathrm{G_d}$ is the activation energy for diffusion.

Similarly, energy needed to jump back from solid (s) to liquid (l) is expressed as,

$$\nu_{sl} = \nu \exp\left(\frac{-\Delta \mathrm{G_d} - \Delta G}{kT}\right) \tag{1.23}$$

where ΔG is the thermodynamic energy balance. This extra energy needed to jump back. Then the net crystal growth rate ‘u’ defined as $u = a_0(\nu_{ls} - \nu_{sl})$ where, a_0 is interatomic distance, can be expressed as

$$u = a_0 \nu \, exp\left(-\frac{\Delta \mathrm{G_d}}{kT}\right) \left[1 - \, exp\left(-\frac{\Delta G}{kT}\right)\right] \tag{1.24}$$

Again, considering the Stokes–Einstein equation for diffusion growth rate can be expressed as:

$$u = \frac{kT}{3\pi a_0^2 \eta}\left[1 - \, exp\left(-\frac{\Delta G}{kT}\right)\right] \tag{1.25}$$

Temperature and time are the two important process variables for nucleation and subsequent growth in the glass melt. The rate of nucleation and growth as a function of temperature and time is shown in Figure 1.10.

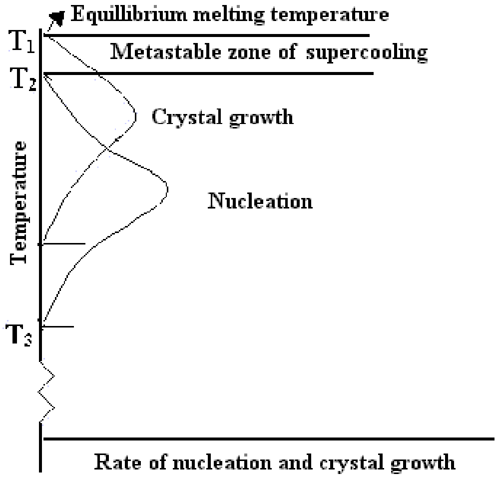

Figure 1.10: Effect of temperature on the rates of nucleation and crystal growth for a glass forming melt.

1.8.3 Time-temperature-transformation (TTT) diagram

In foregoing discussion, nucleation and crystal growth have been treated independently however, in reality these two processes occur simultaneously during cooling of a melt. Therefore, it is easier to find out the over-all transformation rate of nucleation and growth than to measure the isolated rate of nucleation and crystallization process. According to Johnson-Mehl-Avrami overall transformation can be expressed as,

$$\alpha = \frac{V_X}{V} = 1 - exp(kt)^n \qquad (1.26)$$

Here α is the volume fraction of a melt that has crystallized under isothermal conditions; k is the rate constant and 'n' is a constant whose value depends on nature of nucleation and growth.

Under isothermal conditions Eq. (1.26) can be simplified to the form.

$$\alpha = 1 - \exp\left(-\frac{\pi}{3} I u^3 t^4\right) \tag{1.27}$$

where t is the time the sample has been held at the experimental temperature, I and u are rate of nucleation and crystal growth respectively.

Given the nucleation and growth rates at any given temperature, the fraction crystallized can be calculated as a function of time from Eq. (1.27). Repeating the process for other temperatures and joining the loci of points having the same volume fraction transformed yield the familiar time temperature transformation (TTT) diagram, shown schematically in Figure 1.11. From TTT diagram, an estimate of the critical cooling rate (CCR) is given by [86]

$$CCR \approx \frac{T_L - T_n}{t_n} \tag{1.28}$$

where T_L is the temperature of the melt and T_n and t_n are the temperature and time corresponding to the nose of the TTT curve, respectively.

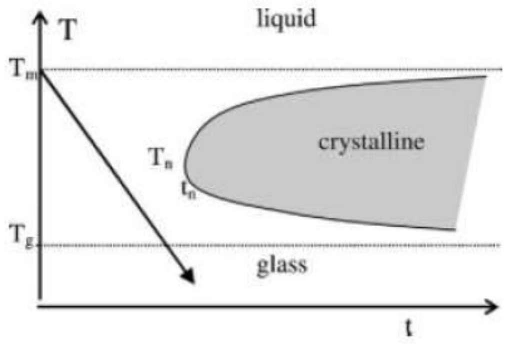

Figure 1.11: A time-temperature-transformation curve for a glass forming melt.

1.9 Scope of the Present Work

In the present work, detailed thermo-physical and structural studies were carried out on phosphate and silicate glasses and glass-ceramics. Silicate glasses and glass-ceramics in the strontium zinc silicate (SZS) and barium zinc silicate (BZS) systems, having potential application as high temperature sealants for planar solid oxide fuel cells (p-SOFCs), have been studied. Phosphate glasses belonging to sodium aluminium titano-phosphate (NATP) system having application in low temperature glass-to-metal sealing and optoelectronic devices are investigated. All the glasses were prepared by melt quench technique and silicate based glasses were converted into glass-ceramics by controlled crystallization.

Detailed information about different types of structural units of P and Si, present in these glasses, was obtained from Raman, Fourier transform Infrared (FTIR) and magic angle spinning nuclear magnetic resonance (MAS-NMR) spectroscopy techniques. The thermo-physical properties like TEC, density, micro-hardness (MH), optical gap have been measured for some of the representative glasses and an attempt has been made to correlate these properties with structural features of these glasses.

In NATP glasses effect of TiO_2 addition on various thermo-physical properties have been studied. Initially T_g, density (ρ) and MH increased, and molar volume, TEC decreased up to 10 mol% TiO_2 incorporation and beyond 10 mol%, a reverse trend in these properties was observed. MAS-NMR, Raman and FTIR spectroscopic studies revealed that substitution of P_2O_5 with TiO_2 up to 10 mol% depolymerizes the phosphate glass network by a systematic conversion of Q^2 structural units into Q^1. For addition of TiO_2 above 10 mol%, Q^1 structural units get converted into Q^0 structural units leading to a Ti-O-Ti/Al based network linked with discrete PO_4 structural units. Observed variation in thermo-physical and optical properties of

NATP glasses was found to be consistent with the structural changes in the NATP glass due to TiO_2 incorporation. Studies also revealed a change in the role of TiO_2 and Al_2O_3 in NATP glasses from network modifier to network former with a change in the composition as TiO_2 substitutes the P_2O_5. In the long-term, NATP glasses were found to be more resistive for moisture attack compared to NAP glasses, as they have P-O-Ti/Al linkages in place of P-O-P linkages. This development of phosphate glass compositions with higher a chemical durability is beneficial to use their unique properties in various fields of technology especially in sealing and optoelectronic devices.

New glass-ceramics in the SZS system have been studied for high temperature sealant application. Crystallization and microstructural studies revealed that in the SZS glass, the phase separated into SiO_2 and ZnO rich regions by a spinodal decomposition mechanism prior to the crystallization. $Sr_3Si_3O_9$ and $Sr_2ZnSi_2O_7$ phases crystallized in these regions upon further heat treatment, respectively. Based on the crystallization kinetics it is inferred that diffusion controlled bulk crystallization with 2-3 dimensional growth occurs for the SZS glass. Raman spectroscopy and XRD together confirm that during an early stage of crystallization, $Sr_2ZnSi_2O_7$ phase and later $Sr_3Si_3O_9$ phase formed in the SZS glass-ceramics. Investigated SZS glasses/glass-ceramics have shown requisite thermo-physical properties like TEC, glass softening (T_{ds}), MH etc., for their use as high temperature sealants in the SOFC. Upon further optimization of the composition of SZS glasses using various additives, it is found that B_2O_3 and V_2O_5 allow better bonding of glasses with SOFC components. In an interesting result Raman spectroscopy revealed the 3 member ring type structure for the $SrSiO_3/Sr_3Si_3O_9$ phase. In accordance with XRD, NMR results also suggest the formation of a solid-solution of $Sr_2ZnSi_2O_7$ phase with substitution of Zn/Si tetrahedral sites with B/Al.

Similarly BZS glasses and glass-ceramics have also shown adequate thermo-physical properties like TEC, T_{ds}, ρ, MH etc, for their application as SOFC sealants. Crystallization kinetics of BZS glasses also revealed a diffusion controlled bulk crystallization with two dimensional growth of crystals from a varying number of nuclei. With the addition of additives, a surface crystallization mechanism starts dominating over the bulk crystallization and activation energy decreases. This information is useful to develop or optimize suitable glass-ceramics sealants and sealing procedure. Crystalline phases having high TEC are formed in these glass-ceramics therefore; resultant glass-ceramic sealants have a consistent TEC for the long-term durability as a sealant.

Thus, in the present investigation, both phosphate and silicate based oxide glasses/glass-ceramics were investigated for their thermo-physical and structural properties. The studies carried out so far demonstrate that SZS and BZS glass-ceramics have potential to be used as a high temperature sealant. Studies also revealed the importance of structural and thermo-physical characterization in optimizing properties of glasses and glass-ceramics for their intended application.

Chapter 2

Experimental Techniques and Procedures

A brief overview of the experimental techniques that have been employed for the preparation and characterization of different types of glasses and glass-ceramics are discussed in this chapter. The relevant theories and working principles are also described. First preparation of glasses and their subsequent conversion to glass-ceramics followed by methods used to characterize them have been described.

Thermal properties have been studied using thermo-mechanical analyzer (TMA) and DTA instruments and mechanical properties using micro-hardness tester. Some optical properties of a few glasses were also measured using absorption and luminescence spectrometers. The structural characterization of glasses and glass-ceramics was carried out using Raman, FTIR and NMR spectroscopies. These techniques have been discussed in brief and relevant references have been cited for detailed description.

2.1 Glass Preparation

All the glass samples in the present work were prepared by melt-quench technique. To obtain homogeneous, transparent and inclusions/bubbles free glasses, a three-step procedure (calcination, melt quenching, annealing) was used and described in the following section. Specific details of the method of preparation for different glass samples are given in the relevant chapters.

2.1.1 Calcination

Starting batches were prepared by weighing calculated amounts of initial precursors based on the composition of the glass. Analytical grade reagents in the form of oxides, phosphates, nitrates or carbonates procured from M/s MERCK, India, M/s MERCK, Germany, M/s S. D. Fine Chem Ltd., India and M/s Loba Chemie, India were used as starting precursors. Phosphates, carbonates and nitrates decompose to oxides according to following reactions:

$$2NH_4H_2PO_4 \rightarrow P_2O_5 + 3H_2O + 2NH_3 \uparrow \qquad (2.1)$$

$$Sr(NO_3)_2 \rightarrow SrO + 2NO_2 \uparrow \qquad (2.2)$$

$$BaCO_3 \rightarrow BaO + CO_2 \uparrow \qquad (2.3)$$

The charge (~50 to 100 g batch) was thoroughly mixed and ground for 20-30 min in a mortar pestle or planetary ball mill (PM 4000 model Retsch, Germany) at a speed of about 300 rpm. This thoroughly mixed charge was taken in an alumina or platinum crucible, depending on the nature of the constituent precursors, for the calcination process.

Calcination is a process to convert precursors into their respective oxides. A few calcination reactions to obtain oxides from different precursors are illustrated in reactions 2.1 to 2.3. The calcination was carried out in a resistance heating furnace having a programmable PID temperature controller (Libratherm 300 series) with a temperature accuracy of ± 0.5°C. An exhaust system is connected to the furnace for removing gases like NO_2, NH_3 during calcination. For calcination, charge was heated in a furnace at a controlled rate (1-3°C/min) to respective decomposition temperatures of various precursors. A dwell time (4-12 h) was provided at each decomposition temperature to allow a complete calcination. After the calcination, measurement of weight loss ascertained a proper decomposition of the precursors. If weight loss was less than expected, indicating an incomplete conversion of the precursors to oxides, then the charge was reground and re-calcined in the same manner.

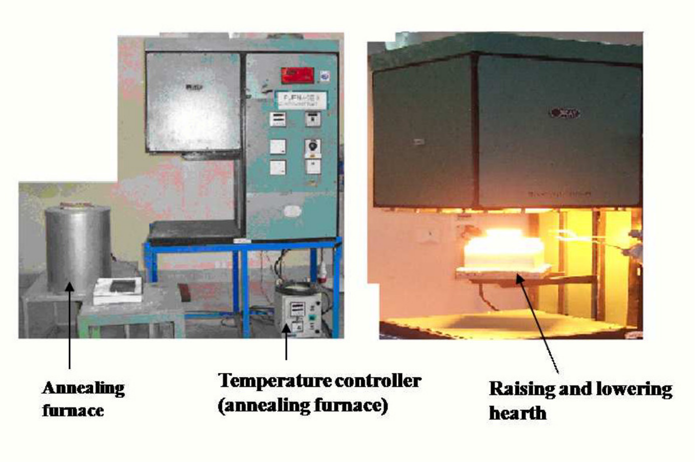

Figure 2.1: Raising and lowering hearth glass melting furnace.

2.1.2 Melt quenching

The calcined charge was melted in a Pt-10%Rh crucible using lowering and raising hearth furnace (Model OKAY 70R 10, M/s Bysakh and Co., Kolkata) (Figure 2.1). To prevent the volatilization of precursors, the crucible was covered with a Pt-10%Rh lid. The glass charges were melted in an air ambient, at temperatures ranging from 1250°C to 1650°C depending on the composition. The melting temperature of glass is decided such that melt viscosity at this temperature is low enough to allow easy pouring. The glass melt was held for 1-2 h, for thorough mixing and homogenization. When the glass melt was thoroughly homogenized and attained a desirable viscosity, it was poured into preheated graphite moulds to obtain glass in the bulk form. In some cases, the glass melt was poured in distilled water to form glass frit.

2.1.3 Annealing

As quenched glasses generally have thermal stresses due to the thermal shock during the quenching process. Therefore, annealing is necessary to relieve the thermal stresses in the melt quenched glasses. Generally annealing is carried out at in the vicinity of T_g (generally 10-20°C below T_g) to allow a rapid removal of thermal stresses. In an annealing procedure, the glass is held at a constant temperature for some time period (usually 1-5 h) and cooled to room temperature at a slower rate. In the present work glasses were annealed in an annealing furnace, in which temperature is control precisely by a PID temperature controller. For annealing, the melt quenched glasses in graphite moulds were immediately transferred to the preheated annealing furnace. Annealing was carried out at temperature close to T_g, for 3-5 h depending upon the glass composition, under flowing N_2 or Ar to prevent oxidation of graphite moulds. The annealed glasses were then cooled to room temperature at the rate of 20°C/ h, to relieve the thermal stresses, generated during quenching.

2.1.4 Glass-ceramic formation

Glass-ceramics are fine grained polycrystalline materials formed when glasses of suitable compositions are crystallized in controlled manner. They consist of high density of small crystals in a glassy matrix. As discussed in the previous chapter to achieve a fine grained microstructure of glass-ceramics, heat treatment procedures for the crystallization of glasses must be optimized and carefully controlled. The thermal characterization that is essential for finding crystallization and nucleation temperature is described separately for completeness. For the base glass, initial thermal parameters were obtained using the DTA. These then served as guidelines for an optimum heat treatment. Glasses to be crystallized were heated up to the crystallization temperature, in an air ambient, at the rate of 1-3°C/min depending upon the composition of glass. The samples were held at this temperature for 1-2 h and then cooled to room temperature at a rate of 1-2°C/min, to yield the glass-ceramics. The exact crystallization schedules for different prepared glass samples are described in the relevant chapters.

2.1.5 Glass/Glass-ceramic processing

Prepared glasses and glass-ceramics were processed to make samples for use in different characterization techniques. They were cut in desired shapes and then polished to get appropriate surface finish. For the cutting process, annealed glass rods were mounted in an aluminium fixture using wax and then cutting was done using diamond wheels on a Buehler ISOMET 4000 linear precision saw. Subsequently, lapping and polishing of the samples were done. Lapping is the removal of material using silicon carbide powder of various grit sizes (200-800 mesh) to produce smooth, flat, rough polished surface. The final polishing was done using alumina powder to obtain mirror finish for optical and micro-hardness measurements.

2.2 Thermo-Physical Characterization

2.2.1 Density

Density (ρ) of glass and glass-ceramic samples was measured using Archimedes principle. Measurement of weight loss of the sample upon immersion in a suitable liquid allows estimation of the density according to the following formula:

$$\rho = \rho_l \frac{W_a}{(W_a - W_l)} \tag{2.4}$$

where W_a and W_l are sample's weights in air and liquids, respectively. The parameter ρ_l is the density of the immersion liquid. Therefore, $(W_a - W_l)$ is the weight loss of the sample upon suspension in the liquid. The choice of immersion liquid is based on convenience and the chemical durability of samples. Water is usually used wherever possible, but toluene or other similar organic liquids are used for samples that react with water. In glasses, the density is an additive property and the density of the glass is the weighted average of the densities of individual components. Crystallization of a glass can significantly alter the density, when the density of the crystalline phase is very different from that of the residual glass. In glass-ceramics, the type of crystalline phases and the relative amounts of glassy and crystalline phases significantly affect the density. The molar volume V_m of the glass samples can be calculated from the following relation:

$$V_m = \frac{M.W.}{\rho} \tag{2.5}$$

where $M.W.$ is the molecular weight of the glass sample. In the present work the reported density values are the average of at least three independently measured values.

2.2.2 Hardness

Hardness is the resistance of a material to permanent deformation under contact loading. The hardness of the glasses is a function of the strength of individual bonds and the density of the packing of atoms in the structure. The most common technique for hardness measurement is micro-hardness (MH) indentation technique. The MH is also called diamond indentation hardness. This technique involves forcing a diamond indenter of specified geometry into the surface of test specimen at loads (forces) ranging from 1-1000 gf. "Force" is the technically correct term however, load is commonly used.

In Vickers micro-hardness (VMH) measurements a diamond indenter tool having the shape of square based pyramid with a peak angle of 136° is used for hardness testing [87]. If the indenter is elongated rhombus pyramid shaped diamond, with angles of 172.5° and 130° at the peak, then the measured hardness is called Knoop hardness [88]. The indents produced on the sample surface are generally observed using an optical microscope. A Vickers micro-hardness tester and typical Vickers indent are shown in Figure 2.2.

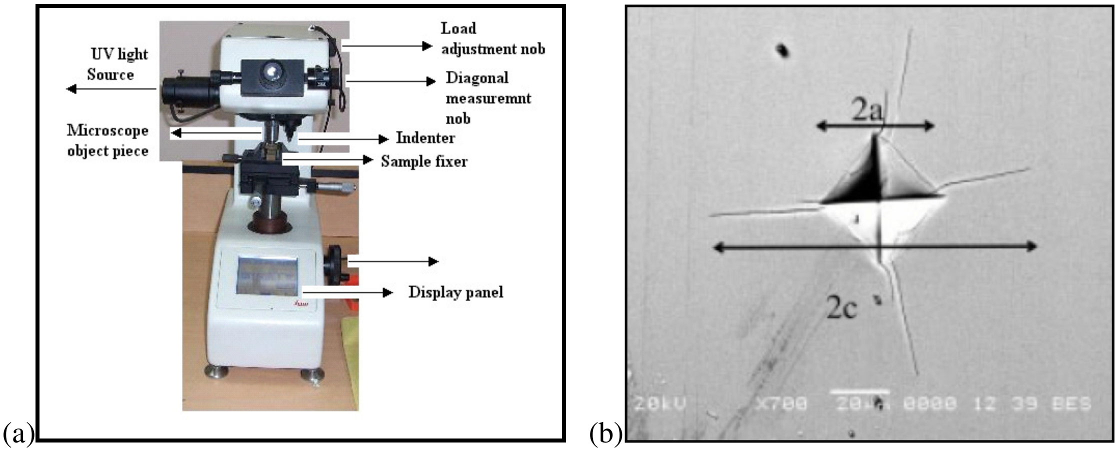

Figure 2.2: (a) Photograph of Vickers micro-hardness tester and (b) Vickers indent showing the diagonals and the presence of cracking.

The hardness (H) is then defined as the ratio of the applied load to the projected area of the indenter.

$$H = \frac{F}{A_p} \tag{2.6}$$

For a Vickers indenter, VMH is given by the following expression:

$$VMH = \frac{2F\sin\frac{\theta}{2}}{d^2} = \frac{1.8544F}{d^2} \tag{2.7}$$

where *F* is the load in Newton, and *d* is the length of diagonal line in mm.

When an indentation is made in a glass, initially the glass is elastically compressed (by the hydrostatic component) and sheared (by the shear component). Next, after reaching the elastic limit, the balance of the hydrostatic stress component permanently densifies the glass under the indentation, whereas the balance of the shear stress component causes the glass to undergo plastic deformation [87,89]. When the indenter is withdrawn, the elastic portion recovers, *i.e*., a slight shrinkage of the impression size is expected. Clearly, the hardness number cannot be independent of the applied load. Also, when large loads are used, cracking from the diagonals is likely to develop. The cracking implies the occurrence of a fracture. Vickers micro-hardness tester (Leica model VMHT30M) was used for the measurement of micro-hardness of the glass/glass-ceramics, in the present study. Mirror polished surface of the sample to be indented was used for the measurement. The loads were then applied in the range of 50-100 g with a dwell time of 5-10 s in all cases, taking care to prevent cracking. Eq. (2.7) was then used to obtain the micro-hardness from the length of the diagonals of the indent. The MH values reported in this thesis are the average values of at least 10 independent indents made on each sample under identical loading conditions.

2.2.3 Thermo-mechanical analysis

Thermo-mechanical analysis is an important technique in the materials science especially for glasses and glass-ceramics to measure the mechanical properties like TEC, T_g and glass softening temperature (T_{ds}) of the sample when it is subjected to temperature regime. A dilatometer allows for the continuous measurement of the length of a given specimen which increases continuously with temperature at a constant heating rate. It is generally in the range 1-50°C/min. It has to be controlled carefully since the T_g depends on the thermal history. The expansion of the specimen is monitored by a stylus/pushrod that contacts the specimen under a small force. Note that only the difference between the expansion of the specimen and the cylindrical support is determined. Therefore, correction of the data has to be made to allow for the expansion of the instrument itself.

In the present investigation, we have used a Setaram TMA instrument (Model: TMA-92 and Setsys) (Figure 2.3). It has a fused quartz sample holder and a silica probe for use up to 1000°C. For higher temperatures, alumina pushrod is used. A schematic diagram of the sample holder and the position of the chromel-alumel (K-type) thermocouple, used to measure sample temperature, are shown in the inset of Figure 2.3. Additional Pt-Rh (R-type) thermocouple is placed inside the furnace to record the furnace temperature. The temperature of the sample and furnace is measured within the accuracy of ±0.1°C, using a PID temperature controller.

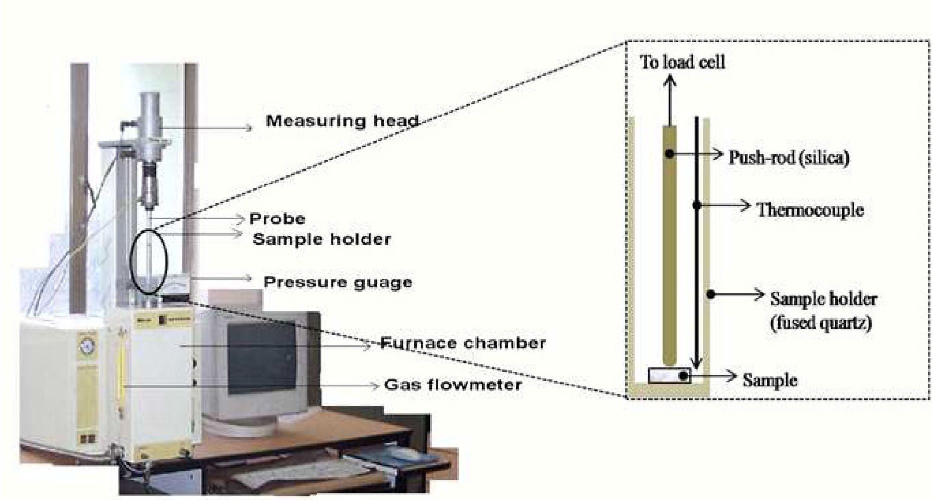

Figure 2.3: Photograph of thermo-mechanical analyzer.

The change in the length can be measured within the range of –2000 to +2000μm. Before starting an experiment the system was calibrated using a standard SS-446 alloys whose expansion is known. The samples used are less than 10 mm in diameter and 20 mm in length. The ends of the samples were ensured to be flat for a perfect contact with the probe. The heating rate was kept the same (10°C/min) for all the measurements. Before starting the experiment the system was evacuated up to 10^{-2} mbar pressure and the chamber was flushed with high purity (IOLAR grade) Ar gas. All the measurements were carried out in flowing Ar atmosphere with a constant flow rate of 4-5 l/h. When the sample is heated it expands and pushes the sample holder and the push rod. This movement is sensed by a linear variable displacement transducer (LVDT) located in the measuring head of the instrument (Figure 2.3). As mentioned earlier, provision was made for correcting the expansion of the instrument itself.

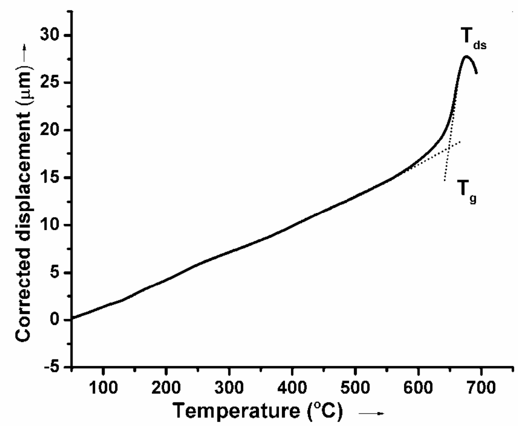

Figure 2.4: Thermal expansion curve for glass showing T_g and T_{ds}.

Figure 2.4 shows a typical TMA curve for a strontium zinc silicate glass. The T_g can be determined at the intersecting point of the tangents of Figure 2.4. In the linear domain the slope of the curve allows to determine the TEC of the solid glass, that is, the relative expansion per temperature unit:

$$\alpha_L = \frac{1}{L}\frac{dL}{dT} \tag{2.8}$$

where L is the sample length and T is the temperature. An increase in the slope after a transition indicates that the thermal expansion of the liquid is larger than that of the glass. From the curve shown in Figure 2.4, the liquid thermal expansion is estimated to be about three to four times larger than that of the solid. However, care has to be taken with the values obtained from dilatometry for $T > T_g$, since expansion is measured by a contacting push-rod which progressively penetrates into the viscous liquid and thermal expansion is underestimated. Further penetration of the push-rod explains the end and maximum of the curve. In fact, when viscosity falls to about 10^{10}–10^{11} Pa.s, the glass becomes so soft that it no longer behaves as a rigid specimen. Depending upon the composition of the samples, the TEC of the glasses may increase or decrease.

2.2.4 Differential thermal analysis

The DTA is the most popular technique to measure a range of thermal events including melting, crystallization, glass transitions and decomposition reactions. Merits of the DTA include small sample size, a wide temperature range of measurement, simple operation, and rapid measurement. The DTA measures the difference in the temperature of the sample (S) and the reference (R) when they are heated or cooled at the same rate under identical conditions [Figure 2.5 (a)]. This differential temperature 'ΔT' is then plotted against time or temperature as shown in Figure 2.5 (b). Chemical, physical, structural and microstructural changes in the sample lead to the absorption (endothermic event) or evolution (exothermic event) of heat relative to R. This reflects in the DTA plot. It gives the information about change in enthalpy and can also be plotted against ΔH. The baseline of the DTA curve exhibits discontinuities at transition temperatures and the slope of the curve at any point gives the information about the physical or chemical changes that are occurring in the sample.

The sample environment consists of a ceramic (or metallic) block, to ensure uniform heat distribution, specimen crucibles and thermocouples (for the sample and reference). Metallic blocks are less likely to cause baseline drifts compared with porous ceramics, but the DTA signal is smaller, due to the higher thermal conductivity of metals. Different types of crucibles i.e. graphite, alumina, Pyrex, silica, and platinum are used depending upon the temperature range and purpose of the experiment.

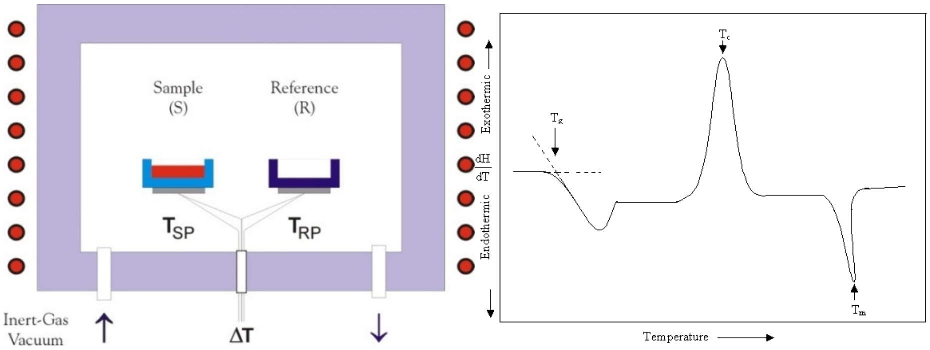

Figure 2.5: (a) Schematic of a DTA cell and (b) a typical DTA curve of a glass.

In our investigation, the DTA measurement was carried out on TG-DTA system (model Labsys and TG-DTA-92 of M/s Setaram, France) with about 40-50 mg of powdered sample (particle size in between 75-210 μm) in a 100μl Pt crucible. The measurements were done at heating rates of 5-30 K/min in flowing Ar atmosphere using an empty Pt crucible as reference. The chamber was initially pumped to 10^{-2} mbar and then flushed by Ar gas, for about 15 min, before starting the experiment. Sample was heated up to different temperatures depending on the type of system under investigation. Based on the non-isothermal DTA measurements, techniques such as Ozawa method [90], Kissinger method [91], Matusita-Sakka methods [92] can be used to study the kinetics of crystallization and to estimate the activation energy for crystallization process.

2.3 Structural Characterization

2.3.1 X-ray diffraction

XRD is an indispensable tool for the material characterization. It is a non-destructive technique and widely used in phase identification and structure delineation for diversified materials from crystalline to amorphous states. The technique is normally useful to collect the data under ambient conditions, but in-situ diffraction as a function of external constraints, such as, temperature, pressure, stress, electric field, atmosphere, etc. is also important for the interpretation of solid-state transformations and material behaviour. The fundamentals of the XRD of crystals are described in various solid state physics books [93,94]. In this section only an overview of the XRD technique in terms of its utility to present work is given.

The principle of XRD technique is based on scattering of X-rays by a crystal consisting of well-defined array of atoms, ions and molecules. Since the crystal lattice consists of parallel arrays of atoms equivalent to the parallel lines of the diffraction grating, the inter-planar spacing could be successfully determined, from the separations of bright fringes of the diffraction pattern. These inter-planar distances are of the same magnitude as the wavelength of X-rays (0.5 to 2 Å) and hence, crystal planes act as diffraction gratings. Interaction of X-rays reflected by a set of parallel planes satisfying Bragg's condition lead to constructive interference only at a particular angle. The Bragg condition/equation for the occurrence of such diffraction can be written as:

$$n\lambda = 2d \sin\theta \tag{2.9}$$

where λ is the wavelength of X-rays, θ is glancing angle, d is the inter planar distance and n is order of diffraction.

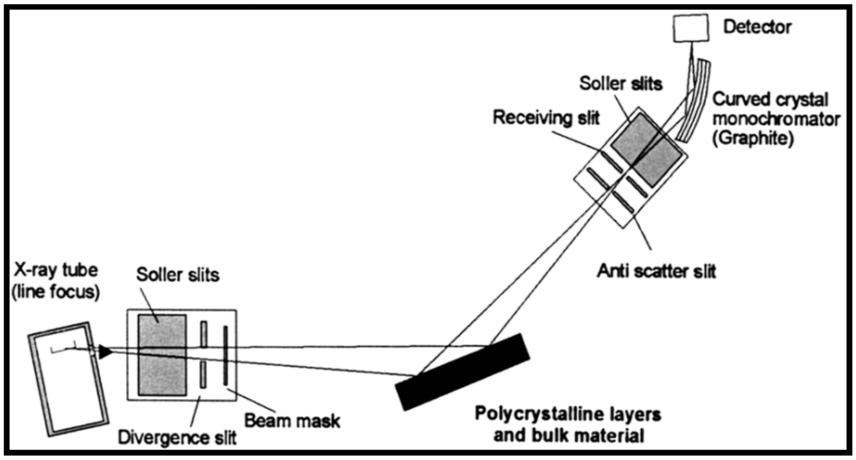

Figure 2.6: A block ray diagram of a typical reflection mode powder diffractometer.

The XRD experiments can be carried out either from single crystals or from polycrystalline samples. The former type samples are studied by Laue method, Weissenberg photograph methods, or most commonly with automated four-circle diffractometer. The later types of samples are studied either by Debye-Scherrer photographic method or by a powder diffractometer [95]. The Powder diffraction method is used for qualitative and quantitative phase identification, refinement of structure solutions of crystalline materials and also for determination of particle size and strain in materials. Powders can be the aggregation of the fine grains with single structure, and each of the fine grains is randomly oriented. A typical block ray diagram of a powder diffractometer is shown in the Figure 2.6. In powder XRD, powdered sample either as smeared layer or compact flat pack or in a capillary is exposed to monochromatic beam of X-ray and the diffracted beam intensity is collected in a range of angles (2θ with respect to the incident beam). For crystalline material, the intensity corresponding to a constructive interference of the diffracted beam from crystallographic plane is observed as a peak corresponding to the Bragg angle (θ). In all other angles, a background is obtained. Therefore, crystalline materials (like glass-ceramics) are characterized by sharp peaks in their diffraction pattern. Unlike this, diffraction pattern of glasses is characterized by a broad hump/halo. This is because glasses have short range order rather than long range periodicity and there is considerable distribution of bond length and bond angles between the constituent atoms.

In the present study, powder XRD was used to verify the amorphous nature of the glasses and identify the crystalline phases in the glass-ceramics [96]. The diffractograms of all the samples were recorded either on Philips PW1710 or Rigaku D-4000, Japan diffractometer based on the Bragg-Brentano reflection geometry. Data were collected using Ni filtered Cu-K_α (1.54 Å) radiation in the $10° \leq 2\theta \leq 70°$ range at a scanning speed of 1°/min for glasses and 0.5°/min for glass-ceramics. The observed diffraction patterns were compared with JCPDS (Joint Committee on Powder Diffraction Standards) files available for reported crystalline samples.

2.3.2 Scanning electron microscopy

The scanning electron microscopy (SEM) is a versatile electron microscopic technique that provide at one end surface information viz. texture, topography etc. up to a length scale of few tens of nanometers and on the other hand provides a three dimensional effect to the images due to depth of focus of the SEM instruments. The electron microscopy provides image of a sample at much higher magnification, higher resolution and depth of focus compared to optical microscopy due to very low wavelength of accelerated electrons. Two types of interactions occur in the SEM between the electron beam and the specimen. These interactions may be either elastic, if the electron beam strikes the sample and there is a change in its direction without change in its energy (backscattered electrons), or on inelastic interaction, which occurs when the beam of electrons strike an orbiting shell electron of the specimen, causing the ejection of secondary electrons, characteristic photon radiation (x-ray and visible radiation), and other types of events from the specimen interaction volume. The backscattered electrons allow element distribution analysis since the intensity of scattering is Z (atomic number) dependent. The secondary electrons on the other hand are liberated from a very small volume in the vicinity of the surface and as a result the secondary electrons can be used to study the surface of samples. These interactions reveal important information about the specimen to determine the surface characteristics and the chemical nature of the specimen.

Figure 2.7 shows the schematic of a typical SEM instrument. In this instrument, a well-focused mono-energetic (~25keV) electron beam is incident and scanned over the sample surface by two pairs of electro-magnetic deflection coils. The signals generated from the surface of the specimen by secondary electrons (SE) and back scattered electrons (BSE) are detected and fed to a synchronously scanned cathode ray tube (CRT) as intensity modulating signals [97,98]. Thus, the specimen image is displayed on the CRT screen. X-ray mode facilities are also present in some SEM, to get qualitative information about the elements present in the probed area. SEM instrument is generally operated in three prominent modes namely secondary electron mode, backscattered electron mode and X-ray radiation mode. In secondary electron (SE) mode, scintillator photomultiplier is used as the detector. In this mode energies of secondary electrons are quite low so the signal results from a depth of approximately 100Å (escape depth of SE) from the sample surface with a resolution of 50Å. Its strength depends on the beam size, beam current, angle of incidence, the topography and the atomic number of the sample. Images obtained in the SE mode show extremely high edge definition and emphasize the small details on the surface of the samples. In backscattered electron (BSE) mode also a scintillator photomultiplier is used as a detector but the escape depth is comparatively large (1000Å) because of the large energy of the back scattered electrons. The very high energy of the back scattered electron permits a resolution of ~200Å. However, the BSE method gives contrast even in flat samples due to compositional distribution. BSE images can give important information about the spatial relationships of adjacent phases, plus about zoning and inclusions within the phases. BSE intensity is, to a first approximation, a function of the chemical composition, the brighter an area, the greater the mean atomic number of that area relative to adjacent areas.

In X-ray radiation mode**,** the X-rays produced due to interaction of the electron beam with the samples are used to characterize the sample. The characteristic X-ray gives the idea about the element present in the sample qualitatively and also quantitatively. In this mode, electron with large beam diameter (up to 1 mm), large beam currents and long integration time are employed for obtaining good signal to noise ratio. Here, the sampling volume is quite large and the resolution is rather limited. X-rays may be collected either in wavelength dispersive or energy dispersive mode. In energy dispersive mode, a liquid nitrogen cooled Li drifted silicon or germanium detector along with multi-channel analyzer is made use of to detect all the elements simultaneously. Nowadays, in SEM instruments, EDS (energy dispersive spectroscopy of X-ray) attachment is also available for compositional analysis.

Each of the method is amenable to obtain images corresponding to the distribution of single element.

The sample to be probed by SEM should be vacuum compatible (~10^{-6} mbar or less). Electrons, being charged particles, require vacuum environment for traversing without change in their number and density. The sample to be analyzed need to be electrically conducting, otherwise there is a charge build up due to the impinging electrons which gives rise to jumping of beam and hence intensity. The surfaces of non-conductive materials are made conductive by coating with a thin film of gold or platinum or carbon.

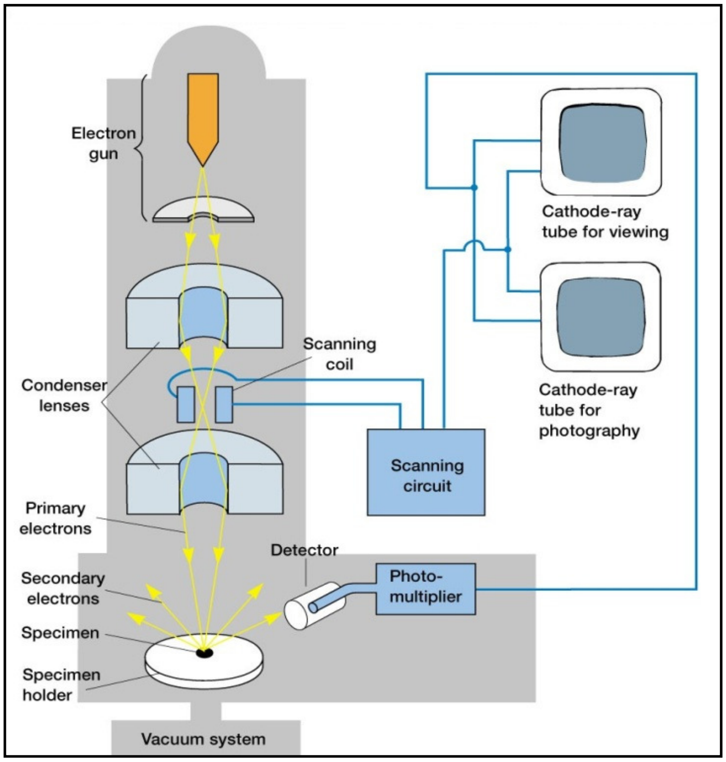

Figure 2.7: Schematic of SEM instrument.

In the present study, SEM has been used to study the microstructure of glass-ceramics and interface of seals. Energy dispersive X-ray analyzer (Model: Oxford INCA Energy 250) fitted with the SEM instrument was used for the compositional analysis and elemental line scan across the interface. The SEM images for various samples have been collected using a SEM instrument (Model: Tescan Vega MV 2300T/40). The BSE and SE images are collected on a fractured or polished sample after etching the surface with 10% HF solution for 10 s. The sample to be analyzed was first coated with a thin layer of Au to render the surface conducting and then mounted on a sample holder placed in a chamber evacuated to a pressure of 10^{-8} mbar. The sample was then imaged by an electron beam of energy 25 keV and micrographs were recorded at different magnifications from 1-30 kx.

2.3.3 Vibrational spectroscopy

Vibrational spectroscopic techniques are extensively used to identify the nature of different linkages present in a material. In vibrational spectroscopy, the changes in the vibrational modes of atoms in a molecule are measured, which are greatly influenced by the mass of atoms, their geometrical arrangement and strength of chemical bonds. IR spectroscopy encompasses a spectral region namely 12500 to 10 cm^{-1} in the electromagnetic spectrum. The most fundamental molecular vibrations occur in mid IR (4000-400 cm^{-1}) region making this region richest in chemical information. These methods can also give valuable information regarding the symmetry of different vibrational units. Vibrational spectroscopy can be broadly classified as Raman and IR spectroscopies. The former is inelastic scattering of photons and the latter is an absorption process. Both IR and Raman spectroscopies result from transition between quantized vibrational states and provide complementary information about the molecular vibrations. These two techniques differ in their instrumentation and origins i.e. the way light interacts with the molecule. Thus, a molecular vibration is IR active when incident IR radiation causes changes in molecular dipole moment while a vibration is Raman active if there is a change in the molecular polarizability due to vibration [99]. Both IR and Raman spectroscopies are used in the present study and the principles as briefly described below.

2.3.3.1 Infrared spectroscopy

Vibrations of bonds and groups, which involve a change in the dipole moment, result in the absorption of IR radiation, which form the basis of the IR spectroscopy. Modern IR instruments are based on Fourier transformation technique to improve the signal to noise ratio. In FTIR instrument, all the frequencies are used simultaneously to excite all the vibrational modes of different types of bonds/linkages present in the sample. This reduces the experimental time considerably.

The FTIR technique is based on a Michelson interferometer, which is an optical device consisting of a fixed mirror, movable mirror and a beam splitter. The interferometer shifts the phase of one of the beam with respect to another by moving one of the mirrors and keeping the other mirror at a fixed position. When the two beams overlap, depending on whether they are in phase or out of phase, constructive and destructive interference takes place. If the light source is monochromatic, the intensity of the interference pattern will rise and fall periodically and the detector will measure a sinusoidal signal as a function of the optical path difference. When the light source contains many frequencies, like the radiation emitted from a Globar IR source, the intensity measured I(x) as a function of optical path difference, x is known as the interferogram. Fourier transformation of the interferogram results in the frequency spectrum, I(ν). The optical path difference 'x' can be accurately obtained from the interference patterns generated from the interferometer using a laser source whose frequency is accurately known.

In the present study all infrared experiments were carried out using a Bomem MB102 FTIR machine with a resolution of 4 cm^{-1} having a range of 400-4000 cm^{-1}. The IR radiation was generated from a Globar source (bonded silicon carbide rod). The instrument used CsI single crystal, as the beam splitter and deuterated triglycine sulphate (DTGS) as the detector. A He-Ne laser having a wavelength of 632.8 nm (with a max power of 25μW) has been used for the calibration purpose. FTIR transmittance spectra were recorded at room temperature on samples in the pellet form. Prior to the measurements, the samples were ground thoroughly after mixing with dry KBr powder (sample to KBr ratio was taken as 2-4 wt.%) and made in the form of a thin pellet. These pellets were introduced into the sample chamber for recording the IR spectra. About 20 scans were co-added and referencing was done by recording a blank KBr pellet.

2.3.3.2 Raman spectroscopy

Raman scattering is an inelastic scattering of electromagnetic radiation (mainly visible) from any excited states (mainly vibrational states) in the material. In Raman spectroscopy a monochromatic incident radiation of frequency ν_0 (typically from some type of laser) is scattered inelastically from different vibrational states of the sample. Most of the incident light scattered elastically (Rayleigh scattering) and only a small fraction of incident light (1 in 10^7 photons) is scattered inelastically at frequency $\nu_0-\Delta\nu$ (or $\nu_0+\Delta\nu$). The small change in frequency of the Raman or inelastically scattered light is called Raman shift. This shift corresponds to the energy required to excite vibration in a molecule.

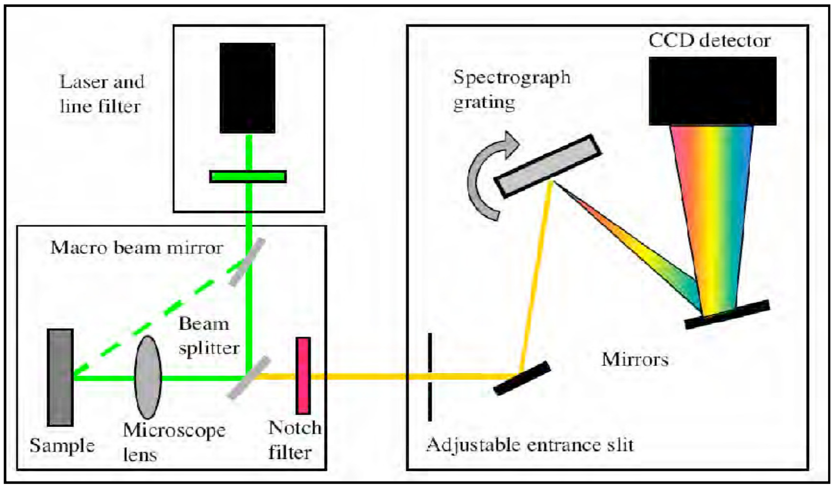

Figure 2.8: Schematic of Raman spectrometer.

Raman scattering setup consists of an excitation source, a spectrometer or spectrograph, a detector and detection electronics with output device as shown in Figure 2.8. Highly monochromatic, directional and high power density excitation radiation in visible range is required for Raman spectroscopy and therefore, lasers are suitable excitation sources. The Raman scattered light is analyzed using a scanning grating spectrometer or spectrograph. The principal requirement of Raman spectrometer is its stray light rejection capacity. Stray light is the Rayleigh scattered radiation which always accompanies the Raman scattered light and is ~10^3-10^5 times stronger. A notch filter having high and sharp absorption about the laser light is used in front of the entrance slit in single stage spectrometer to block the stray light. However, the width of the absorption band about the laser line for these filters are finite and Raman shifts below 100-150 cm^{-1} cannot be observed. Raman signals are very weak and a sensitive and low noise detector is of primary importance. The detectors employed in the present day multichannel spectrographs are charge coupled devices (CCD). A CCD is a 2D array of potential wells (known as pixels), which stores the information generated by photo-electron.

The main advantage of this technique is that an ambient atmosphere can be used and no special sample preparation is required for analyzing samples. The intensity of bands in the Raman spectrum of a compound are governed by the change in polarizability, α, that occurs during the vibration and given by following expression:

$$I_{Raman} = K\, I_L\, (v_0 - v_i)^4 x \left(\frac{d\alpha}{dQ}\right)^2 \qquad (2.10)$$

where I_L is the power of the laser at the sample, v_0, v_i are the frequencies of the incident and scattered lights respectively and $d\alpha/dQ_i$ is change in the polarizability with the normal coordinate of the vibration. The constant of proportionality, K, is dependent on the optical geometry, collection efficiency, detector sensitivity and amplification.

In the present study, Raman spectra were recorded on a home-made Raman spectrometer using 532 nm line from an air cooled Argon ion laser [100]. The spectra were collected using a grating with 1200 groves/mm with a slit width of ~50 micron (yielding a resolution of ~2cm^{-1}) along with Peltier cooled CCD and a holographic notch filter. The Raman spectra of glasses in particular have a strong frequency and temperature dependence, and therefore the intensity at lower frequencies have an unwanted scattering component, which can be taken care by appropriate corrections. Raman spectra have been corrected by multiplying the correction factor 'R' for the unwanted scattering component. We have used a correction factor 'R' of the form employed by Mysen et al [101]

$$R = \nu_0^3\left(1 - e^{-\nu/kT}\right)\frac{\nu}{(\nu_0 + \nu)^4} \tag{2.11}$$

where ν_0 and ν are the frequencies (in cm^{-1}) of excitation line and Raman shift, respectively. For the analysis, a baseline correction has been employed. Since, the glasses exhibit broad-band features we have not included the instrumental line width in the analysis.

2.3.4 NMR spectroscopy

NMR spectroscopy is a very powerful technique for the structural elucidation in disordered and compositionally complex materials like glasses and glass-ceramics. It gives valuable information about the structure, dynamics and chemical environment of the particular nucleus in the material. NMR is an element selective technique as Larmor precession frequency is quite different for nuclei of different elements or for different isotopes of the same element. Further, it is a non-destructive technique and does not require elaborate sample preparation.

2.3.4.1 Fundamentals of NMR

A nucleus with a spin quantum number, I, can have (2I+1) different orientations relative to reference axis, that are distinguished by quantum number m_I and are degenerate in the absence of a magnetic field. The m_I can have values, I, I-1, I-2….-I. There is nuclear magnetic moment for such nucleus associated with nuclear spin as follows:

$$\mu = \gamma \boldsymbol{I} \tag{2.12}$$

where γ is the gyromagnetic ratio of nucleus and $\boldsymbol{I} = [I(I+1)]^{\frac{1}{2}}\hbar$

$$\mu_z = \gamma m_{\boldsymbol{I}}\hbar \tag{2.13}$$

Interaction between the nuclear magnetic moments and applied magnetic field, B_o, known as the Zeeman interaction, lifts the degeneracy of the 2I+1 spin states. And transitions between these non-degenerate energy levels form the basis of nuclear magnetic resonance spectroscopy. The force exerted by the applied static magnetic field on the nuclear magnetic moments causes them to precess about the field direction and the precessional frequency, known as Larmor frequency, is given by

$$\omega_o = \gamma B_o \tag{2.14}$$

NMR signals arise when an ensemble of nuclear spins placed inside a strong static magnetic field B_o is perturbed from the equilibrium by the application of radiofrequency (RF) pulses causing transitions between non-degenerate spin states. The applied RF frequency must exactly match with the precessional frequency in order to cause the transition. In addition to the applied field, nuclei may also experience a smaller internal field due presence of neighbouring atoms. Then Larmor frequency of a particular nucleus would depend on the chemical environment around the nucleus and is be expressed as,

$$\omega_o = \gamma B_{net} \tag{2.15}$$

where B_{net} is the net magnetic field felt by the nucleus and is the vector sum of the applied field B_0 and the local field at the site of the nucleus B_{loc} . Thus each nucleus would exhibit a shift in its resonance frequency based upon its chemical surrounding, known as the chemical shift. However, representation of the chemical shift in terms of frequency is not intuitive because the resonance frequency is dependent upon the applied field. Therefore the resonance frequency is quoted in relation to a reference compound so that the line position becomes independent of the applied field. As an example, ^{29}Si NMR spectra use tetramethyl silane (TMS) as the reference. Since the sample and reference resonance shift with the field in the same manner, defining chemical shift according to Eq. (2.16) ensures that the reported chemical shift is independent of the applied field.

$$\delta = \frac{\omega - \omega_{ref}}{\omega_{ref}} \times 10^6 \qquad (2.16)$$

where ω, ω_{ref} represent resonance frequencies of nuclei in the sample and in the reference, respectively.

2.3.4.2 Solid state NMR

In contrast to solution NMR, solid state NMR spectra are characterized by the presence of very broad line shapes. This broadness of NMR lines is due to the effect of various anisotropic or orientation dependent interactions viz, chemical shift anisotropy, dipolar and quadrupolar interactions in solids, which average out in solution due to random tumbling of molecules. However, during recent years, several specialized techniques have been developed for averaging these interactions to zero, or reduce them to their isotropic values in solids allowing the registration of high-resolution NMR spectra of solids. The broad NMR line shapes, however, contain valuable structure and dynamic information. Technique has been developed where by choosing appropriate experimental protocols, one can access the anisotropic part of NMR interaction while maintaining high resolution. Broadening of the NMR lines in solid samples occurs mainly because of (i) anisotropic effect, (ii) dipolar interaction and (iii) quadrupolar effect, for the nuclei with spin >1/2. The anisotropic and dipolar interaction can be overcome by magic angle spinning NMR technique, where as the quadrupolar broadening is overcomed using MQ MAS-NMR and choosing coherence transfer pathways that are not influenced by the quadrupolar interactions.

2.3.4.3 MAS-NMR

MAS-NMR technique involves rotating the powder samples at high speeds, at an angle of 54.7° (magic angle) with respect to the applied magnetic field direction. When $\theta = 54.7°$, the term $3\cos^2\theta$ becomes unity. Since Hamiltonian for different anisotropic interactions have $3\cos^2\theta - 1$ term, these anisotropic interactions get averaged out in time during fast spinning thereby giving rise to sharp NMR peaks. Thus the MAS-NMR technique simplifies the solid state NMR patterns and individual chemical environments can be correlated with corresponding chemical shift values obtained from these samples [102].

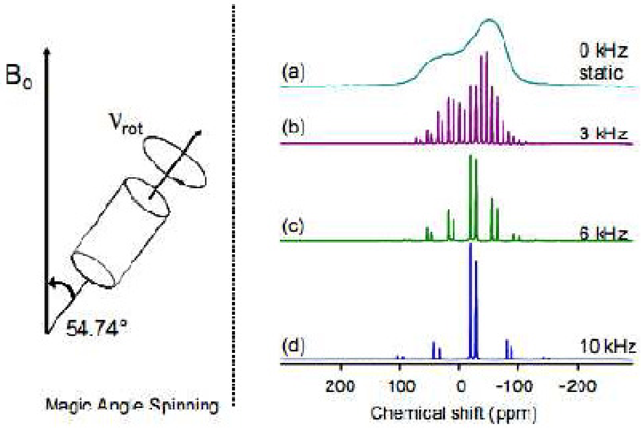

Figure 2.9: Schematic representation of MAS-NMR (left) and the effect of various MAS rates on the ^{31}P NMR of $NaAl_2P_2O_7$ (right).

A schematic view of magic angle spinning is shown in Figure 2.9 (left). On the right, the effect of various spinning speeds is shown in ^{31}P MAS-NMR of $NaAl_2P_2O_7$. From the figure it is clear that the value of spinning frequency must be higher than the frequency of the anisotropic interactions to get a single resonance at the isotropic position. In most cases, even a spinning speed of upto 60 kHz is insufficient to fully average out the anisotropic interactions and the broad line is then broken up into a series of spinning sidebands flanking the isotropic resonance and separated from it by a frequency equal to the spinning frequency (Figure 2.9).

Modern NMR instruments are based on the principle of Fourier transformation. In FT-NMR, all frequencies in a spectrum are irradiated simultaneously with a radio frequency pulse. Following the pulse, the nuclei return to thermal equilibrium. A time dependent variation in magnetization is recorded immediately after the pulse. A frequency domain spectrum is obtained by employing Fourier transformation technique. Figure 2.10 shows a schematic of typical NMR instruments.

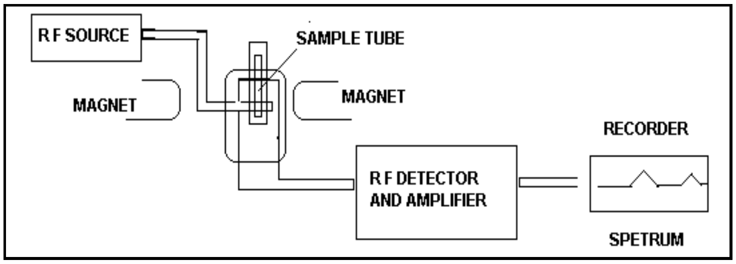

Figure 2.10: A schematic of NMR instrument.

In the present study ^{29}Si, ^{27}Al, ^{11}B and ^{31}P MAS-NMR spectra for various samples were recorded on Bruker AVANCE spectrometers with different static field. Details of the experiments are given in relevant chapters.

2.4 Optical Characterization

2.4.1 Ultraviolet-visible absorption spectroscopy

Ultraviolet-visible (UV-Vis) absorption spectroscopy is based on the measurement of the attenuation of a beam of light after it passes through a sample or after reflection from a sample surface. Oxide glasses generally absorb strongly both in the far IR and UV spectral region. The former is associated with the interaction of light with the molecular vibrations and the latter with the electronic transitions between the valence band and the conduction band or between the excitation levels. Most of the oxide glasses are highly transparent in the visible region with a broad absorption edge in the UV region. The position and shape of the absorption edges depend on the composition as well as the nature of the network former and modifier cations.

The absorption coefficient 'α' of a transmitting medium can be expressed by Lambert-Beer law as $I = I_0 \exp(\alpha l)$, where I_0 is the intensity of the incident light and I is the intensity of the light transmitted through a sample of length l. Optical absorption spectra of glasy material are characterized by a broad absorption edge. The onset of optical absorption can be obtained from the extrapolation method and can be correlated with the $E_{optical}$ values of the glasses.

In a commercial UV-vis spectrometer usually a deuterium discharge lamp is used as light source for UV measurements and a tungsten-halogen lamp for visible and NIR measurements. The instruments automatically swap lamps when scanning between the UV and visible regions. The wavelengths of these continuous light sources are typically dispersed by a holographic grating in a single or double monochromator or spectrograph. The spectral bandpass is then determined by the monochromator slit width or by the array-element width in array-detector spectrometers. Spectrometer designs and optical components are optimized to reject stray light, which is one of the limiting factors in quantitative absorbance measurements. Photodiode, phototube, or photomultiplier tubes (PMT) are commonly used as detector in UV-Vis spectrometer. UV-Vis-NIR spectrometers utilize a combination of a PMT and a Peltier-cooled PbS IR detector. The light beam is redirected automatically to the appropriate detector when scanning between the visible and NIR regions. The diffraction grating and instrument parameters such as slit width can also be changed during the measurement.

A commercial dual beam UV-Vis-NIR spectrophotometer (JASCO V- 670) was used in the present study for recording the absorption curves of glass samples. The glass samples in the form of a disc having diameter more than 12 mm and thickness in the range 2-4 mm were prepared and polished with 0.3 μm alumina powder for optical measurements. The optical absorption measurements were carried out in the 200-2500 nm range with 2 nm resolution.

2.4.2 Photoluminescence spectroscopy

Photoluminescence (PL) is a process, in which a substance absorbs photons and then re-emits photons of lower energy. Quantum mechanically, this can be described as an excitation to a higher energy state by absorption of photon and then a return to a lower energy state accompanied by the emission of a photon.

The schematic of spectrofluorometer is shown in Figure 2.11. The light from an excitation source passes through a monochromator, and strikes the sample. A proportion of the incident light is absorbed by the sample, and sample fluoresces. The fluorescent light is emitted in all directions. Some of this fluorescent light passes through a second monochromator and reaches to a detector, which is usually placed at 90° to the incident light beam to minimize the risk of transmitted or reflected incident light reaching the detector. Various light sources may be used as excitation sources, including lasers, photodiodes and lamps (xenon arcs and mercury-vapor lamps). Xenon arc lamp has a continuous emission spectrum with nearly constant intensity in the range from 300-800 nm and a sufficient irradiance for measurements down to 200 nm. The most common type of monochromator utilizes a diffraction grating, that is, collimated light illuminates a grating and exits with a different angle depending on the wavelength. The monochromator can then be adjusted to select which wavelengths to transmit. The most commonly used detector is PMT.

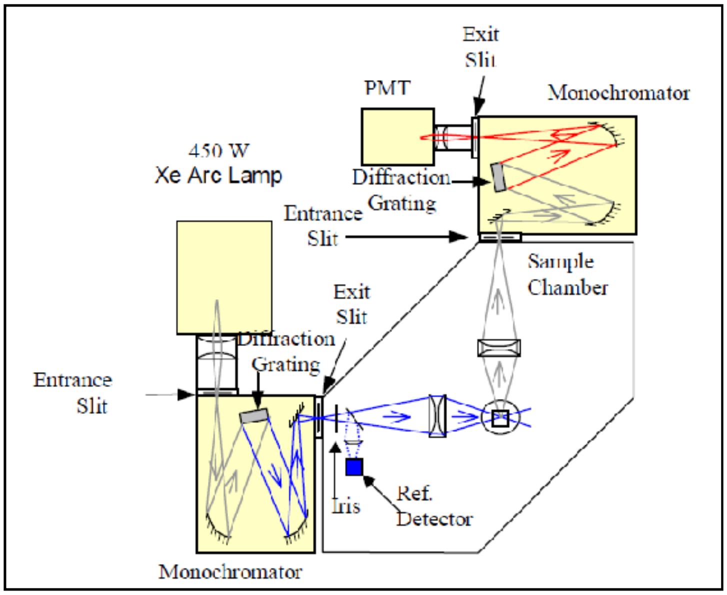

Figure 2.11: Schematic representation of spectrofluorometer.

The spectrofluorometer with dual monochromators and a continuous excitation light source can record both excitation and emission spectrum. When measuring emission spectrum, the wavelength of the excitation light is kept constant, preferably at a wavelength of high absorption, and the emission monochromator scans the spectrum. For measuring excitation spectra, the wavelength passing through the emission monochromator is kept constant and the excitation monochromator is subjected to scanning. The excitation spectrum generally is identical to the absorption spectrum.

In the present study all luminescence measurements were carried out at room temperature by using an Edinburgh FLSP 920 Instrument, having a 450W Xe lamp as the excitation source. Polished glass samples were mounted on the front face solid sample holder in the sample chamber of the instrument. Emission spectra were recorded with a resolution of 5 nm and all emission spectra were corrected for the detector response.

2.5 Adhesion Property and Seal Fabrication

To demonstrate the potentiality of investigated strontium zinc silicate glasses/glass-ceramics, as a high temperature sealants for SOFC application, seals with few fuel cell components like YSZ (electrolyte) and Crofer-22-APU (an interconnect material) have been prepared. In the formation of a hermetic seal, the bonding/adhesion property of glass to wet metal/ceramic was exploited. Glasses have random network structures, as a result of which, the number of bonds broken per unit area during surface creation is lower than in the case of crystalline solids. Further, the open structure of glasses, readily allows minor structural rearrangements allowing the minimization of the energy penalty incurred during surface creation. As a result of this, glasses readily wet metals and oxide ceramics as well. In order to enhance the wetting of metal by the glass, the metal surface is cleaned suitably before the sealing process.

For assessing adhesion property of glass, glass disks were placed between two YSZ or Crofer metal in sandwich geometry and assembly was heated in a controlled manner in air up to 900-1050°C for 1-2 h. Seals in a sandwich geometry (Crofer/glass/Crofer) were prepared by putting the glass powder in paste form between two Crofer plates having dimension 20 mm length, 20 mm wide and 1 mm thickness. The glass paste was prepared by mixing the glass powder with alcohol. The whole assembly was heated in a vertical split resistance furnace upto 1050°C in air for 1-2 h. A little pressure was applied during the sealing process for a better contact of the glass paste with Crofer plate.

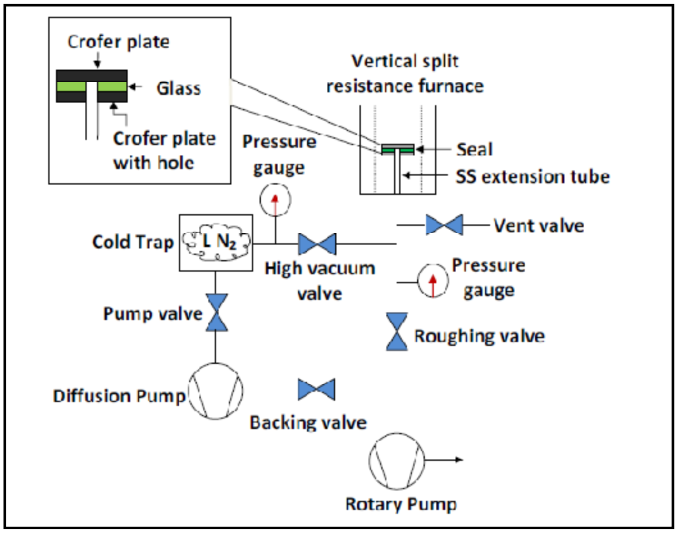

Figure 2.12: Schematic of leak testing setup.

For testing of vacuum integrity of seal, one Crofer plate having a 5 mm hole in the centre with an SS extension tube was used in the seal formation. For leak testing of the seal, the extension tube was connected to the vacuum system as shown in schematic of leak testing setup Figure 2.12. Seals of glass with Crofer-22-APU were tested for vacuum integrity at different elevated temperatures up to 950°C. For this, the seal was heated in a vertical split resistance furnace and changes in pressure if any were continuously monitored. The seals were also tested after exposure to high temperatures for different times.

Chapter 3

Studies on Sodium Aluminium Titano-Phosphate Glasses

3.1 Introduction

Phosphate glasses are finding ever-increasing applications in different emerging fields viz: vitrification of radioactive waste [103-105], photonics [39], fast ion conductor [106], glass-to-metal seals [107], biomaterials etc [108-109]. These glasses have a series of interesting properties such as low T_g, lower T_m (compared to silicate glass), high TEC, high ultraviolet transmission and biocompatibility [38] which make them potential candidates for various technological applications. Earlier, phosphate glasses have been of limited interest due to their hygroscopic nature and poor chemical durability however, the development of novel compositions of superior physical and chemical properties, of these glasses have revived new interest in phosphate glasses and glass-ceramics. In recent years there has been much research on improving the physical properties and chemical durability of phosphate glasses by introducing intermediate type metal oxides (MO) like Al_2O_3, Fe_2O_3, TiO_2, ZnO, which generate additional O-M-O type cross-linkages among different polyphosphate anions.

Alkali alumino-phosphate glasses are technologically important for low temperature hermetic sealing and vitrification of radioactive waste. These glasses are also important as laser host materials. These glasses with high alkali concentration have potential applications in solid state ionic devices. Sodium alumino-phosphate (NAP) glasses have T_g below 400°C and TEC greater than 150×10^{-7}/°C and are used for making glass-to-metal seals with low melting and high thermal expansion materials like Al, Cu etc. The NAP glasses have been the subject of various investigations [110-115]. The role of Al_2O_3, on structure and other properties of these phosphate glasses, has been extensively studied [111-113]. It has been reported that addition of Al_2O_3 up to ~10 mol% to the phosphate glasses resulted in improved chemical durability and modifications in their thermo-physical properties like TEC and T_g. These properties have shown marginal changes upon addition of more than 10 mol% Al_2O_3 [110]. Similarly, sodium titano-phosphate (NTP) glasses without Al_2O_3 have also been investigated by many researchers [116-119]. Incorporation of TiO_2 improves the chemical durability of the phosphate glasses, while also increasing the nonlinear refractive index (n_2 values) [120], thereby facilitating their application as active materials in optical switches and telecommunication fibers. Presence of Al_2O_3 and TiO_2 together in the glass matrix is expected to significantly modify the optical and thermo-physical properties of the glassy system. Therefore, effect of TiO_2 in NAP glasses in terms of thermo-physical and optical properties has been investigated in the present work and correlated with the structural changes in the glass.

3.2 Experimental

3.2.1 Synthesis of glass samples

Sodium aluminium titano-phosphate (NATP) glasses having compositions (in mol%): $40Na_2O$-$10Al_2O_3$-$xTiO_2$-$(50-x)P_2O_5$, where x = 0-20 were prepared by melt quench method. Analytical grade $NaNO_3$, Al_2O_3, TiO_2 and $NH_4H_2PO_4$, were used as starting materials in such proportions that the O/P ratio changed from 3.2 to 4.33. Glasses were prepared following the procedure as described in chapter 2 of the thesis. Depending on the composition, glass charges were melted in temperature range from 1250°C to 1350°C in the air ambient.

Annealing of these glasses was done in the temperature range ~400-460°C for 4 h. Annealed glasses were stored in a desiccator for further characterization.

3.2.2 Thermo-physical characterization

Density of glass samples was measured at room temperature by Archimedes principle using toluene as an immersion liquid with an accuracy of ± 0.03 g/cm^3. Molar volume of the glass was also obtained from the density. TEC and T_g were measured by TMA. The TEC being reported here are an average in the range of ~30-300°C. The MH of optically polished glass samples was measured by the Vickers indentation technique.

The effect of ambient moisture on the NATP glasses was also investigated. For this purpose, optically polished transparent glass discs of all compositions were exposed to air ambient and surface of glasses was examined by an optical microscope after different time intervals.

3.2.3 Optical characterization

Optical absorption and luminescence measurements of glass samples at room temperature were carried out as described in chapter 2. Polished glass samples having diameter more than 12 mm and thickness in the range 2-4 mm were used for these measurements. The samples were excited at 273 nm.

3.2.4 Structural characterization

Information regarding the structural aspect of the glass is essential to explain and understand the observed variation in the physical properties of the system as a function of the composition. Therefore, structural aspects of these glasses have been investigated through ^{31}P and ^{27}Al MAS-NMR, Raman and FTIR techniques.

Raman spectra on polished glass discs were recorded as described in chapter 2. FTIR spectra of all glasses were recorded over the frequency range 400-4000 cm^{-1} with a resolution of ~ 4 cm^{-1} as detailed in chapter 2.

^{31}P and ^{27}Al MAS-NMR spectra were recorded with the Bruker Avance 500WB spectrometer with a static field of 11.7 T. The spinning frequency of 15 kHz and 10 kHz were used for recording ^{31}P and ^{27}Al spectra, respectively. ^{31}P spectra were recorded at Larmor frequency 202.4 MHz and chemical shift values are expressed with respect to 85 % H_3PO_4. Typical 90° pulse duration and delay times are 3.5 μs and 4s, respectively. A number of NMR experiments had been carried out with different delay times and found that the 4s delay time for these samples was optimal. ^{27}Al spectra were recorded at Larmor frequency of 130.287 MHz with 2.5 μs pulses and 2s recycling time and chemical shift values are expressed relative to 1M aqueous solution of $AlCl_3$. The ^{31}P MAS-NMR spectra were deconvoluted based on Gaussian fit, by independently varying the peak maximum, line width and intensity. The quality or the goodness of the fit was judged from the χ^2 values and the fit with lowest χ^2 value was used to calculate the relative concentration of different P structural units.

3.3 Results and Discussion

3.3.1 XRD

Clear, transparent and bubble-free glasses were obtained for all the investigated compositions. Nominal batch compositions and O/P ratio of all NATP glasses are given in

Table 3.1. Powder X-ray diffraction patterns for all the glass samples showed a broad hump at around 2θ = 30° as shown in Figure 3.1, characteristic of the amorphous nature of the glass samples.

Table 3.1: Nominal composition and O/P ratio for NATP glasses.

Glass ID	Composition (Nominal) (mol%)				O/P ratio
	Na_2O	Al_2O_3	P_2O_5	(x) TiO_2	
NATP0	40	10	50	0	3.2
NATP2	40	10	48	2	3.27
NATP5	40	10	45	5	3.39
NATP10	40	10	40	10	3.63
NATP15	40	10	35	15	3.93
NATP20	40	10	30	20	4.33

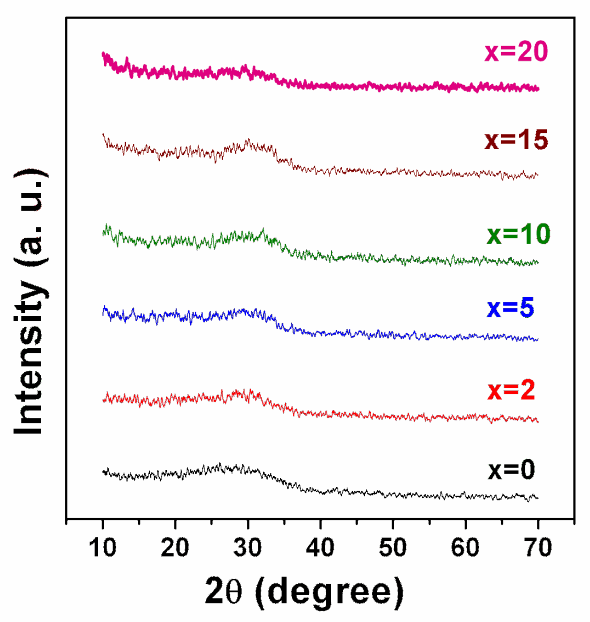

Figure 3.1: XRD patterns of NATP glasses having x mol% TiO_2 (x = 0-20).

3.3.2 Thermo-physical properties

Various thermo-physical properties like T_g, TEC, MH, ρ and V_m for the prepared glass samples are given in Table 3.2.

Table 3.2: TiO_2 content (x), T_g, TEC, MH, ρ, V_m and $E_{optical}$ for different NATP glasses.

Sample	**TiO_2 content x (mol%)**	**$E_{optical}$ (eV)**	**T_g± 2 (°C)**	**TEC± 5% (10^{-7}/°C)**	**MH± 5% (GPa)**	**ρ ± 0.03 (10^3kg/m^3)**	**V_m (10^{-6}m^3)**
NATP0	x = 0	3.57	386	186.40	2.90	2.63	40.29
NATP2	x = 2	3.43	415	168.50	3.05	2.66	39.37
NATP5	x = 5	3.34	448	158.06	3.25	2.68	38.38
NATP10	x = 10	3.32	479	157.50	3.35	2.72	36.67
NATP15	x = 15	3.30	472	168.27	3.31	2.70	35.80
NATP20	x = 20	3.29	462	165.25	3.23	2.46	37.03

Variations in ρ and V_m of the NATP glasses as a function of TiO_2 content (x) are shown in Figure 3.2. The ρ first increases up to 10 mol%, and then decreases with further addition of the TiO_2. However, the V_m first decreases and then increases. The observed variation, particularly below 10 mol% TiO_2 contents, is in contrary to one's expectation as the molecular weight of P_2O_5 and TiO_2 are 142 g/mol and 79.9 g/mol, respectively and replacement of P_2O_5 by TiO_2 is expected to decrease the ρ and increase the V_m. Observed variation in the above properties indicates that the Ti polyhedra form some new interconnections within the network and thus densify the glass network up to 10 mol% TiO_2. For glass samples with TiO_2 more than 10 mol% the ρ decreases and V_m increases. This indicates that for more than 10 mol% TiO_2 content, interconnections provided by titanium polyhedra are not sufficient to overcome the depolymerization of phosphate network and result in decrease in ρ and increase in the V_m.

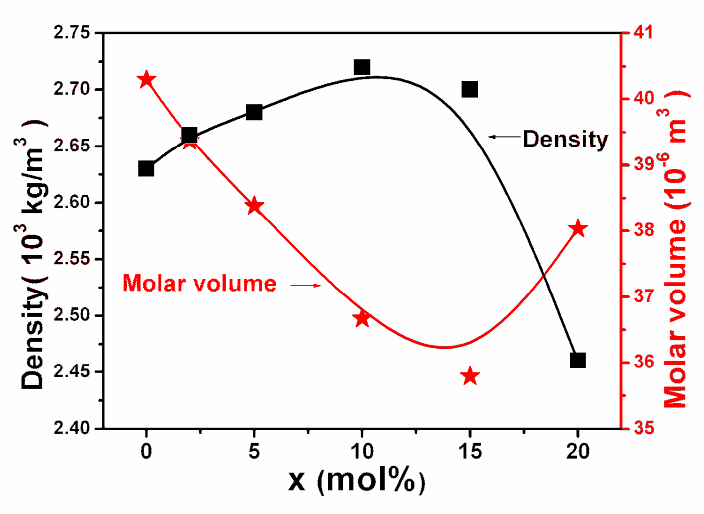

Figure 3.2: Variation of density and molar volume of NATP glasses as a function of TiO_2 concentration (x) in mol%. Solid lines are drawn as guide to the eyes.

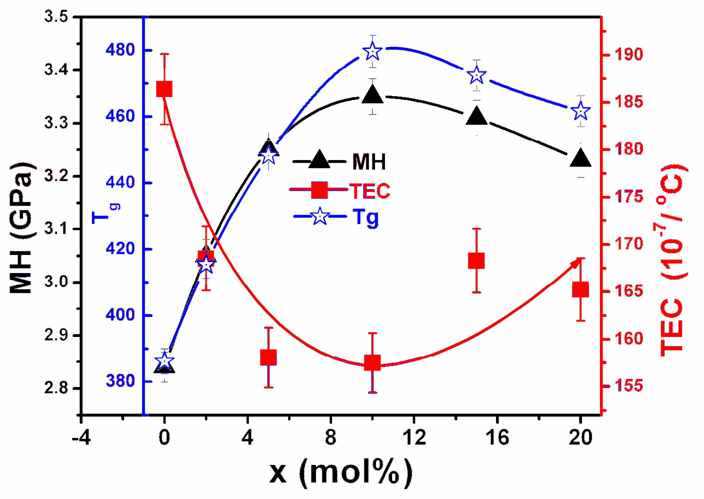

Figure 3.3: Variation of MH, TEC and T_g of NATP glasses as a function of TiO_2 concentration (x) in mol %. Solid lines are drawn as guide to the eyes.

Variation in the values of MH, TEC and T_g of the NATP glasses as a function of TiO_2 content are shown in Figure 3.3. It is clear from the figure that the T_g and MH increase while TEC decreases up to 10 mol% TiO_2. With the increase of TiO_2, beyond 10 mol%, the T_g and MH decrease and TEC increases. The initial increase in T_g and MH values for replacement of TiO_2 by P_2O_5 up to 10 mol% indicates the formation of strong and rigid bonding. However, beyond that the network bonding weakens. The results of TEC measurement also support the observation that glass structure becomes more stable and rigid up to 10 mol% TiO_2 and beyond that network stabilization and rigidity start to reduce.

3.3.3 Optical properties

UV-Vis optical absorption spectra of the NATP glass samples containing different amounts of TiO_2 are shown in Figure 3.4. All the absorption curves are characterized by a broad onset of absorption edge over the region of 500-300 nm, which is characteristic of the glassy nature of the sample. The broad onset is arising due to the disorder in structural units existing in the glass. There is a distribution in the bond angles and bond lengths corresponding to different structural units in the glass and this is associated with the relaxation of selection rules for various optical transitions [121-122]. Such relaxation in the selection rules leads to broadening of the onset corresponding to the absorption edge. For the glass sample without any TiO_2 the onset of absorption is found to be around 350 nm. With incorporation of TiO_2, the onset of absorption was found to be red shifted for all the samples. Further, there is a weak absorption over the region of 400-500 nm in all the spectra. A similar weak absorption has also been observed in many phosphate and silicate based glasses [123-124]. Based on those reports we attribute this to the absorption due to the localized centers/structural inhomogeneities present in the glass. (Presence of Ti^{3+} in glass is characterized by an absorption in the visible region around 500-600 nm. However, formation of Ti^{3+} species is unlikely in the glass samples of present study as the glass samples are prepared by melting the constituents in air at 1350°C).

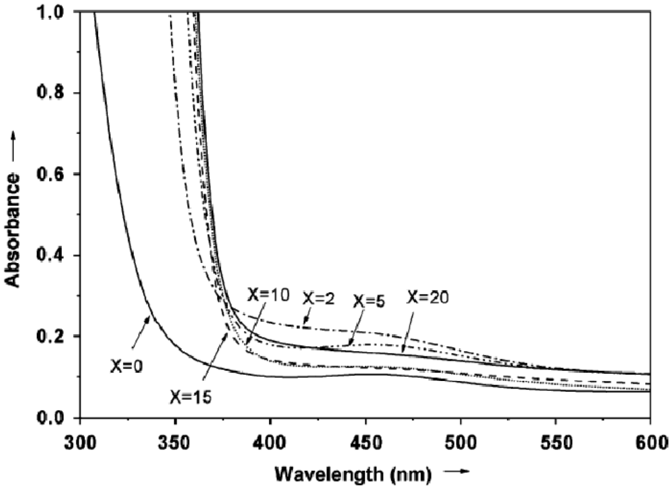

Figure 3.4: UV-visible optical absorption spectra of NATP glasses containing different amounts of TiO_2 (x) in mol%.

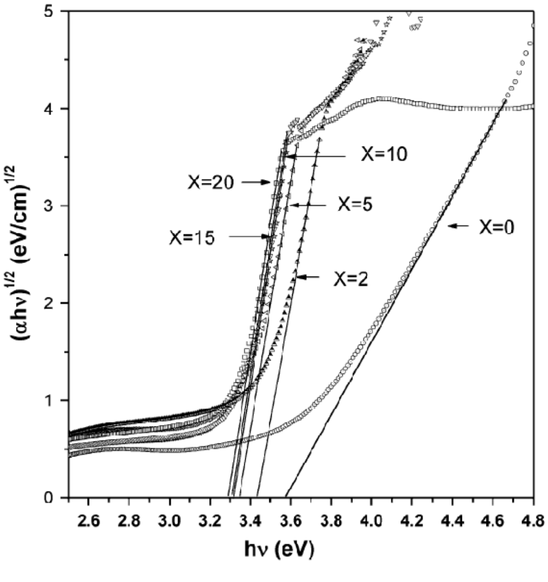

Figure 3.5: Tauc plots for NATP glasses containing different amounts of TiO_2 (x) in mol%.

As the onsets of absorptions are quite broad, attempt was not made to exactly calculate the onset wavelength of absorption. However, the absorption coefficient (α) in these glasses can be related to $E_{optical}$ values of the glass by a power law suggested by Mott and Davis [125], which can be expressed as $\alpha h\upsilon = A(E-h\upsilon)^r$, where A is a constant and r is a parameter which depends on the type of transitions and can have values 2, 3, ½ etc. As reported by Tauc [121] and, Mott and Davis [125] for indirect transitions in glassy materials, the value of r can be assumed to be 2. Hence, a plot of $(\alpha h\upsilon)^{1/2}$ versus hυ (known as a Tauc plot), will results in a curve, extrapolation of the linear region of the curve to the x-axis with $\alpha = 0$ can give the value of the optical gap in the glass. Tauc plots (variation of $(\alpha h\upsilon)^{1/2}$ as a function of hυ) of NATP glasses are shown in Figure 3.5. The $E_{optical}$ values obtained from these Tauc plots are summarized in Table 3.2. For glass sample without any TiO_2 content, the $E_{optical}$ value is found to be 3.57 eV. Incorporation of 2 mol% TiO_2 resulted in reduced $E_{optical}$ value to 3.43 eV. Further, reduction in $E_{optical}$ value (3.34 eV) was noted for the glass containing 5.0 mol% TiO_2. The $E_{optical}$ values for the glasses containing 10, 15 and 20 mol% TiO_2, as mentioned in the Table 3.2, are comparable with that of the glass sample with 5 mol% TiO_2. The observed variation in the $E_{optical}$ values can be explained based on the conversion of BO to NBO atoms brought about by the TiO_2 incorporation in the glass. Optical transitions from these glasses are thought to be arising from the excitation of electrons from the levels, mainly constituted by oxygen atoms to the levels made by the metal ions. The negative charge present on the NBO atoms facilitates the excitation of its electrons to a higher energy level compared to BO atoms where there is no negative charge. Hence an increase in the concentration of NBO atoms is associated with a decrease in the $E_{optical}$ values. Similar a decrease in the $E_{optical}$ values with increase in NBO atoms content has been reported in many phosphate and silicate glasses [126-127]. In the present study, for glasses containing

2 and 5 mol% TiO_2 the relative concentration of NBO atoms are higher and hence their $E_{optical}$ values are lower, when compared to the glass without any TiO_2. However, for the glass samples containing more than 5 mol% TiO_2, there is no significant change in the $E_{optical}$ values indicating that the relative concentration of NBO atoms attached with P structural units remains more or less same. From these results it can be inferred that at higher concentration of TiO_2, Ti^{4+} mainly goes to the network rather than further modifying the network and increasing the concentration of NBO atoms. There are no charge transfer phenomena taking place in these glasses, as this will lead to the reduction of Ti^{4+} to Ti^{3+} species, which is unlikely for glass samples prepared at 1350°C in air. Indeed, it is worth mentioning here, that the Ti^{3+} species are mainly observed in glass samples prepared under reducing conditions [128-131].

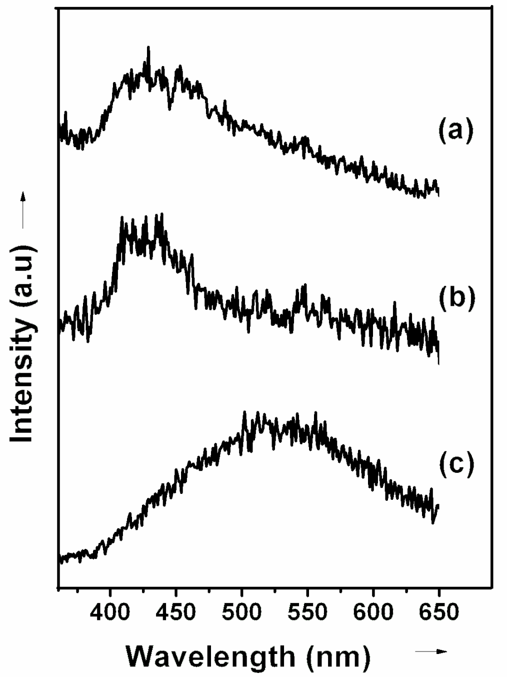

Figure 3.6: Emission spectrum of NATP glasses with (a) x = 0, (b) x = 10 and (c) x = 20 TiO_2 content (in mol%). The samples were excited at 273 nm.

Emission spectra of a few representative NATP glass samples are shown in Figure 3.6. For the glass sample without any TiO_2, a broad peak centered about 435 nm with significant tailing towards higher wavelength region occurs (Figure 3.6(a)). The broad emission spectrum has been attributed to the different types of luminescent centres present in the glass. It is reported that in binary silicate [123] and phosphate glasses [132-133] linkages like $Si\text{-}O^{-}\ldots Na^{+}$, $P\text{-}O^{-}\ldots Na^{+}$ etc form and these linkages act as localized levels in the optical gap of the glasses and can trap the electrons. Such levels are generally known as L-centres or modified L-centres [123,132-133]. Recombination of electrons form this level with the holes in the lower levels leads to light emission. In a multi-component glass there can be a variety of L-centres and depending upon their concentration in the glass a broad emission spectrum is observed. With incorporation of TiO_2 at the expense of P_2O_5, upto 10 mol%, the wavelength corresponding to the emission maximum remained the same, even though there is a slight change in the line shape (Figure 3.6(b)). However, above 10 mol% TiO_2 incorporation in the glass, the emission maximum got significantly shifted to higher wavelength (528 nm) indicating a decrease in the energy corresponding to localized levels. From the UV-visible optical absorption spectrum it is confirmed that the $E_{optical}$ value decreases with increase in TiO_2 content in the glass. In accordance with this the emission maxima also get red shifted. Based on UV-Visible optical absorption and luminescence studies described above, it is inferred that, the glass network and the electronic environment around the NBOs change significantly with TiO_2 incorporation in the glass. The changes are with respect to the creation of more NBO atoms and formation of relatively more ionic P-O-Ti linkages at the expense of more covalent P-O-P linkages. Similar changes in the L-centre emission characteristics have also been observed in $PbO\text{-}Na_2O\text{-}SiO_2$ glasses [123]. At this stage it is worthwhile to mention that no Ti^{3+} emission is observed from the sample as reported by Bausa et al [129] and Batyaev et al [131].

3.3.4 Structural studies

In order to understand the observed variation in thermo-physical properties and $E_{optical}$ values, structural studies were carried out using ^{31}P and ^{27}Al MAS-NMR, Raman and FTIR techniques.

3.3.4.1 MAS-NMR

^{31}P MAS-NMR spectra for NATP glasses, prepared with different amounts of TiO_2, are shown in Figure 3.7.

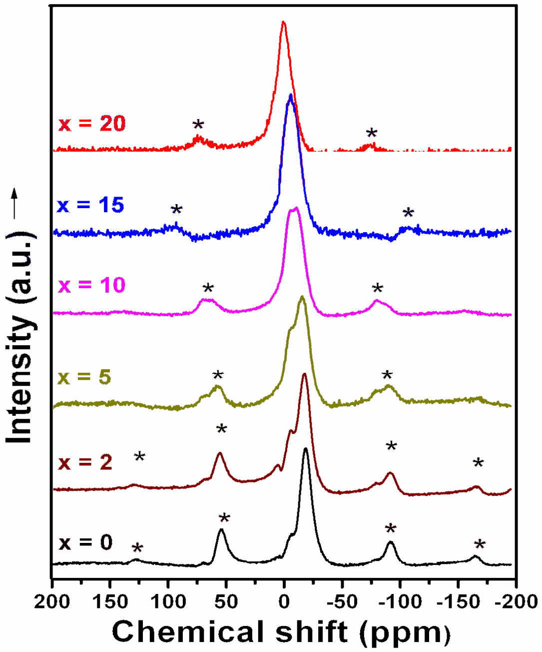

Figure 3.7: ^{31}P MAS-NMR spectra of NATP glasses having x mol% TiO_2 (x = 0-20). Side bands are marked with an asterisk (*).

For the glass with x = 0, an asymmetric peak around -18 ppm with shoulders around -4 and +4 ppm has been observed. Deconvolution based on a Gaussian fit, revealed three peaks around -18.8, -4 and +4 ppm, which are characteristic of Q^2, Q^1 and Q^0 structural units of 'P', respectively (where Q^n represents the 'P' structural units having 'n' number of bridging oxygen atoms) [134-135]. With the increase of TiO_2 concentration in the glass up to 10 mol%, the concentration of Q^1 structural units increases at the expense of Q^2 structural units as shown in the Figure 3.8(a). Furthermore, the Q^2 structural units show systematic increase in the chemical shift values from –18.8 ppm (for x = 0 mol%) to –11 ppm (for x = 10 mol%), while that of Q^1 structural units remain more or less the same, as shown in Figure 3.8(b). Beyond 10 mol% TiO_2, featureless ^{31}P MAS-NMR spectra were observed with peak maxima shifting towards more positive values.

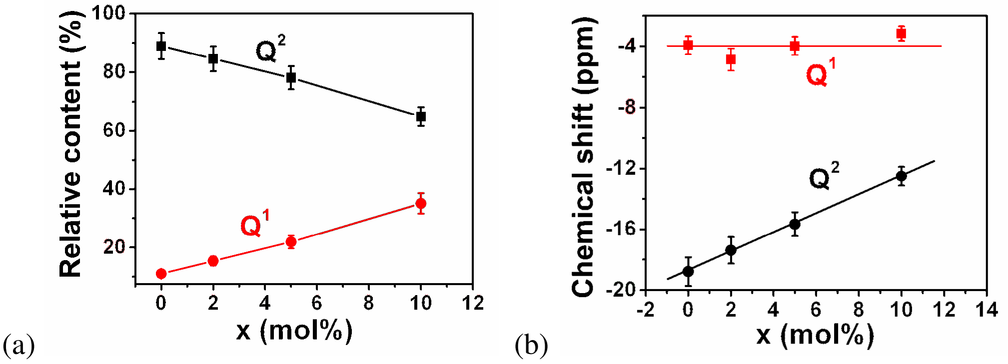

Figure 3.8: (a) Relative contents and (b) chemical shift values of Q^1 and Q^2 structural units as a function of TiO_2 content (x) in mol% in the glasses. Solid lines are drawn as guide to the eyes.

Increase in the concentration of Q^1 structural units in the glass is due to the depolymerization of polyphosphate chains as TiO_2 replaces the P_2O_5 in the glass (thus O/P ratio of the glass also increases). The increase in chemical shift of Q^2 structural units has been attributed to a combined effect of decrease in chain length as well as the formation of P-O^- Ti^{4+} linkages (where Ti^{4+} exists at the network modifying positions in the glass) at the expense of P-O-P linkages [117]. Due to lower Z/r values of Ti^{4+} compared to P^{5+}(where Z is the valency of the ion and r is the ionic radius), replacement of the P-O-P linkages with P-O^- Ti^{4+} linkages results in an increase in ^{31}P chemical shift values. For TiO_2 content >10 mol%, only one peak was observed with peak maxima shifting towards more positive values with increase in TiO_2. Based on the chemical shift values and O/P ratios of the glass samples (Table 3.1), it is inferred that glass NATP15 (O/P ratio = 3.93) consists mainly of Q^0 structural units along with some Q^1 structural units and glass NATP20 (O/P ratio = 4.33) contains only Q^0 structural units connected to different cations. For the glass sample containing more than 5 mol% TiO_2, the observed changes in the ^{31}P MAS-NMR spectra can be explained by the formation of covalent P-O-Ti linkages (where Ti^{4+} act as network former) at the expense of P-O-P linkages. This is because the P structural units like Q^1 and Q^0 can not form a network of its own at this stage. In other words, TiO_2 acts as a network former in these glasses when their concentration is above 10 mol%. Similar network former and modifying behaviour of TiO_2 has also been observed in borosilicate glasses containing different amounts of TiO_2 [126].

^{27}Al MAS-NMR spectra of NATP glasses are shown in Figure 3.9. The spectra clearly show a change in the coordination environment around Al^{3+} ions in the glass as TiO_2 substitutes the P_2O_5. The NMR spectrum of NAP (x=0) glass shows a single peak around -20 ppm, characteristic of AlO_6 structural units [136]. With increasing x, two additional peaks around +6 and +40 ppm start appearing. These peaks have been assigned to the five fold AlO_5 and four fold AlO_4 coordination of Al^{3+} ions respectively based on ^{27}Al MAS-NMR studies on alumino-phosphate crystals [136]. Intensity of these peaks increases progressively beyond x=10 mol%. For x=20, most of the Al^{3+} ions exist as AlO_4 structural units. Based on ^{27}Al MAS-NMR studies it is inferred that Al^{3+} ions mainly extend the glass network by forming P-O-Al type of linkages, where the Al^{3+} is having a tetrahedral configuration.

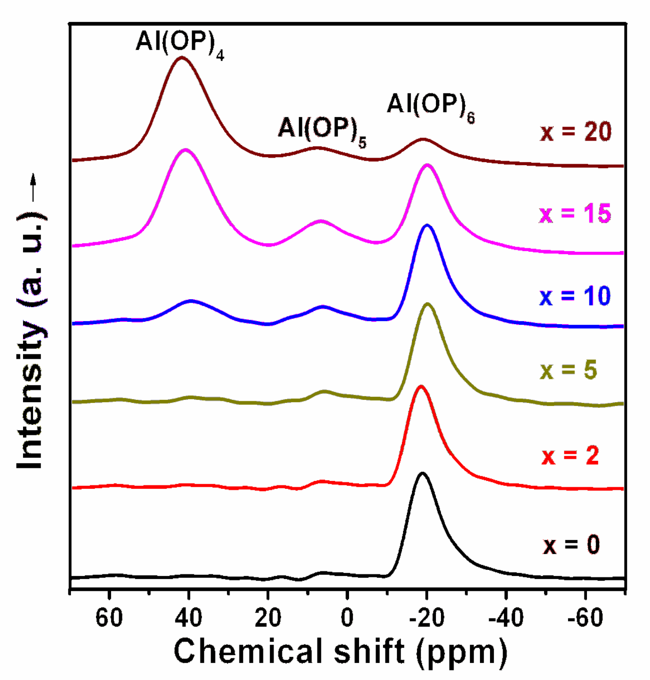

Figure 3.9: ^{27}Al MAS-NMR spectra of NATP glasses.

3.3.4.2 Raman spectroscopy

The Raman spectra of NATP glasses in three frequency ranges, namely, low frequency (200-400 cm^{-1}), medium frequency (400-800 cm^{-1}) and high frequency (800-1400 cm^{-1}) ranges are shown separately in Figure 3.10. The low frequency Raman spectra are shown in Figure 3.10(a). A Raman band observed at ~300-400 cm^{-1} is typical of rocking motion of PO_4 tetrahedron and/ or the motion of cationic polyhedrons [137]. The evolution of this peak 'A' (for NATP0), shows red shift towards the peak 'B' (for NATP20) with increasing TiO_2 content. Corresponding red shift is shown in the inset of Figure 3.10(a). Position of this band depends on the covalent interactions of metal cation with oxygen present in different coordination polyhedral units [137]. Therefore effect of TiO_2 on the extent of ionicity and/or covalency between the cations and its surrounding oxygen atoms is related to this low frequency Raman mode. We correlate the observed red shift in this peak to an increase in the ionicity with increasing TiO_2 content in accordance with the observation of Nelson and Exarhos [137]. This is quite understandable, as the covalency, which is related to the Z/r ratio (where, Z is the valency of the ion and r is the ionic radius), decreases with increase in TiO_2. A new peak 'C' at ~ 440 cm^{-1}, that starts developing for $x > 10$ mol% may be a characteristic of Na-O-P-O-Ti linkages. Similar structural units have been observed in compounds having NASICON type structure [138] exhibiting a Raman band at ~438 cm^{-1}.

The Raman spectra in the medium frequency range are shown in Figure 3.10(b). The band in the range ~650-750 cm^{-1}, associated the P-O-P symmetric stretching [139,140] is composed of two peaks namely 'F' and 'G' [Figure 3.10(b)]. This band in case of NATP0 has an intense peak 'F' at ~693 cm^{-1}, followed by a shoulder peak 'G' at ~737 cm^{-1}. Similar features are observed in the Raman spectra of $NaPO_3$ (sodium metaphosphate) as reported by Nelson and Tallant [140]. It has been reported that unlike in metaphosphates (Q^2 units), the pyrophosphates (Q^1 units) have only one peak centered at ~740 cm^{-1} [140]. These results indicate that the peak 'F' is arising due to metaphosphate (Q^2) units and the shoulder 'G' is arising due to terminal PO_3 (Q^1) structural units. The decreasing intensity of peak 'F' and increasing intensity of peak 'G' with x, indicate that the terminal Q^1 structural units are evolving at the expense of the Q^2 structural units. These Q^2 structural units finally diminish beyond x = 10 mol%. The width of this peak in the NATP20 glass (140 cm^{-1}) has been almost compared to that doubled of NATP0 (70 cm^{-1}). Yifen et al [141] have reported a Raman peak at 740 cm^{-1} for AlO_4 structural units while Sakka et al [142] have assigned this Raman peak to Ti-O_{nb} (O_{nb}: non-bridging oxygen) stretching vibrations in TiO_4 units. Thus the random distribution of distorted TiO_4 and AlO_4 tetrahedra connected to different phosphate structural units may be responsible for the increase in the width of this peak. An additional peak 'E' at ~ 620 cm^{-1} (in NATP2) starts developing with addition of TiO_2. The intensity of this peak increases with increasing TiO_2. Based on previous studies, this peak is assigned to the stretching vibrations of Ti-O bonds in TiO_6 units [139,142].

Figure 3.10(c) shows the Raman spectra in high frequency range 850-1300 cm^{-1} where, the different peaks are marked as 'H' through 'L'. Inset of Figure 3.10(c) shows the shift in these peaks with TiO_2 content. The NATP0 glass shows the most intense peak at ~1160 cm^{-1} (peak 'K') and a relatively less intense peak at ~1277 cm^{-1} (peak 'L'). The line profile of the band (constituting peaks 'K' and 'L' in NATP0) is systematically altered as the concentration of TiO_2 is increased. The symmetric and asymmetric stretching vibrations of Q^2 structural units of 'P' (PO_2 groups) appear at 1155 and 1280 cm^{-1}, respectively [117,143].

Thus, the peaks 'K' and 'L' are assigned to the symmetric and asymmetric stretching vibrations of Q^2 structural units of 'P'. The peak 'L' is observed to show a red shift from 1273 cm^{-1} (for NATP0) to 1174 cm^{-1} (for NATP20). The peak 'K' appearing at 1163 cm^{-1} (for NATP0) also shows a red shift up to 1147 cm^{-1} (for NATP5), but to a lesser degree than peak 'L'. At x = 10 mol% and beyond, this peak disappears completely and is taken over by the shoulder peak 'J'.

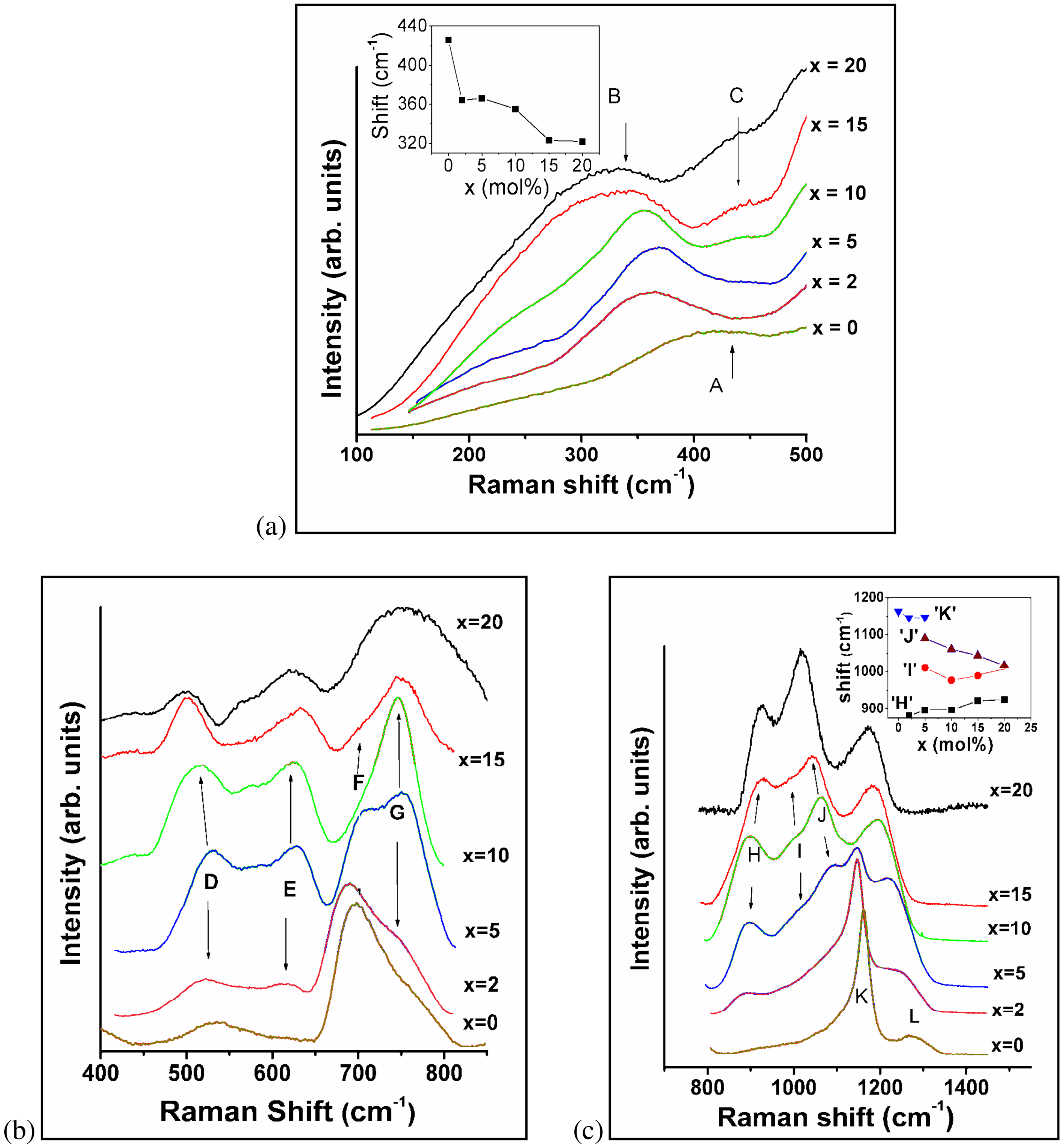

Figure 3.10: Raman spectra of NATP glasses having x mol% TiO_2 (a) Low frequency (200-400 cm^{-1}) Raman spectra; inset shows the shift of peak 'A' as a function of x (TiO_2 content), (b) Medium frequency (400-800 cm^{-1}) Raman spectra, (c) High frequency (800-1400 cm^{-1}) Raman spectra; inset shows the shift of various peaks as a function of x (TiO_2 content).

At a higher concentration of TiO_2, the shoulder at the left hand side of peak 'K' (in NATP2), develops into well defined peaks 'I and J'. For the NATP5 glass, peaks 'I and J' appear at ~1010 cm^{-1} and ~1090 cm^{-1} respectively. For TiO_2 above 10 mol%, these peaks are further intensified, and the peak 'K' (quite intense at x = 0 mol%) is completely diminished. The peaks ('I' and 'J') in NATP10 are red shifted to ~980 and 1060 cm^{-1}. The line profiles in NATP15 and NATP20 have completely changed from that of NATP0. At x = 15 mol%, the intensity of peak 'I' is more as compared to that of peak 'J' and therefore the combination peak ('I' and 'J') appears as a single asymmetric peak at ~1040 cm^{-1}. For NATP20 glass, there is a considerable overlap between peak 'I' and peak 'J' and appears as a single peak at 1015 cm^{-1}. The Q^1 units of pyrophosphate have Raman peaks in the range ~1050-1010 cm^{-1} [139], similar to what we have observed in the form of peaks 'I' and 'J'. The extinction of 'K-L' band together with the evolution of 'I' and 'J' peaks indicate that most of the Q^2 structural units are being gradually converted into Q^1 structural units. An additional peak 'H' at ~ 880 cm^{-1} (in NATP2) is evolved with addition of TiO_2. This peak for NATP5 and NATP10 is shifted to ~900 cm^{-1} and finally to ~925 cm^{-1} for NATP15 and NATP20. The intensity of this peak increases with increasing TiO_2. Therefore, this peak is attributed to Ti-O stretching vibrations in TiO_4 units [139,142].

This peak shows blue shift [inset of Figure 3.10(c)]. At lower content of TiO_2, Ti-O-P linkages exist but as TiO_2 content increases these Ti-O-P linkages are replaced by more of Ti-O-Ti linkages. In Ti-O-P linkages, the Ti-O bond strength is reduced compared to Ti-O bond strength in Ti-O-Ti linkages due to different charges of Ti and P (+4 and +5 respectively). As a result peak 'H' is shifted towards higher frequency, as more and more Ti-O-Ti linkages formed. The systematic red shift in 'K' and 'L' peaks, suggests redistribution of π bonding of terminal P=O bond, among various spectroscopically equivalent NBO's as the Q^2 units are systematically being converted into Q^1 units [144]. In other words the ionicity of PO bonds increases with an increase in TiO_2 content in the glasses.

3.3.4.3 FTIR spectroscopy

Room temperature infra-red spectra of all the NATP glass samples are shown in Figure 3.11. For the glass without TiO_2 (x = 0 mol%), five absorption bands approximately at 1280, 1200, 1120, 900, 750 cm^{-1} are observed. Up to 10 mol% TiO_2, the IR patterns essentially remain the same except the intensity of bands around 1200 and 1280 cm^{-1}. The intensity of 1280 band keeps on diminishing and finally disappears at x = 10 mol%, while that around 1210 cm^{-1} becomes pronounced. Above 10 mol% TiO_2, the IR spectra change significantly and the band at 900 cm^{-1} disappears with the development of bands around approximate 1000, 1070 and 1170 cm^{-1}.

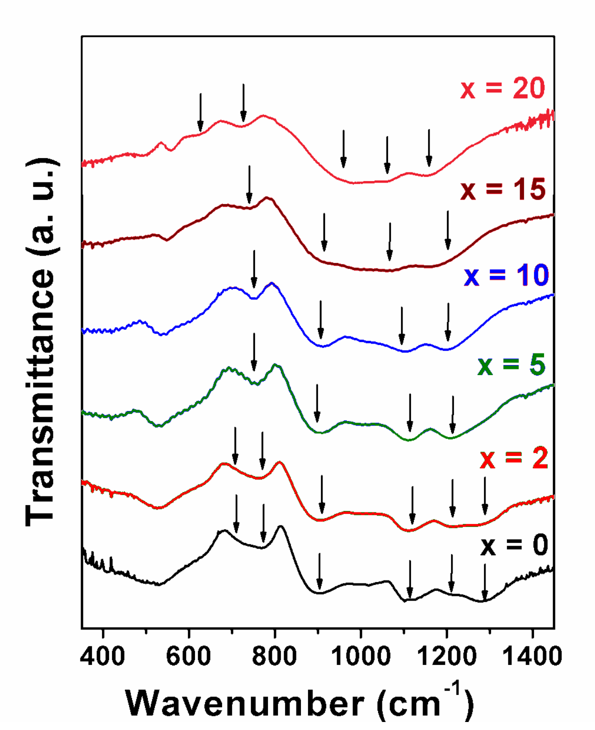

Figure 3.11: FTIR spectra of NATP glasses.

The band at 1280 cm^{-1} has been attributed to the asymmetric stretching vibration of PO_2 groups (equivalent to Q^2 structural units) [145]. Both the absorptions bands around 1200 and 1120 cm^{-1} are assigned to asymmetric stretching of PO_3 groups (chain end group equivalent to Q^1 structural units). According to Montagne et al [146] the band around 1120 cm^{-1} is due to the vibration of PO_3 groups with a smaller number of aluminium neighbours than those PO_3 groups which are vibrating around 1200 cm^{-1}. The band at 900 cm^{-1} is assigned to asymmetric stretching of P-O-P bridges [145-147]. The bands at 700 and 750 cm^{-1} are due to the symmetric stretching of P-O-P bridges [147-148]. A reduction in the intensity of the band at 1280 cm^{-1}, while an increase in that around 1200 cm^{-1} indicate that as TiO_2 content increases, the phosphate network depolymerize with the conversion of PO_2 groups (Q^2 structural units) into PO_3 groups (Q^1 structural units). This observation is in agreement with the NMR results that suggested a conversion of Q^2 structural units to in Q^1 structural units. Above 10 mol% TiO_2, the band at 900 cm^{-1} (corresponding to Q^1 structural units) disappears with the development of bands approximately around 1000, 1070 and 1170 cm^{-1} characteristic of the isolated PO_4 groups (equivalent to Q^0 structural units) connected to different cations. These changes suggest that the phosphate network is highly depolymerized with isolated orthophosphates, which is in agreement with the NMR results.

MAS-NMR, Raman and FTIR spectroscopic studies revealed that the substitution of P_2O_5 with TiO_2 up to 10 mol% depolymerizes the phosphate glass network by a systematic conversion of Q^2 structural units into Q^1. Even though Q^2 to Q^1 conversion occurs by breaking of P-O-P linkages, the formation of P-O-Ti (along with P-O-Al) bonds provide cross linking between 'P' structural units, which make the glass network more rigid. Therefore the net effect is an increase in T_g, density and MH, and a decrease in molar volume and TEC, up to 10 mol% TiO_2. For the addition of TiO_2 above 10 mol%, the Q^1 structural units get converted into Q^0 units and TiO_4 structural units leading to a Ti-O-Ti based network linked with discrete PO_4 structural units. Further as the bond energy of Ti-O-Ti linkages is lesser than P-O-P and P-O-Ti linkages, the formation of Ti-O-Ti type network connected with discrete 'P' structural units is expected to weaken the glass network. This is consistent with the decrease in T_g, density and MH, and an increase in molar volume and TEC for the glasses containing TiO_2 more than 10 mol%. The changes observed in the nature of the linkages present in the glass are also clear from the variation in the $E_{optical}$ values and wavelength corresponding to the emission maxima of the glass samples as a function of composition. When the strong P-O-P linkages are replaced by progressively weaker P-O-Ti or Ti-O-Ti linkages, the optical gap is expected to reduce. This will eventually lead to a decrease in the energy corresponding to the localized luminescence centres.

3.3.5 Surface degradation studies

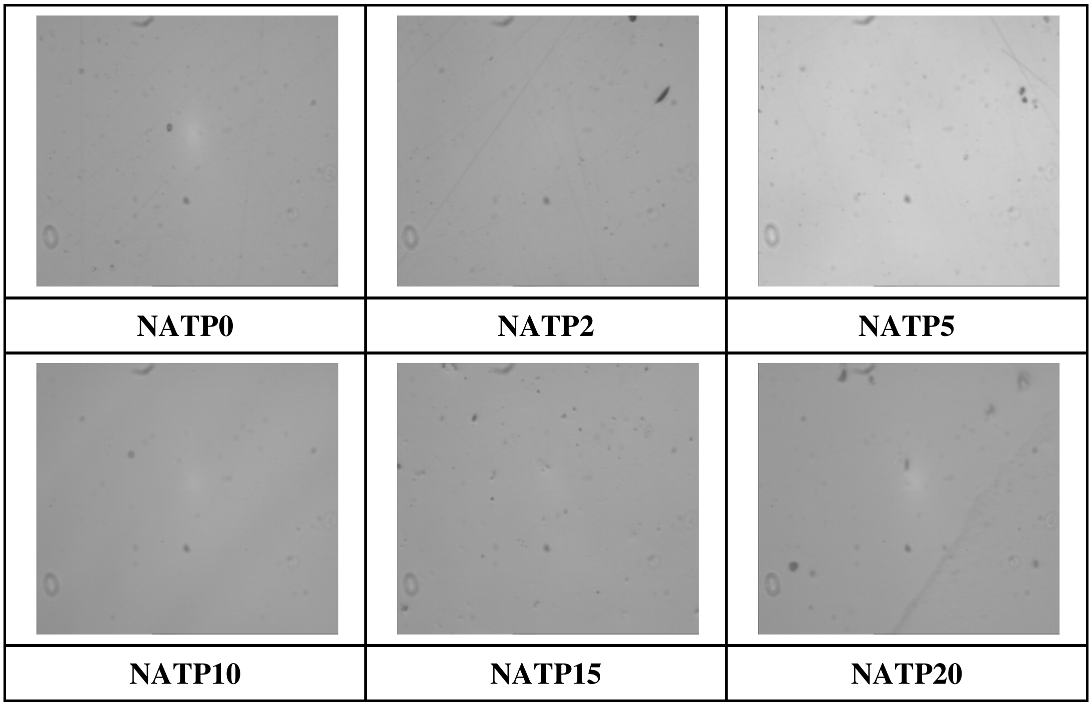

NATP0 **NATP2** **NATP5**

NATP10 **NATP15** **NATP20**

Figure 3.12: Initial optical photographs of NATP glass surfaces at 10x magnification.

Optical photograph of polished surfaces of all the NATP glasses are shown in Figure 3.12. We found no change in the surface of these glasses after exposure in air ambient for several months. However, after a long time exposure of the NATP0 glass (x = 0) resulted in the degradation of glass surface compared to other TiO_2 containing NATP glasses. Optical photograph of the same glass samples after an exposure to air ambient for 2 years are shown in Figure 3.13. These photographs clearly indicate a higher resistance of the NATP glasses having 5 mol% or higher amount of TiO_2 confirming the higher chemical durability of NATP glasses compared to NAP glass

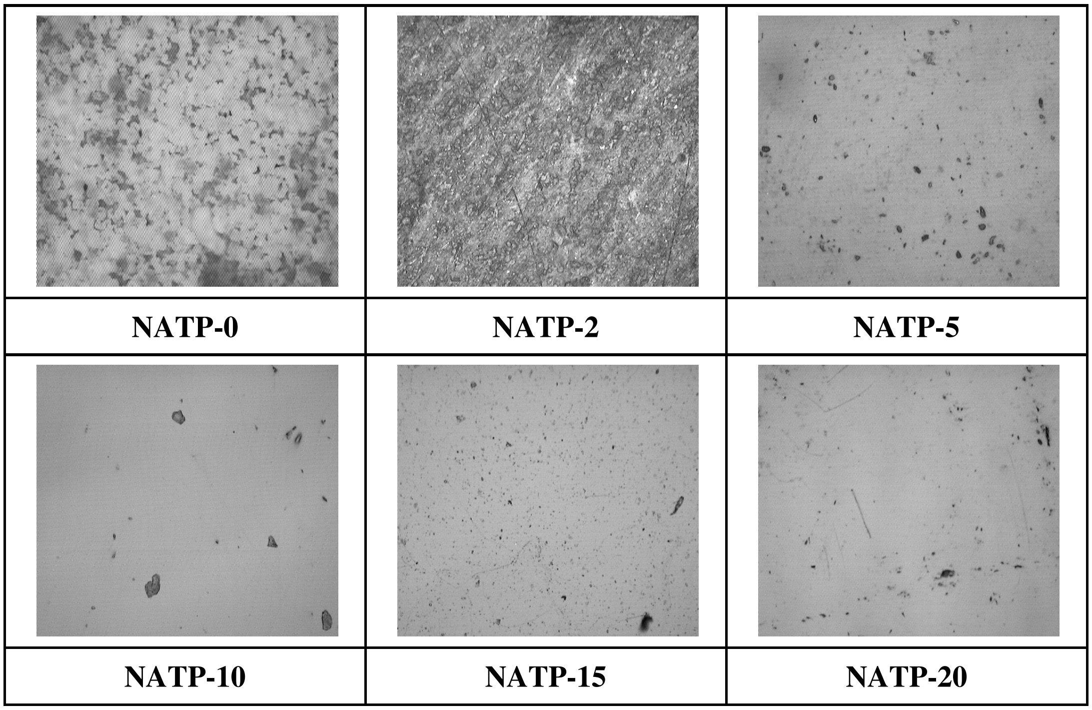

NATP-0 **NATP-2** **NATP-5**

NATP-10 **NATP-15** **NATP-20**

Figure 3.13: Optical photographs of different NATP glass surfaces, after an exposure to open air ambient for 2 years, at10x magnification.

3.4 Conclusion

Raman, FTIR and ^{31}P MAS-NMR studies confirm that the addition of TiO_2 in the NATP glass results in the progressive conversion of Q^2 structural units into Q^1 (up to 10 mol%) and Q^0 structural units (more than 10 mol%). The Raman spectra revealed that TiO_2 enters in the glass network in the form of octahedral and tetrahedral structural units and at a higher content of TiO_2 (for $x > 10$ mol%), existence of tetrahedral structural units of Ti are more favourable. Cross-linking provided by P-O-Ti and P-O-Al bonds between shortened discrete 'P' structural units (for $x \leq 10$ mol%) results into a more strong and rigid glass network.

Based on thermo-physical and structural studies it is concluded that TiO_2 behaves as a network modifier upto 10 mol% and above that a Ti-O-Ti based network connected with discrete PO_4 structural units exist in the glass. Al coordination changes significantly from octahedral to tetrahedral for glass samples having more that 10 mol% TiO_2. Above 10 mol% TiO_2 the incorporation depolymerization of glass network is significant with the formation of Ti-O-Ti type of linkages along with Q^0 structural units of P at the expense of strong P-O-P linkages leading to a less rigid structure. Variation in T_g, MH, density, TEC and $E_{optical}$ values for these glasses are in accordance with the structural changes taking place in the glass as a function of composition.

Chapter 4

Studies on Strontium Zinc Silicate Glasses/Glass-ceramics

4.1Introduction

The development of high temperature sealant materials is an important field of research due to their possible use in planar solid oxide fuel cells (p-SOFC) and planar solid oxide electrolyzer cells (p-SOEC) [149-152]. The planar design of SOFC has an advantage of high power generation efficiency with ease in fabrication over the tubular design. But it also requires stable, gas tight seals at high temperatures to prevent mixing and leakage of fuel gas and oxidant [153-156]. Alkaline earth based silicate glasses and glass-ceramics are promising materials as high temperature sealants for such applications [150-152,157]. Glasses based on barium silicate or barium aluminosilicate composition have been investigated in the recent past by many researchers [158-161]. These materials have requisite thermal properties to make suitable seals to different cell components of the SOFC. However, issues concerning the long-term thermal and chemical stabilities with the fuel cell materials have been raised due to the formation of $BaCrO_4$ phase as a result of interfacial reactions of BaO with Crofer-22-APU (most widely used interconnect material for SOFC), which is detrimental to the long-term stability of seal [152,162-165]. Another limitation of these sealant materials is the formation of the monocelsian ($BaAl_2Si_2O_8$) and its polymorph hexacelsian crystalline phases having low TEC. The difference between TEC of these two polymorphic phases (TEC of monocelsian phase: 22.9 x 10^{-7}/°C and TEC of hexacelsian phase: 80 x 10^{-7}/°C) develops thermal stresses in the seal [165]. Because of these shortcomings there is an increasing need to search new glass or glass-ceramics for high temperature sealing applications. Other alkaline earth oxides like, SrO, MgO based silicate systems have been comparatively less explored as a sealant for SOFC [166-169]. In order to minimize/prevent the chromate phase formation at the interface, strontium zinc silicate based glass system has been investigated in the present work to develop high temperature sealants for SOFC. Recently, Zhang et al [170] have reported the role of ZnO in the reduction of chromate formation at the interface. At high operating temperatures of SOFC (800-850°C) the glass gets converted into glass-ceramic due to nucleation and growth of crystalline phases in the glassy matrix. The kinetics of growth and microstructure of these crystalline phases affect the properties of sealant material and thereby influence the working of SOFC. Knowledge of crystallization kinetics and mechanism is also important to develop suitable materials and processes for the glass-ceramic sealant [171]. Therefore, crystallization kinetics of a few glasses has also been studied. Glasses and glass-ceramics in the strontium zinc silicate (SZS) system have also been studied for various other technological applications like dielectrics, optical connectors and as prospective bone graft materials [172-176].

In this chapter, the thermo-physical properties, crystallization kinetics and structural aspects of SZS glasses and glass-ceramics with different additives are described. To demonstrate the suitability of the material as SOFC sealants, the preparation of hermetic seals with SOFC components has also been described.

4.2 Experimental

4.2.1 Synthesis of glass samples

Glasses of different composition as listed in Table 4.1 in the SrO-ZnO-SiO_2 (SZS), system with different additives like B_2O_3, Al_2O_3, V_2O_5/Cr_2O_3, TiO_2 and Y_2O_3, were prepared by melt-quench method. Analytical grade $Sr(NO_3)_2$ (MERCK, India), B_2O_3 (MERCK, Germany), SiO_2 (Loba Chemie, India), and ZnO, Al_2O_3, V_2O_5, Cr_2O_3, TiO_2 and Y_2O_3 (all from S. D. Fine Chem Ltd., India), were used as starting precursors. The initial charge (~100 gm) was prepared by thoroughly mixing and grinding for 20-30 min in a mortar pestle. This was calcined in an alumina crucible by heating first at temperature 620°C for 4 h to decompose $Sr(NO_3)_2$ and then at 750°C for 15 h. This charge was re-ground and re-calcined in the same manner. Glasses were prepared following the procedure as described in chapter 2. Depending on the composition, glass charges were melted in the temperature range 1500-1600°C in the air ambient. The glass was then annealed in the temperature range of 600-650°C for 4 h. Discs of bulk glasses were used for crystallization and other measurements.

4.2.2 Formation of glass-ceramics samples

Based on DTA data, SZS glasses either in disc or pellet forms, were crystallized by one step heat treatment at their respective crystallization temperatures for 2 h. A few representative glasses namely SZS-1 and SZS-9 were also crystallized according to different heat treatment schedules (at different temperatures for different durations).

4.2.2.1 DTA

Crystallization temperature of glasses was determined from DTA as described in chapter 2. The non isothermal experiments were performed on ~50 mg powdered glass samples (particle size in the range of 75-210 μm), using a heating rate of 10°C/min. To study the crystallization kinetics of glasses, the DTA scans were also recorded from room temperature to 1050°C in an air atmosphere with heating rates of 5, 10, 15 and 20°C/min.

4.2.3 Thermo-physical characterization

T_g, T_{ds} and TEC of all the glass/glass-ceramics were measured using TMA. Flat circular discs of diameter 10 mm and thickness 3-4 mm were used for the measurement. TEC being reported is the average in a temperature range from 30°C to T_g. Density was measured at room temperature by Archimedes principle using DM water as an immersion liquid with an accuracy of ±0.03 g/cm^3. The MH of glass/glass-ceramics samples was measured using the Vickers indentation technique. Indentation was obtained by applying a 50 g load for 5 s.

4.2.4 XRD

The amorphous nature of SZS glasses and various crystalline phases in the glass-ceramics samples were identified using powder XRD with Cu K_α as X-ray source. Diffractograms were recorded in a 2θ range from 10 to 70° with a speed of 0.5°/min (steps of 0.01°).

4.2.5 Structural characterization

Structural studies of glasses were carried out using Raman, FTIR and NMR spectroscopic techniques. Raman spectra on powdered glass and glass-ceramics samples were recorded using a homemade Raman spectrometer with ~532 nm wavelength as an excitation source [100]. Details of the measurement and data correction are described in chapter 2. Infrared spectra of all glasses were recorded over the frequency range 400-4000 cm^{-1} with a resolution of ~4cm^{-1} as detailed in chapter 2.

^{29}Si, ^{27}Al and ^{11}B MAS-NMR spectra for representative SZS glasses and glass-ceramics were recorded at 2.34, 18.8 and 18.8T, respectively, on Bruker AVANCE spectrometers. Probes used were: 3.2 mm probe at 20 kHz spinning speed for ^{11}B and ^{27}Al and a 7 mm probe at 4 kHz spinning speed for ^{29}Si. Powdered samples (~3 mg, 5 mg and 30 mg for 3.2 mm, 4 mm rotors and 7 mm rotors, respectively) used for these measurements were packed densely in ZrO_2 rotors to ensure stable spinning. The Larmor frequencies were 19.8, 161.9 and 256.8 MHz for ^{29}Si, ^{27}Al and ^{11}B, respectively. For ^{11}B, the pulse duration was 2 μs (π/6) and the recycle delay was 10 s. For ^{27}Al the pulse duration was 1.5 μs (π/8), and the recycle delay was 2 s. For ^{29}Si, the pulse duration was 1.6 μs (π/5) and the recycle delay was 180 s. All relaxation delays were chosen long enough to enable complete relaxation at the respective fields. The ^{29}Si chemical shifts are relative to tetramethyl silane (TMS) at 0 ppm, those of ^{27}Al are relative to $AlCl_3$ at 0 ppm and those of ^{11}B nuclei are given relative to BPO_4 at 3.6 ppm. The deconvolution of NMR spectra was carried out using origin software and peaks were fitted using the Gaussian line shape.

4.2.6 Microstructural characterization

Microstructure of glasses/glass-ceramics and interface of seal between glass-ceramics and SOFC components were investigated using SEM as described in chapter 2. Elemental line scanning was done across the interface of seals using EDS to find out the inter-diffusion of elements.

4.2.7 Bonding properties and interface studies

Adhesion/bonding property of a few glasses with YSZ and Crofer-22-APU was also investigated according to the method describe in chapter 2. Seals of a few representative SZS glasses with YSZ and Crofer-22-APU were fabricated and tested for vacuum integrity following the process described in chapter 2.

Table 4.1: Chemical compositions (in wt.% and mol%) of investigated SZS glasses.

Glass ID	Composition	SrO	ZnO	SiO_2	B_2O_3	V_2O_5	Cr_2O_3	Al_2O_3	TiO_2	Y_2O_3
SZS-1	(wt.%)	51	9	40	-	-	-	-	-	-
	(mol%)	38.8	8.7	52.5	-	-	-	-	-	-
SZS-3	(wt.%)	51	9	30	5	-	2	3	-	-
	(mol%)	40.5	9.1	41	5.9	-	1.1	2.4	-	-
SZS-4	(wt.%)	51	9	30	10	-	-	-	-	-
	(mol%)	39.5	8.9	40.1	11.5	-	-	-	-	-
SZS-6	(wt.%)	49.1	8.9	29.2	8.5	4.4	-	-	-	-
	(mol%)	39	9	40	10	2	-	-	-	-
SZS-7	(wt.%)	49.4	9	29.4	8.5	-	3.7	-	-	-
	(mol%)	39	9	40	10	-	2	-	-	-
SZS-8	(wt.%)	48.8	8.8	27.6	6.7	-	3.7	2.5	1.9	-
	(mol%)	39	9	38	8	-	2	2	2	-
SZS-9	(wt.%)	48.1	9.4	27.9	1.6	-	3.7	2.4	1.9	5.2
	(mol%)	40	9	40	2	-	2	2	2	2

4.3 Results and discussion

Transparent and bubbles/inclusion free glasses were obtained for all the investigated compositions. Glasses were colourless except those having Cr_2O_3 or V_2O_5 oxides. Glasses having Cr_2O_3 were dark greenish in colour that might be due to the presence of Cr^{3+} ions and glasses having V_2O_5 were light greenish in colour due to the presence of V^{3+} ions [177].

4.3.1 Thermo-physical properties

Various thermo-physical properties of glasses are listed in Table 4.2. It is clear from Table 4.2 that investigated glasses have densities in the range of 3.66-3.78 x 10^3 kg/m^3 and MH in the range of 6.26-7.17 GPa. The MH of all glasses is high, reflecting higher bond strength thereby indicating a higher load withstanding capability of these glasses [178]. Molecular weights of B_2O_3 and Al_2O_3 are higher compared to SiO_2 therefore, the density of SZS glasses increases with the addition of these oxides, for SZS-3 and SZS-4 glasses. The density remains almost the same with the addition of V_2O_5 along with B_2O_3 for glass SZS-6. It can be explained on the basis of two opposing effects; higher molecular weight increases the density but more open glass network due to a network modifying effect of V_2O_5, decreases the density.

Table 4.2: Thermo-physical properties of investigated SZS glasses.

Glass ID	$T_g \pm 2$ (°C)	$T_{ds} \pm 2$ (°C)	TEC ± 5% (10^{-7}/°C) (30°C-T_g) Glass	TEC ± 5% (10^{-7}/°C) (30-900°C) Glass-ceramics	$T_p \pm 2$ (°C)	MH ± 5% (GPa)	$\rho \pm 0.03$ (10^3 kg/m^3)
SZS-1	722	745	108	112	920	6.26	3.68
SZS-3	671	707	112	104 (30-700°C)	885	6.26	3.78
SZS-4	643	676	105	115	878	7.13	3.71
SZS-6	640	664	115	118	865	7.17	3.66
SZS-7	666	697	115	114	910	7.05	3.73
SZS-8	668	698	112	115	915	7.02	3.72
SZS-9	730	750	111 (200-700°C)	116 (200-900°C)	930	6.33	3.88

It is observed that with the addition of B_2O_3, T_g and T_{ds} reduce and TEC remains almost the same. Since B_2O_3 decreases the viscosity of the glass, it results in the reduction of T_g and T_{ds}. With the addition of V_2O_5 a further reduction in the T_g and T_{ds} for the SZS-6 glass was also observed. This is because V_2O_5 reduces the surface tension of liquid and therefore reduces the T_g and T_{ds}. Addition of V_2O_5 along with B_2O_3 increases the TEC of the glass. The TEC for the investigated glasses are in the range of 105-115 x 10^{-7}/°C (30°C-T_g), which is closely matched with the TEC of other SOFC components like interconnect, electrodes and electrolytes [168,179]. It is found that TEC of glasses after a 2h crystallization did not change much as shown in Table 4.2. Softening temperature for all the glass-ceramics was observed higher than 1000°C which is advantageous for high temperature sealants.

4.3.1.1 Viscosity

The viscosity of glasses was also calculated from the dilatometric data using a method based on the Vogel-Fultcher-Tamman (VFT) equation as reported by Wang et al [180]. Although this is not a very accurate method but it is very convenient and significant one for the viscosity measurement. According to the simple liquid theory (Mott and Gurney) [180], there is a relationship between pseudo-critical temperature (T_k) and the absolute melting point (T_m)

$$\frac{T_k}{T_m} = \frac{2}{3} \tag{4.1}$$

Beaman [[181,182] showed that this rule could be applied on glass/glass-ceramics and there the terms T_k and T_m of Eq.(4.1) can be replaced with T_g and liquid temperature (T_l), respectively of the glass. Thus Eq.(4.1) becomes

$$\frac{T_g}{T_l} = \frac{2}{3} \tag{4.2}$$

Hence T_l can be calculated using the value of T_g. The viscosity (η) values at T_g , T_{ds} and T_l are fixed and independent of materials and are reported [183] to be $10^{13.6}$, $10^{11.3}$ and 10^6 dPa.s, respectively, at these temperatures. Then, according to VFT equation [184,185].

$$\log\eta = A + \frac{B}{T - T_0} \tag{4.3}$$

where A, B and T_0 are all constants.

Table 4.3: Constant of VFT equation and viscosity values at 950°C and 1000°C for SZS glasses.

Glass	A	B	T_0	η at 950°C (dPa.s)	η at 1000°C (dPa.s)
SZS-1	5.04	535.21	932.44	6.88	6.6
SZS-4	4.34	923.82	816.19	6.61	6.37
SZS-6	4.46	843.54	815.75	6.53	6.30
SZS-8	4.9	789.54	853.42	6.72	6.47

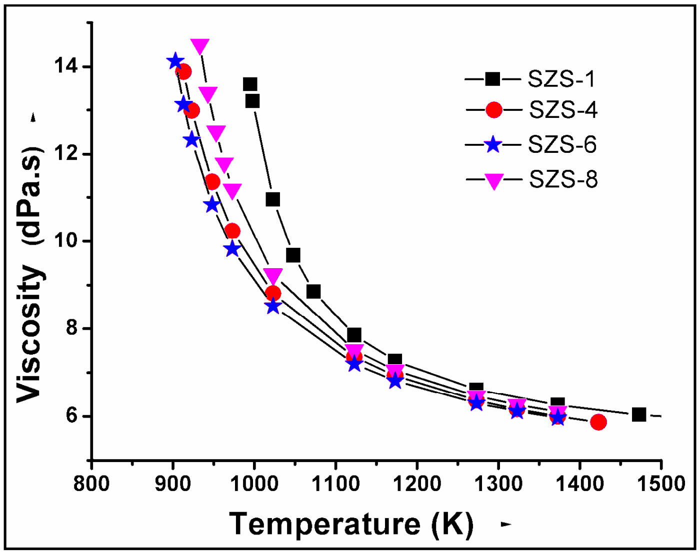

Figure 4.1: Temperature dependence of viscosity of SZS glasses.

Using the value of T_g, T_d and T_s from Table 4.2 in Eq.(4.3) constants A, B and T_0 were determined for SZS glasses and listed in Table 4.3. The viscosity of glasses at different temperature was obtained using the calculated constants and obtained viscosity-temperature curve of SZS glasses, are shown in Figure 4.1. The viscosity of SZS glasses at the sealing temperature (950°C) (Table 4.3) are well within the required range of viscosity (10^6 to 10^9 dPa.s) for sealing applications [157].

It is clear from Figure 4.1 that the viscosity varies more steeply with temperature for SZS-1 glass compared to other SZS glasses. It is required that the viscosity of the glass sealant should vary smoothly with temperature around sealing temperature for a better joining. The variation in the viscosity with temperature is smoother for SZS-6 glass in all the investigated SZS glasses which is advantageous for sealing application.

4.3.2 DTA analysis

DTA plots of investigated glasses are shown in Figure 4.2. Endothermic base line shift in the DTA trace indicates the T_g and exotherm indicates the crystallization temperature (T_p). It is clear from Figure 4.2 that for the SZS-1 glass exotherm comprises of 2 overlapping peaks around 890°C and 930°C. This indicates the crystallization of two phases in the SZS-1 glass. T_g and T_p reduce significantly with the partial replacement of SiO_2 by B_2O_3. B_2O_3 reduces the viscosity of the glass and increases the diffusion of ions. This reduces the T_g and causes crystallization of glass at a lower temperature. Addition of V_2O_5 in the SZS-6 glass further reduces T_g and T_p. V_2O_5 is known for its ability to reduce the surface tension of glasses, therefore it seems that presence of this oxide in the SZS-6 glass resulted in a lower thermodynamic free energy barrier for the crystallization. It is found that addition of Cr_2O_3 in place of V_2O_5 in the SZS-7 glass results in higher T_g and T_p. Chromium generally exists in Cr^{3+} and Cr^{6+} states in glassy matrices. Of these Cr^{3+} in octahedral coordination acts as a network modifier whereas Cr^{6+} ions as CrO_4^{2-} structural units that takes part in the network formation [186,187]. Dark green colour of Cr_2O_3 containing SZS glasses indicates the presence of Cr^{3+} ions in the glass. However, observed variation in T_g, T_{ds} and T_p indicate that most of Cr_2O_3 might be playing the role of network former in the form of Cr^{6+} ions in the SZS glass [186,187]. For other SZS glasses like SZS-3, SZS-8 which contains Cr_2O_3 and Al_2O_3, T_g is found to be higher. For SZS-9 glass also T_g and T_p are quite high. This might be due to the lesser amount of B_2O_3 and network forming behavior of the added additives. Presence of Al_2O_3 also retards the crystallization of the glass.

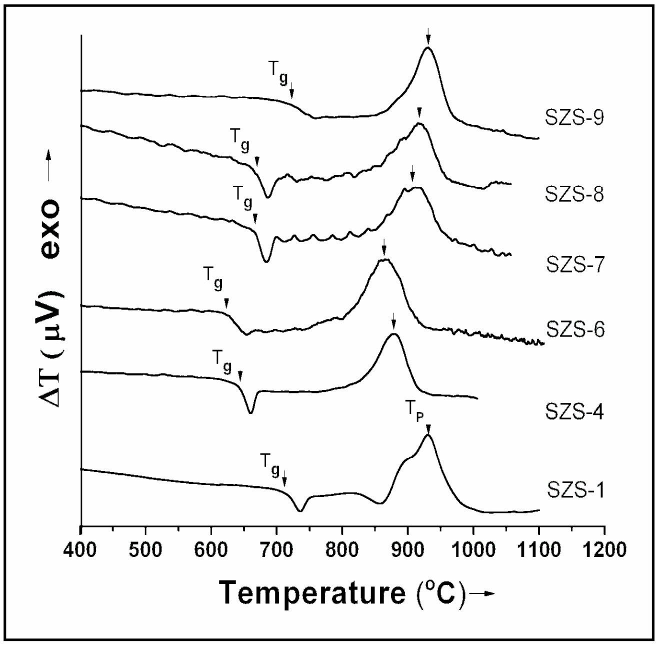

Figure 4.2: DTA plots of SZS glasses at a heating rate of α = 10°C/min.

4.3.3 X-ray diffraction analysis

A characteristic broad hump at around $2\theta = 28°$ in the powder XRD pattern of SZS glasses confirmed the amorphous nature of the prepared glasses. Figure 4.3 shows the X-ray diffractograms of SZS-1 glass and glass-ceramics produced by heat treatment schedules as given in Table 4.4. As a result of the crystallization, the physical appearance of the glass changes from clear, transparent and colourless to white tinged translucent and finally to white and opaque.

Table 4.4: Heat treatment schedules and crystalline phases of the SZS-1 glass-ceramics.

Glass-ceramic ID	Heating Temp. (°C)	Dwell Time (h)	Crystalline Phases
SZS1-GC-1	750	1	amorphous
SZS1-GC-2	750	5	amorphous
SZS1-GC-3	820	1	amorphous
SZS1-GC-4	820	2	SiO_2, $ZnSiO_3$, $Sr_3Si_3O_9$, $Sr_2ZnSi_2O_7$
SZS1-GC-5	850	2	Mainly $Sr_3Si_3O_9$, $Sr_2ZnSi_2O_7$ and Minor amount of SiO_2, $ZnSiO_3$
SZS1-GC-6	925	2	$Sr_3Si_3O_9$, $Sr_2ZnSi_2O_7$

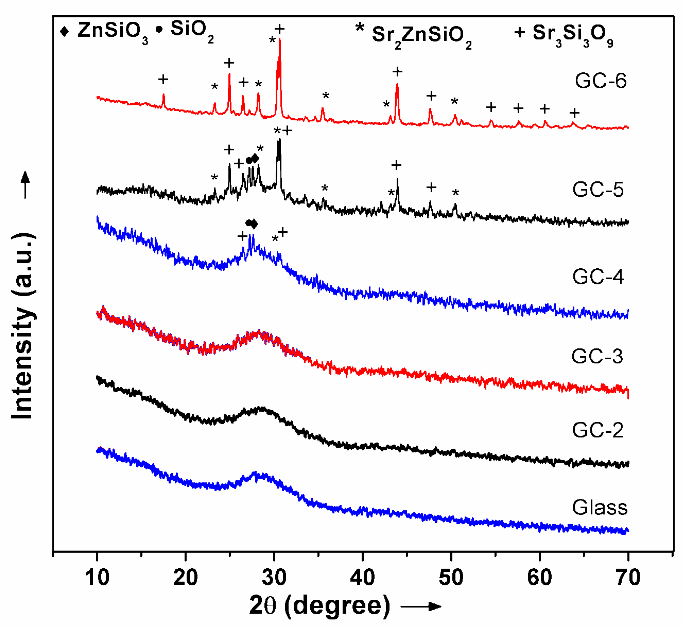

Figure 4.3: X-ray diffractograms of SZS-1 glass-ceramics.

The samples heat treated at 720°C for 1 h, 750°C for 5 h and 820°C for 1 h are amorphous. In the sample heat treated at 820°C for 2 h, $ZnSiO_3$ (JCPDS No: 83-2473), SiO_2 (JCPDS No: 83-2473), Sr_2ZnSiO_2 (JCPDS No: 39-0235) and $Sr_3Si_3O_9$ (JCPDS No: 77-0233) crystalline phases are evident in the X-ray diffractograms (Figure 4.3). In the glass sample heat treated at 850°C for 2 h, the fraction of $ZnSiO_3$ and SiO_2 decreases in comparison to Sr_2ZnSiO_2 and $Sr_3Si_3O_9$. For the glass sample heat treated at 925°C for 2 h, only Sr_2ZnSiO_2 and $Sr_3Si_3O_9$ phases are evident. $Sr_3Si_3O_9$/$SrSiO_3$ [188] and $Sr_2ZnSi_2O_7$ [189] are quite stable phases while SiO_2 and $ZnSiO_3$ (o) [190] are reported as metastable phases. Initially SiO_2 and $ZnSiO_3$ (o) metastable phases crystallize in the glass and later only more stable $SrSiO_3$/$Sr_3Si_3O_9$ and $Sr_2ZnSi_2O_7$ phases crystallize. It is postulated that as temperature and time increase during the crystallization both SiO_2 and $ZnSiO_3$ (o) metastable phases converted to more stable $Sr_3Si_3O_9$ and $Sr_2ZnSi_2O_7$ phases, respectively according to the following reactions [191]:

$$SiO_2 \text{ (hexagonal)} + SrO \text{ (glass)} \longrightarrow SrSiO_3 \text{ (monoclinic)} / Sr_3Si_3O_9 \text{ (monoclinic)}$$

$$ZnSiO_3 \text{ (orthorhombic)} + 2SrO \text{ (glass)} + SiO_2 \text{ (glass)} \longrightarrow Sr_2ZnSi_2O_7 \text{ (tetragonal)}$$

XRD patterns for all other SZS glass-ceramics heat treated at their crystallization temperatures for 2h are presented in Figure 4.4. It is observed that at crystallization temperature (925°C) two crystalline phases $Sr_2ZnSi_2O_7$ and $Sr_3Si_3O_9$ are formed for SZS-1 glass. For glass SZS-4 also both the phases crystallize but intensity of peaks corresponding to $Sr_3Si_3O_9$ is very less compared to that of peaks of the $Sr_2ZnSi_2O_7$ phase. This indicates the suppression of crystallization of this phase. For the SZS-6 glass mainly the $Sr_2ZnSi_2O_7$ phase crystallized. For the SZS-7 glass the $Sr_3Si_3O_9$ crystallized as a major phase with a small amount of $Sr_2ZnSi_2O_7$. XRD results indicate that in the base composition (SZS-1) $Sr_2ZnSi_2O_7$

and $Sr_3Si_3O_9$ phases crystallize and addition of additives (B_2O_3/V_2O_5) suppress the crystallization of $Sr_3Si_3O_9$ phase. Unlike this, additive Cr_2O_3 enhances the formation of $Sr_3Si_3O_9$ phase.

Figure 4.5 shows the XRD patterns of SZS-9 glass-ceramics heat treated according to the schedule given in Table 4.5. All the peaks are analyzed with JCPDS files. It is observed that first $Sr_2ZnSi_2O_7$ phase crystallized and the amount of crystalline phase increases with increase in the dwell time at 950°C, as the intensity of peaks corresponding to the $Sr_2ZnSi_2O_7$ phase was found to increase. At a higher temperature (1100°C) or prolonged dwell at lower temperature (950°C) the $SrSiO_3$/$Sr_3Si_3O_9$ phase also crystallized.

Table 4.5: Heat treatment schedules and crystalline phases of the SZS-9 glass-ceramics.

Sample Name	Nucleation temperature (°C)	Dwell time (h)	Crystallization temperature (°C)	Dwell time (h)	Crystalline Phases
SZS9-GC1	800	2	-	-	$Sr_2ZnSi_2O_7$
SZS9-GC2	800	2	950	1	$Sr_2ZnSi_2O_7$
SZS9-GC3	800	2	950	2	$Sr_2ZnSi_2O_7$, $Sr_3Si_3O_9$
SZS9-GC4	800	2	1100	1	$Sr_2ZnSi_2O_7$, $Sr_3Si_3O_9$
SZS9-GC5	800	2	1100	2	$Sr_2ZnSi_2O_7$, $Sr_3Si_3O_9$
SZS9-GC6	-	-	950	50	$Sr_2ZnSi_2O_7$, $Sr_3Si_3O_9$
SZS9-GC7	-	-	1100	50	$Sr_2ZnSi_2O_7$, $Sr_3Si_3O_9$

Table 4.6 summarizes the different crystallization phases observed in SZS glass-ceramics. For glasses namely SZS-4 to SZS-9, the peak maximum of the diffraction peaks corresponding to $Sr_2ZnSi_2O_7$ phase shifted slightly to higher 2θ value. This has been

attributed to the partial substitution of Zn/Si sites by Al/B in $Sr_2ZnSi_2O_7$. In other words a solid solution formation is taking place in these glass-ceramics. The $Sr_2ZnSi_2O_7$ (Sr-Hardystonite) phase is a member of a melilite family of silicate mineral and $Sr_3Si_3O_9$ crystalline phase belongs to cyclo-silicate mineral group. Similar solid solution formation, among the members of melilite silicate minerals like hardystonite, gehlenite etc, has been previously reported in the literature [192,193].

It is reported that melilite silicate and cyclo-silicate phases have high TEC [194,195], high chemical durability, high insulating properties and high mechanical strength [192,196,197]. It is also reported that glass ceramics containing crystalline phases of theses silicate groups have high TEC [198]. Therefore, formation of these crystalline phases in all the SZS glass-ceramics is advantageous for their use in SOFC sealant application.

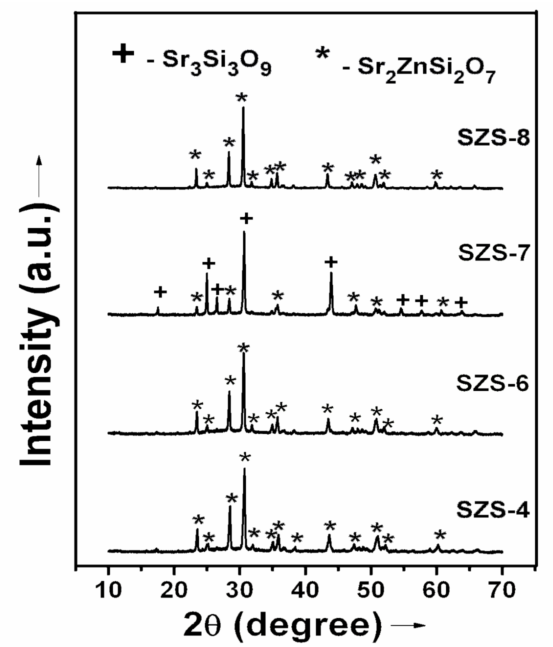

Figure 4.4: X-ray diffractograms of SZS glass-ceramics.

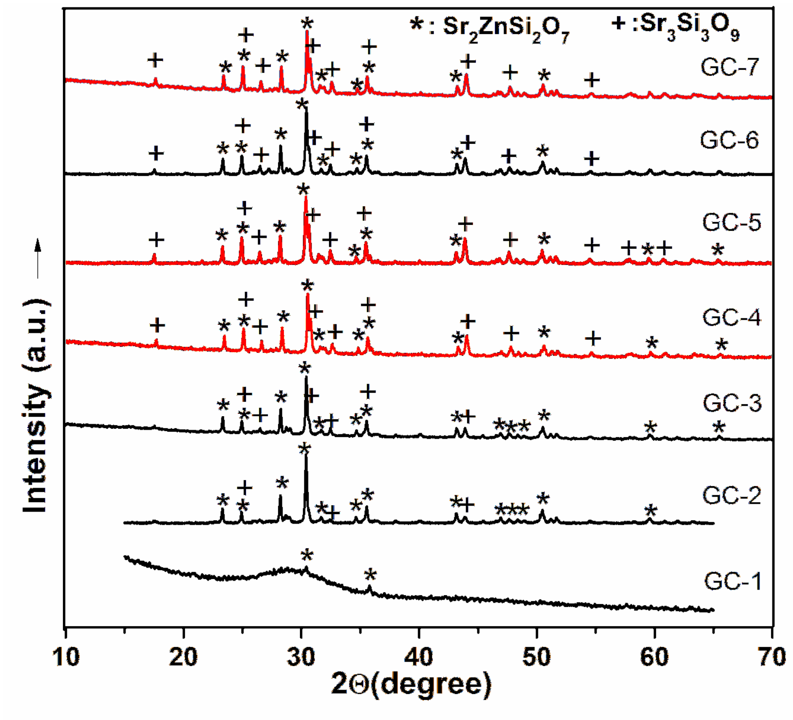

Figure 4.5: X-ray diffractograms of SZS-9 glass-ceramics.

Table 4.6: Crystalline phases in SZS glass-ceramics.

Glass ID	Crystalline phases in glass-ceramics
SZS-1	$Sr_2ZnSi_2O_7$, $Sr_3Si_3O_9$
SZS-3	$Sr_2ZnSi_2O_7$ solid solution, $Sr_3Si_3O_9$
SZS-4	$Sr_2ZnSi_2O_7$ solid solution , $Sr_3Si_3O_9$ (Minor)
SZS-6	$Sr_2ZnSi_2O_7$ solid solution, $Sr_3Si_3O_9$ (Minor)
SZS-7	$Sr_2ZnSi_2O_7$ solid solution, $Sr_3Si_3O_9$ (Major)
SZS-8	$Sr_2ZnSi_2O_7$ solid solution, $Sr_3Si_3O_9$
SZS-9	$Sr_2ZnSi_2O_7$ solid solution, $Sr_3Si_3O_9$

4.3.4 Structural studies of SZS glasses

4.3.4.1 Raman spectroscopy

Raman spectra of investigated glasses revealed the information regarding the modification in the structure of glasses with the addition of different additives as shown in Figure 4.6. Bands in the 700-1100 cm^{-1} region are characteristic of Si-O$^-$ stretching vibrations in different SiO$_4$ tetrahedra. The silica network is expressed in terms of Q^n structural units, where 'Q' represents the Si tetrahedron and 'n' the number of bridging oxygen per tetrahedron. For the silica network n varies between 0 and 4. Raman spectrum of the SZS-1 glass has intense bands at ~860, 940 and 1040 cm^{-1}, a medium intense asymmetric band at ~620 cm^{-1} and a weak band at around 360 cm^{-1}. Based on the previous studies on silicate, borate and borosilicate glasses, bands at ~940 cm^{-1} and ~860 cm^{-1} are assigned to Si-O$^-$ stretching vibrations of NBO in Q^2 and Q^1 Silicate structural units [199-202]. Another band at around 1040 cm^{-1} is attributed to Si-O^0 vibrations of BO (Si-O-Si) in different Q^n silicate structural units. The concentration of Q^3 units in glasses is very low since a band around 1100 cm^{-1}, characteristic of stretching vibrations of Q^3 units, appears to have very weak intensity. Raman spectrum of SZS-4 glass having B$_2$O$_3$ is quite similar to the SZS-1 glass except 3 additional bands. Vibrational bands corresponding to 'Si' structural units remain almost unchanged with the addition of B$_2$O$_3$ which indicate that B$_2$O$_3$ is participating part in the glass network and not directly interacting with silicate structural units. For SZS-6 to SZS-9 glasses with the addition of other constituents like Al$_2$O$_3$, V$_2$O$_5$, Cr$_2$O$_3$, intensity of the band at 860 cm^{-1} increases and intensity of bands at 940 and 1040 cm^{-1} decreases. This indicates that Q^1 structural units are increasing at the expense of Q^2 structural units in the glass network. Incorporation of other additives whether network former or modifier creates NBO atoms, thereby leading to the formation of Q^n silicate structural units with lower number of 'n' values. The band at ~620 cm^{-1} is assigned to mixed stretching and bending vibrations of Si-O-Si bridges in various silicate units [201]. However, this band has also been attributed to the bending vibration of Si-O-Si bridges by many researchers [203]. Asymmetry of this band towards higher wave number is assigned to the analogous vibration in Q^1 silicate structural units. An increase in the frequency of this band with the additives in the glass also indicates the depolymerization of Si network. A weak broad band at ~360 cm^{-1} is attributed to the rocking motion of silicate units and/or motion of cationic polyhedral units [204].

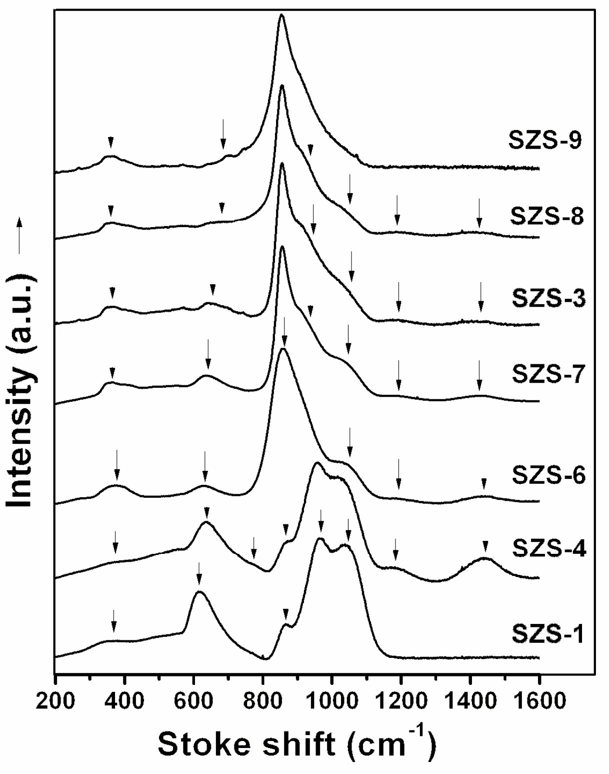

Figure 4.6: Raman spectra of SZS glasses.

New bands appeared in the Raman spectra of B_2O_3 containing glasses at ~1200 cm^{-1} and ~1450 cm^{-1}. The intensity of these bands is higher for glasses having higher concentration of B_2O_3. Bands at ~1200 cm^{-1} and ~1450 cm^{-1} are attributed to stretching vibrations of $B\text{-}O^-$ bond in triangular (BO_3) borate units [205-207]. The band at ~780 cm^{-1} in the spectra of SZS-4 glass is assigned to vibrations of $B\text{-}O^-$ bond in the tetragonal (BO_4) borate units [205-207]. This indicates that initially B_2O_3 is going into the network as triangular (BO_3) borate units. For higher concentrations of B_2O_3 (as in SZS-4 glass) a part of the B_2O_3 goes into the glass network as tetragonal (BO_4) borate units.

4.3.4.2 FTIR spectroscopy

The room temperature FTIR transmittance spectra of investigated SZS glasses are shown in Figure 4.7. All recorded spectra show three broad bands in the mid infrared region (400-1500 cm^{-1}). Most intense bands are observed in the 1200-800 cm^{-1}region and the next one is observed in the 600-400 cm^{-1} region. The least intense band is observed in the 800-600 cm^{-1} region. The presence of broad bands and lack of sharp features indicate the general disorder in the silicate glass network mainly due to the presence of wide distribution of Q^n structural units in these glasses. It has been known that the band in the 1200-800 cm^{-1} region is characteristic of asymmetric vibrations of $Si\text{-}O^-$ within SiO_4 tetrahedron [205]. It is clear from the spectrum of SZS-1 glass that the broad band in the 1200-800 cm^{-1} region is composed of three bands at ~1020 cm^{-1}, ~910 cm^{-1} and ~860 cm^{-1}, respectively. A new band around 1220 cm^{-1} is appeared in the spectra of B_2O_3 containing glasses. Intensity of this band is more for the glasses having higher concentration of B_2O_3.

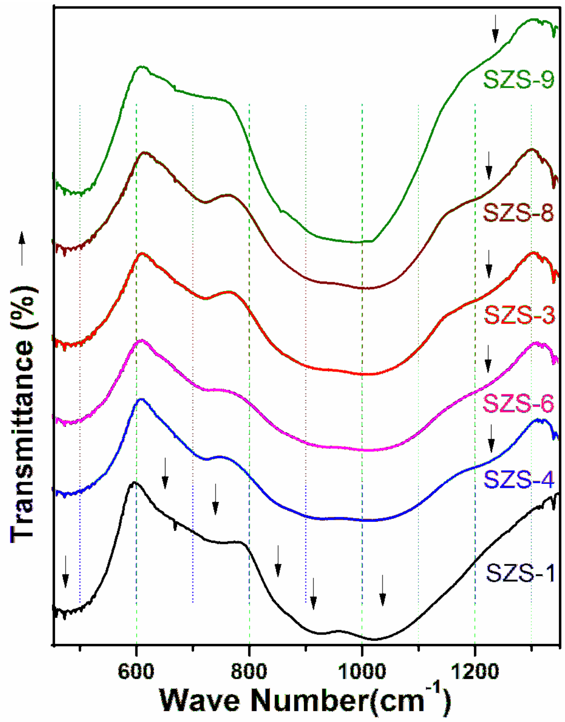

Figure 4.7: FTIR spectra of SZS glasses.

According to previous vibrational studies on silicate glasses, bands at ~910 cm^{-1} and ~860 cm^{-1} are assigned to Si-O^{-} asymmetric stretching vibrations in Q^2 and Q^1 silicate structural units respectively [202]. The band at ~1020 cm^{-1} is assigned to the Si-O^{o} vibration in various silicate structural units (Q^1, Q^2 and Q^3). The presence of Q^3 units in SZS-1 glass is indicated by an asymmetry of broad band at 1200-800 cm^{-1} towards higher wave numbers. This is because the concentration of Q^3 structural units, which is responsible for the peak at 1100 cm^{-1}, is having very low concentration in the glass. When other additives (network modifier or former) added into the glass, the position of this broad band shifts toward lower wave number due the formation of Q^n silicate structural units having higher number of NBO atoms. The width of this band also reduces with the addition of other additives which reflects the decrease in the distribution of Q^n silicate structural units in the network. The band between 800-600 cm^{-1} is assigned to Si-O^- symmetric stretching in various silicate units [208]. The band at ~1220 cm^{-1} is attributed to stretching vibrations of B-O^- bond in triangular (BO_3) borate units [208]. The band at ~500 cm^{-1} is assigned to Si-O-Si bending vibration in various silicate units [208]. Thus, FTIR spectra also revealed that the glass network mainly composed of Q^2 and Q^1 silicate structural units. It is also inferred that the silicate glass network depolymerizes with the addition of different additives and B_2O_3 enters into the network as triangular BO_3 borate structural units.

4.3.4.3 MAS-NMR spectroscopy

The ^{29}Si MAS-NMR spectra of a few SZS glasses are shown in Figure 4.8. These show a broad feature in the −70 to −105 ppm range. Considering that the content of modifying oxide (~48 mol%) for SZS-1 glass, one can expect the glass network to have low degree of polymerization and thus mainly composed of Q^2 structural units along with Q^3 and Q^1 units. A deconvolution based on Gaussian fitting resulted in the appearance of three peaks around chemical shift values -91.4, -85 and -78 ppm (for SZS-1) which are characteristic of Q^3, Q^2 and Q^1 structural units of 'Si', respectively [209-211]. For SZS-6 glass the resonance remain almost at the same chemical shift value. However, there is a slight increase in the asymmetry of the peak towards lower chemical shift value. This is due to the slight increase in network polymerization. This indicates that B_2O_3 takes part in the glass network and there is no direct interaction between the borate and silicate structural units. The Borate network may be indirectly interacting with the silicate network through modifier cation M (where M is Sr/Zn/V) to form Si-O-$(M\text{-}O)_n$-B type linkages. For the SZS-9 glass the resonance shifts towards more positive chemical shift values compared to other SZS-1 and SZS-6 glasses. This is in accordance with the higher amount (~58 mol%) of modifier oxides in the glass. The overall resonance is assumed to be a convolution of 3 resonances at -66, -81 and -87 ppm which can be attributed to Q^0, Q^1 and Q^2 structural units, respectively.

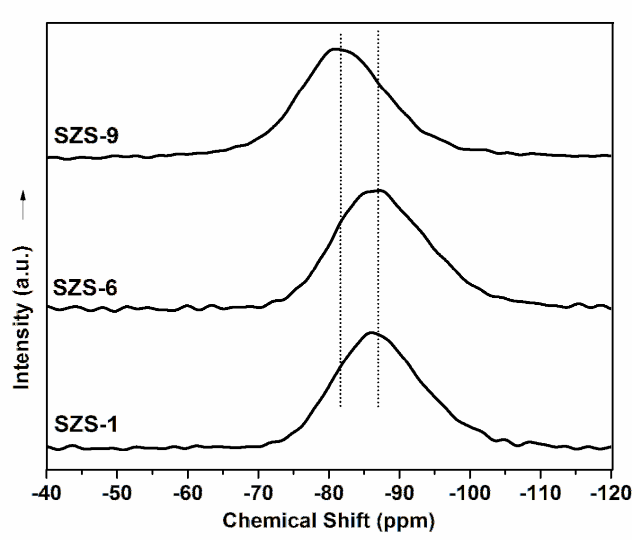

Figure 4.8: ^{29}Si MAS-NMR of few representative SZS glasses.

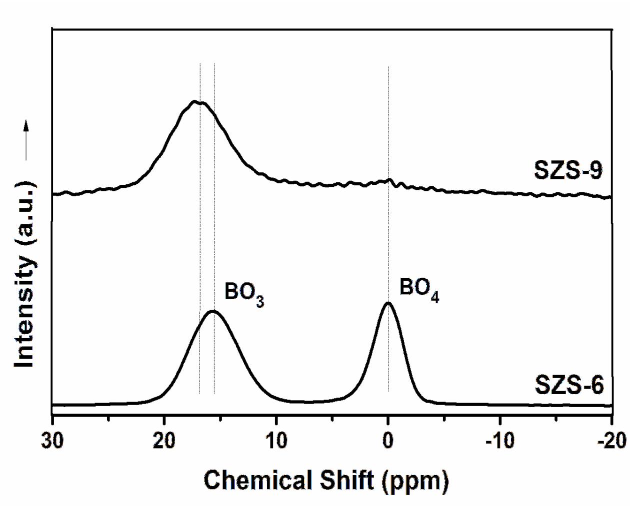

Figure 4.9: ^{11}B MAS-NMR of few representative SZS glasses.

Figure 4.9 shows the ^{11}B MAS-NMR spectrum of representative SZS glasses. The ^{11}B MAS-NMR of SZS-6 glass revealed the presence of two well resolved resonances centered around 15 and 0 ppm, the former peak is broader compared to latter and are arising due to boron in BO_3 and BO_4 structural units, respectively [212]. As ^{11}B is a quadrupolar nucleus, it will have significant quadrupolar interaction, when it occupies a non-cubic symmetry (i.e. in BO_3 structural unit), leading to a broad line shape. Unlike this boron in a tetrahedral configuration (BO_4 structural units) has got a cubic symmetry and negligible quadrupolar interaction, resulting in a sharp NMR peak. The use of a high field (18.8T) spectrometer enables us to obtain well resolved resonances, almost free of the second order quadrupolar broadening. The relative concentrations of BO_3 and BO_4 structural units were estimated from area under the corresponding resonances and found that 61% boron exits as BO_3 structural units and remaining 39% boron exists as BO_4 structural units for the SZS-6 glass composition. The presence of BO_3 and BO_4 units can be attributed to the direct interaction of B_2O_3 with the network modifiers SrO/ZnO brought about by a decreased concentration of SiO_2 in the glass. This interaction leads to the conversion of some part of B_2O_3 to BO_4 structural units. Boron in B_2O_3 is deficient of an electron and has a tendency to get converted to BO_4 structural units by interaction with O^{2-} ions generated by SrO/ZnO. It is clear from Figure 4.9 that SZS-9 glass has only BO_3 units and no BO_4 units. This indicates that although the glass has higher modifier content but there is paucity of charge compensation for forming BO_4 units.

4.3.5 Microstructural analysis

SEM micrographs of SZS-1 glass samples, heat treated according to various schedules given in Table 4.4, are presented in Figure 4.10.

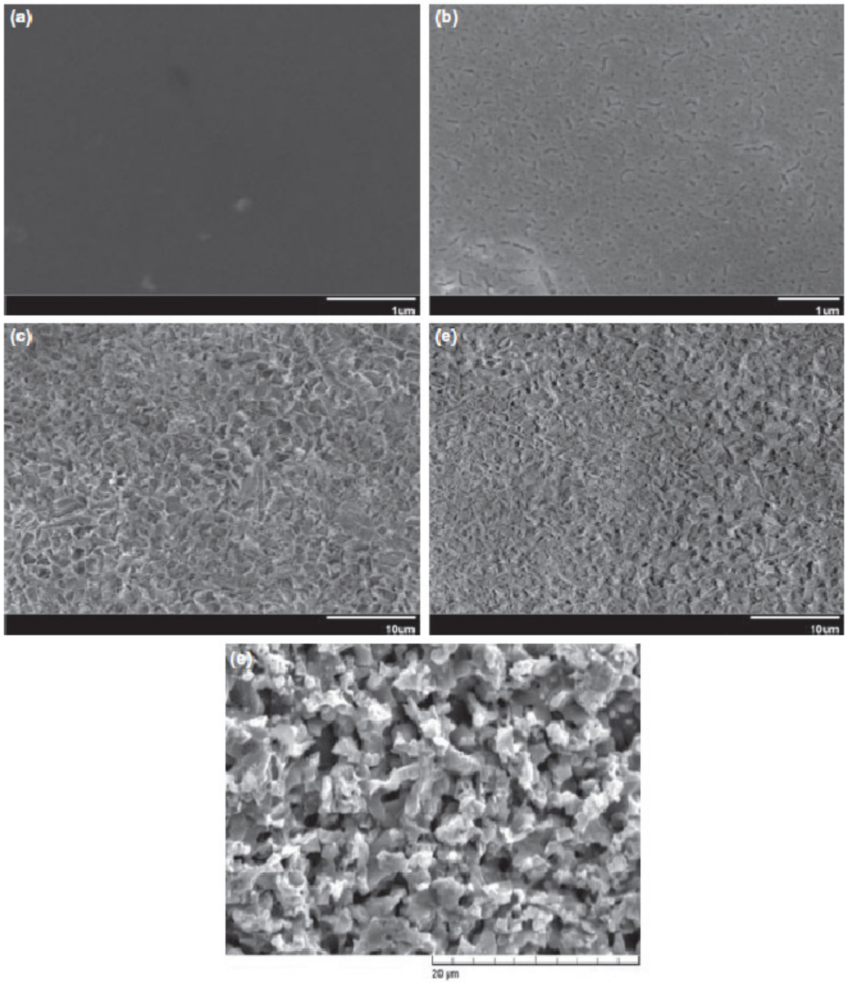

Figure 4.10: SEM micrographs of the SZS-1 glass and glass-ceramics (a) as prepared glass (b) glass-ceramic SZS1-GC-2, crystallized at 750°C for 5 h, (c) glass-ceramic SZS1-GC-4, crystallized at 820°C for 2 h, (d) glass-ceramic SZS1-GC-5, crystallized at 850°C for 2 h, (e) glass-ceramic SZS1-GC-6, crystallized at 925°C for 2h.

No distinct microstructure is observed for the as-prepared SZS-1 glass [Figure 4.10(a)], which reflects the good homogeneity of the prepared glass. Similar homogenous glass formation has been reported in other ternary silicate glasses around 40 wt.% of SiO_2 [173]. For the sample heat treated at 750°C for 5 h, a vermicular phase separated structure is evident. It is likely that the SZS-1 glass undergoes a liquid in liquid phase separation by the spinodal decomposition mechanism on the length scale of 50-500 nm, leading to the characteristic interconnected morphology [Figure 4.10(b)] [213-215]. Phase separation tendencies in binary SrO-SiO_2 [188] and ZnO-SiO_2 [189] systems are well known and it is therefore not really surprising that such behaviour persists in the ternary SZS glasses. Liquid-in-liquid immiscibility has also been reported in other similar ternary systems [216]. Upon heat treating at 820°C, the phase separation, driven by the higher temperature becomes more evident and the boundaries between the phase separated regions become more distinct, growing to a length scale of 1-2 μm [Figure 4.10(c)]. In the sample heat treated at 850°C, which is close to the crystallization onset temperature (Figure 4.2), the phase separated regions begin crystallizing and some granular/prismatic crystals about 2-4 μm in size are evident [Figure 4.10(d)]. These crystals are more numerous in the sample heat treated at 925°C and the interconnected structure is very clearly evident for this sample [Figure 4.10(e)]. High crystallinity of the glass-ceramics at this temperature is also evident which is in accordance with the XRD. Thus, microstructural evolutions suggest that the SZS-1 glass undergoes a phase separation by a spinodal decomposition mechanism prior to crystallization during heating of the glass and resulted in highly interconnected microstructure of the two crystalline phases. Similar spinodal decomposition was also reported in diopside based glass-ceramics [217]. On the basis of XRD and microstructural studies it is proposed that upon heat treatment SZS-1 glass, phase separated into SiO_2 rich region and ZnO rich region by the spinodal decomposition [215]. Compositions of both the regions continuously vary with time, and reached to equilibrium compositions close to $SrSiO_3$ and $Sr_2ZnSi_2O_7$ phases, respectively. At the crystallization onset temperature, both the regions start to crystallize almost simultaneously into metastable ‘SiO_2’ and ‘$ZnSiO_3$ (o)’ phases, respectively and later, more stable $SrSiO_3$/$Sr_3Si_3O_9$ and $Sr_2ZnSi_2O_7$ phases crystallized.

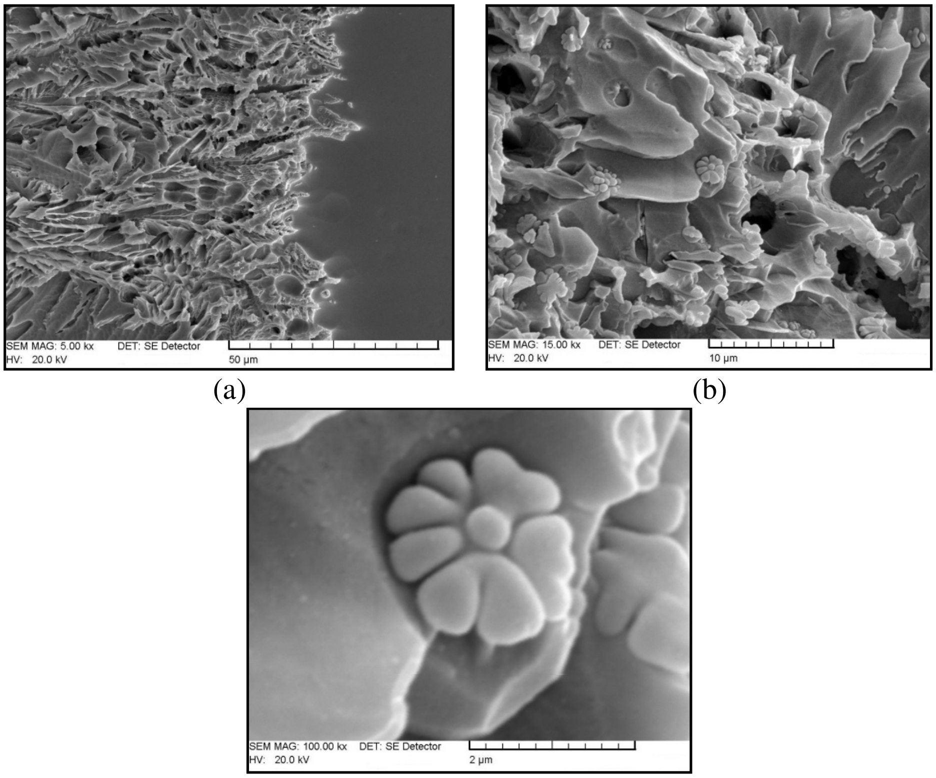

(a) (b)

(c)

Figure 4.11: SEM micrographs of SZS-4 glass-ceramics at different magnification (a) 5 kx (b) 15 kx and (c) 100 kx.

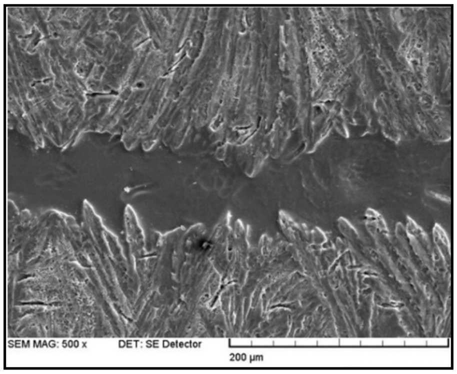

Figure 4.12: SEM micrographs of SZS-6 glass-ceramic at 0.5kx magnification.

SEM micrographs of SZS-4 glass-ceramics at different magnification are shown in Figure 4.11. This figure clearly indicates the occurrence of surface crystallization for this glass. Figure 4.11(a) also indicates the dendrite growth of crystals in the glass. Figure 4.11(b) shows two different types of crystallites in the microstructure; one is layer type and the second one is flower type which might be corresponding to the two different crystalline phases. However, EPMA is required to distinguish these two phases. Similarly, the surface crystallization was observed for the SZS-6 glass, as shown in SEM micrograph of the SZS-6 glass-ceramic (Figure 4.12). This also indicates the dendrite growth of crystals in the glass-ceramic.

SEM micrographs of SZS-8 glass-ceramics in BS and SE mode are shown in Figure 4.13. Figure 4.13(a) indicates the dendrite growth of elongated crystals of $Sr_2ZnSi_2O_7$ and Figure 4.13(b) shows two to three dimensional growth of these crystallites.

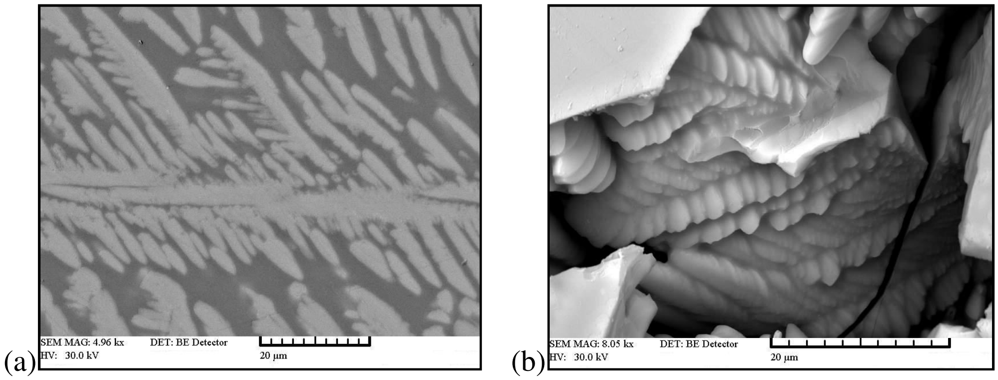

Figure 4.13: SEM micrographs of SZS-8 glass-ceramic at 5kx magnification (a) back scattered electron mode (b) secondary electron mode.

SEM micrographs of SZS-9 glasses heat treated at different temperatures and time are shown in Figure 4.14. Microstructure of the SZS9-GC-1 clearly indicates the formation of prismatic crystals at surface of the glass. The micrograph of SZS9-GC-3 [Figure 4.14(b)] revealed a fine microstructure with island type growth of crystals (1-2 μm in size). Glass-ceramics crystallized at higher temperature (Figure 4.14(c)) have a coarser microstructure compared to the glass-ceramics crystallized at lower temperature [Figure 4.14(b)].

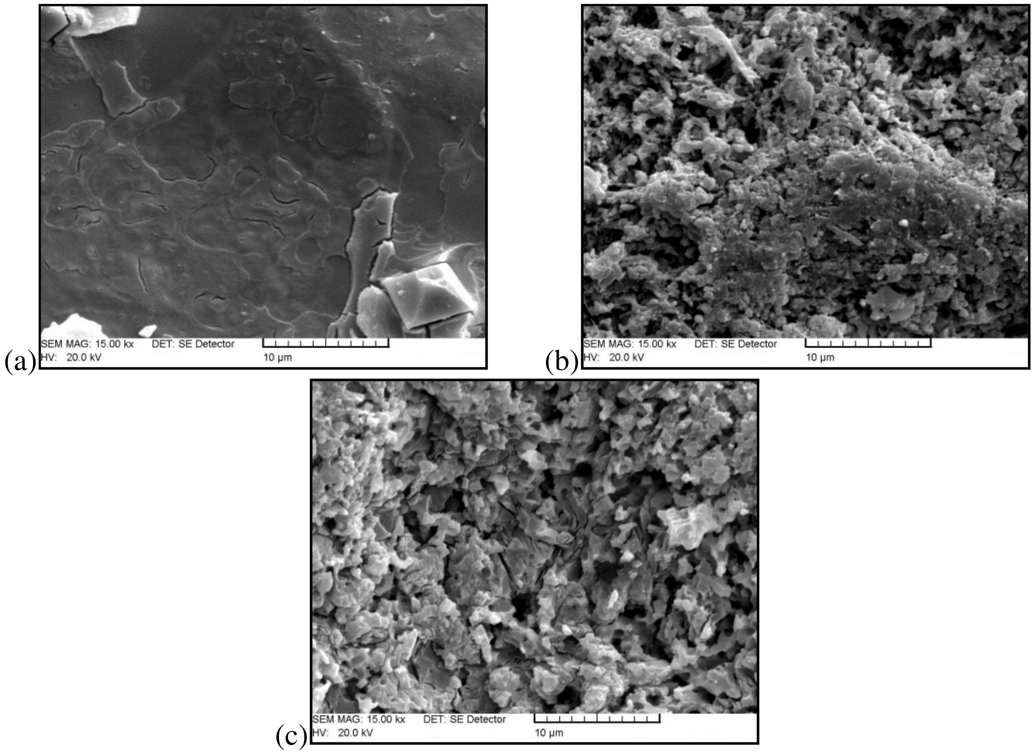

Figure 4.14: SEM micrographs of SZS-9 glass-ceramics (a) SZS9-GC-1, (b) SZS9-GC-3 and (c) SZS9-GC-5, at 15kx magnification.

4.3.6 Crystallization kinetics and mechanism of SZS glasses

The crystallization kinetics of glass powder was studied using the DTA. The crystallization peak temperature (T_p) was measured at different heating rates for all SZS glasses and collated in Table 4.7.

Table 4.7: Values of T_p at different heating rate for SZS-glasses.

Heating rate α (°C/min)	SZS-1		SZS-4	SZS-6	SZS-7	SZS-8	SZS-9
	T_{p1} (°C)	T_{p2} (°C)	T_p (°C)	T_p (°C)	T_p (°C)	T_p (°C)	T_p (°C)
5	860	896	839	844	888	895	930
10	877	917	858	863	909	912	949
15	889	929	871	878	922	926	965
20	895	942	882	892	947	939	977

The non-isothermal crystallization kinetics based on DTA data was investigated using modified Kissinger equation proposed by Matusita and Sakka [92,218]. It distinguishes the crystallization process that occurs on a fixed number of nuclei from those where nucleation and growth take place simultaneously and given as:

$$\ln\left(\frac{\alpha^n}{T_p^2}\right) = \frac{-mE_a}{RT_p} + constant \tag{4.4}$$

where T_p is peak crystallization temperature, α is heating rate, E_a is activation energy for the crystallization, R is ideal gas constant, n is a constant known as Avrami parameter and m represents the dimensionality of the crystal growth.

The Avrami parameter '*n*' was determined from the DTA data using Ozawa equation [90]

$$\frac{d\ \ln(-\ln(1-x))}{d\ln\alpha} = -n \tag{4.5}$$

where, x is volume fraction crystallized at any temperature when heated at a heating rate of α. The crystallized volume fraction x is calculated from the ratio of the partial area of the crystallization peak at any temperature to the total area of the crystallization peak.

Once '*n*' is known from Ozawa equation, activation energy E_a can be obtained from Matusita equation if value of m is known. Matusita et al have reported $m = n$-1 for a quenched glass containing no nuclei and $n = m$ for a glass containing large number of nuclei before the thermal analysis [92]. Additionally, the value of m can be calculated form Matusita equation using value of E_a, obtained from Marseglia equation [219]

$$\ln\left(\frac{\alpha}{T_p}\right) = \frac{-E_a}{nRT_p} \tag{4.6}$$

For comparison, the activation energy for the crystallization E_{ak} was also obtained using the Kissinger equation [91],

$$\ln\left(\frac{\alpha}{T_p^2}\right) = \frac{-E_{ak}}{RT_p} + constant \tag{4.7}$$

The DTA thermographs of the SZS-1 glass recorded at different hating rates exhibited a well defined exotherm consisting of two overlapping peaks. Typical thermograph at a heating rate of 10°C/min is shown in Figure 4.15, where deconvoluted Gaussian peaks are shown by dotted lines. It is observed that with increasing heating rate the peak temperature of the exotherm (T_p) shifted towards the higher temperature side. The shift in T_p with the heating rate is due to the lesser extent of crystallization during the heating, as crystallization occurs over a period of time.

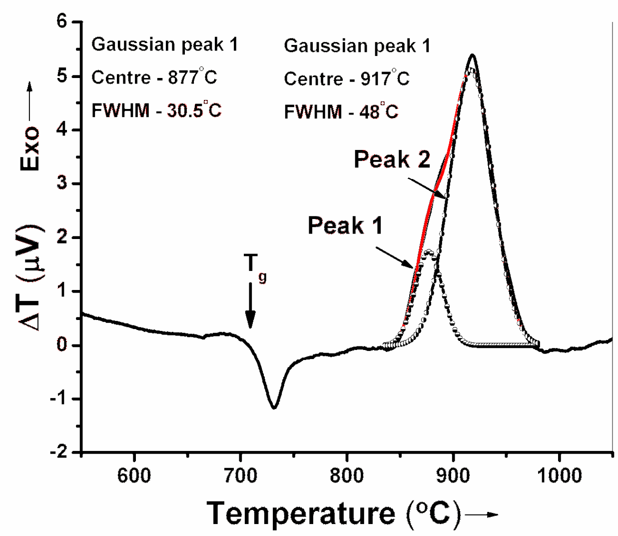

Figure 4.15: DTA curve of the SZS-1 glass at a heating rate of α = 10°C/min.

The Avrami parameter n was determined through the Ozawa method [Eq.(4.5)] from the crystallized fraction 'x' obtained at different temperatures for different heating rates. Ozawa plots of both the peaks of SZS-1 glass are shown in Figure 4.16 (a) and (b). The fitting of data to straight lines ($R^2 \geq 0.95$) gives values of n, which increased gradually for both the peaks when temperature decreases. The average values of 'n' are $\langle n \rangle = 2.67$ for the first and $\langle n \rangle = 1.95$ for the second crystallization peak, which are close to 2.5 and 2, respectively [220]. An intermediate value of n between 3 and 1 indicates the simultaneous occurrence of bulk and surface nucleation in the SZS-1glass. Figure 4.17(a) and (b) show the Marseglia plots of first and second exothermic peaks, of SZS-1 glass, respectively. Using the value of n, the activation energy E_a (Marseglia) for both the peaks was calculated from the slope of these straight lines and tabulated in Table 4.8. Figure 4.18(a) and (b) show the Matusita-Sakka plots of first and second exothermic peaks, respectively. Data were fitted to straight lines with simple least squares method with $R^2 \geq 0.99$. The value of 'mE_a' for both the peaks was calculated from the slope of these straight lines. The value of m can be taken equal to n-1 when no heat treatment is given to nucleate the as-prepared glass before the thermal analysis [92] and activation energy (Matusita) found to be 700 kJ/mol for the first peak and 704 kJ/mol for the second peak, as summarized in Table 4.8. Similar bulk crystallization with activation energy of 714 kJ/mol has been reported for barium zinc silicate glasses [171]. The value of m was also calculated from Matusita equation by using the value of E_a (Marseglia) in 'mE_a' and found to be $m = 1$ for both the peaks as given in Table 4.8. It is clear from the Table 4.8 that the calculated m does not match with the assumed value of $m = n$-1 for the first peak probably due to the existence of mixed two to three dimensional growth of crystals. The Kissinger plots of both the exothermic peaks of the SZS glass are shown in

Figure 4.19(a) and (b). Data were fitted to straight lines with simple least squares method, obtaining $R^2 \geq 0.99$. The Kissinger activation energy ‘E_{ak}’ was calculated from the slope of these plots and given in Table 4.8.

The growth morphology parameters ‘*n*’ and ‘*m*’ for both the peaks (Table 4.8) indicate the diffusion controlled bulk dominant crystallization for the SZS-1 glass with varying number of nuclei [220]. This bulk crystallization occurs via three and two dimensional growth of crystals. It can be seen from Table 4.8 that the activation energy ‘E_a’ is quite high compared to the ‘E_{ak}’. Relatively higher activation energies for both the peaks indicate that the crystallization kinetics is more activated with temperature for SZS-1 glass that may result into a poor control over the crystallization process.

Table 4.8: Activation energy and growth morphology parameters for crystallization of the SZS-1 glass.

Sample		Average ‘*n*’ (Ozawa)	*m* (calculated)		E_{ak} (kJ/mol) (Kissinger)	E_a (kJ/mol) (Marseglia)	E_a (kJ/mol) (Matusita)
			m=*n*-1	(Matusita)			
SZS-1	Peak-1	2.67 (~2.5)	1.5	1	409	1046	700 (*m*=1.5)
	Peak-2	1.95 (~2)	1	1	342	703	704

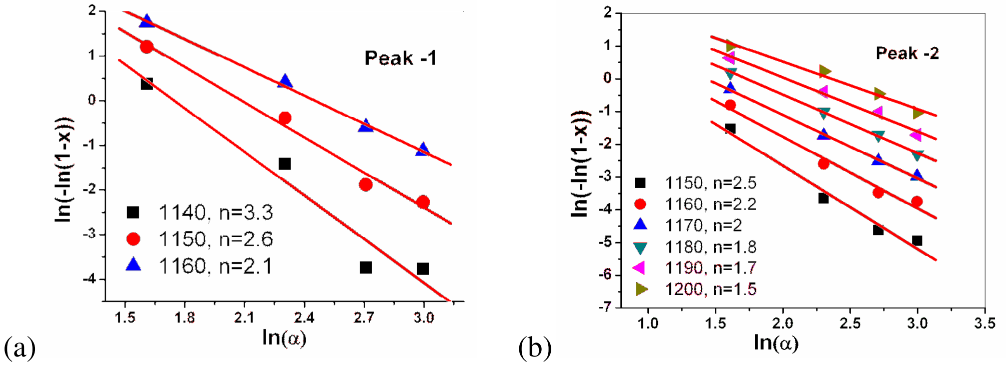

Figure 4.16: Ozawa plots of (a) peak-1 and (b) peak-2 of SZS-1 glass.

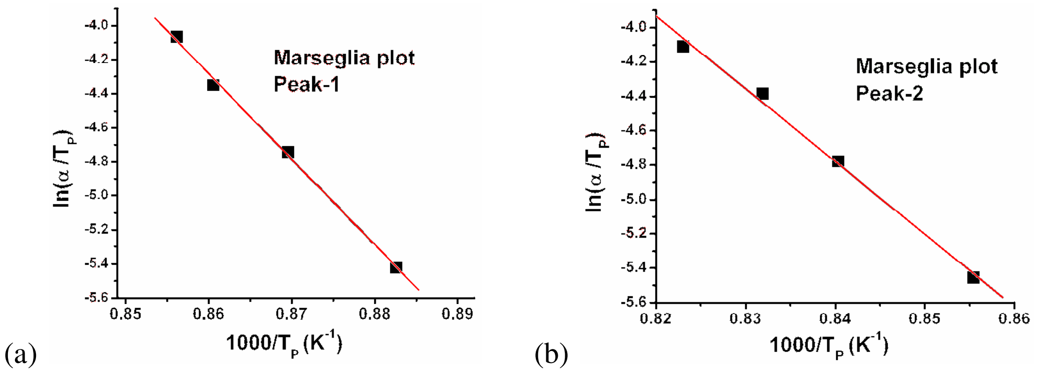

(a) (b)

Figure 4.17: Marseglia plots of (a) peak-1 and (b) peak-2 of SZS-1 glass.

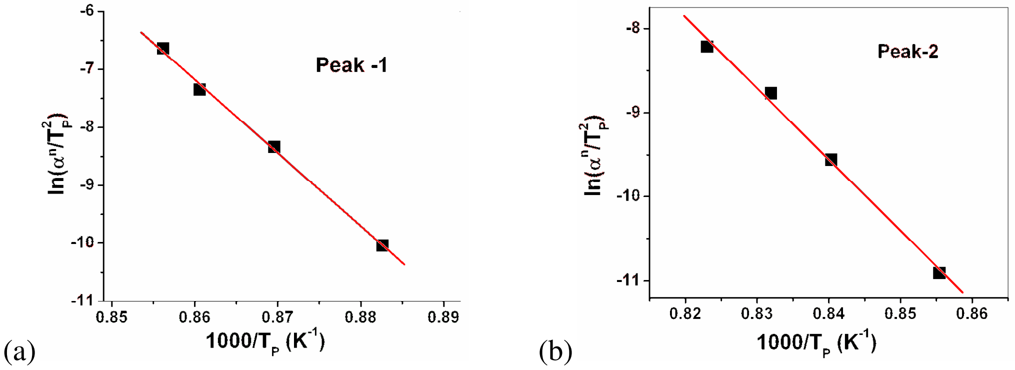

(a) (b)

Figure 4.18: Matusita plots of (a) peak-1 and (b) peak-2 of SZS-1 glass.

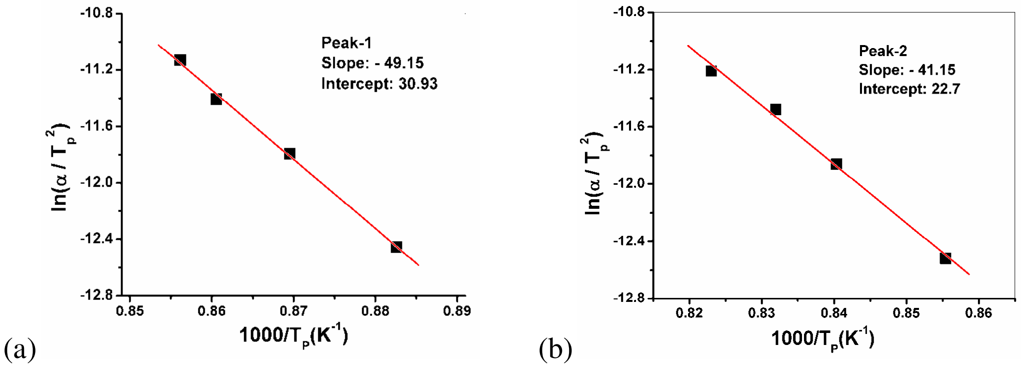

(a) (b)

Figure 4.19: Kissinger plots of (a) peak-1 and (b) peak-2 of SZS-1 glass.

Table 4.9: Activation energy and growth morphology parameters for crystallization of the SZS glasses.

Sample ID	Average '*n*' (Ozawa)	*m* (calculated) (Matusita)	E_{ak} (kJ/mol) (Kissinger)	E_a (kJ/mol) (Marseglia)	E_a (kJ/mol) (Matusita)
SZS-4	2.23	1	328	674	674
SZS-6	1.5	1	295	469	464
SZS-7	1.4	1	329	469	497
SZS-8	1.5	1	349	543	538
SZS-9	1.77	1	347	746	746

Similarly detailed studies of crystallization kinetics were also carried out for other SZS glasses in the series and the results are summarized in Table 4.9. A value of *n* between 3 and 1 indicates the simultaneous occurrence of bulk and surface nucleation in the investigated SZS glasses. For the SZS-1 glass the value of *n* is close to 3 which reflect the dominancy of bulk nucleation over surface nucleation mechanism. For SZS-4 glass and other SZS glasses lesser value of *n* suggests the dominancy of the surface nucleation mechanism. Microstructures of SZS-4 and SZS-6 glasses also confirm the surface crystallization for these glasses. It is also clear from Table 4.9 that $m = n$-1 is not valid for all the SZS glass samples. This is possibly due to the existence of mixed nucleation and growth mechanism in these glasses.

4.3.7 Thermal expansion and structural aspects of SZS-9 glass-ceramics

4.3.7.1 Thermo-mechanical analysis

It is also important to know the TEC of glass-ceramics when subjected to long term heat treatment. Figure 4.20 shows the representative TMA plots of different glass-ceramics obtained from the SZS-9 glass. The TEC values are summarized in Table 4.10. The values are found to be the same (within the error limit) for all the SZS-9 glass-ceramics. These results suggest the compatibility of SZS glass-ceramics for long term thermal and mechanical stabilities at elevated temperatures.

Table 4.10: TEC of SZS-9 glass-ceramics

Sample ID	Nucleation Temp. (°C)	Dwell Time (h)	Crystallization Temp. (°C)	Dwell Time (h)	TEC ± 5% (10^{-7}/°C)
SZS9-Glass	-	-	-	-	111
SZS9-GC-1	800	2	-	2	112
SZS9-GC-3	800	2	950	2	110
SZS9-GC-5	800	2	1100	2	116
SZS9-GC-9	-	-	850	50	105

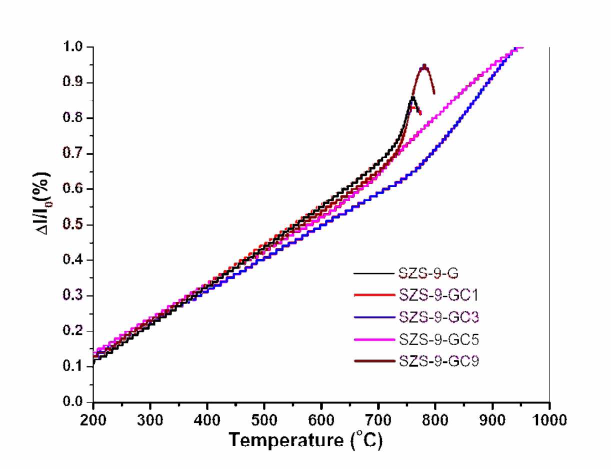

Figure 4.20: Thermal expansion curves of SZS-9 glass-ceramics

4.3.7.2 Raman studies

Raman spectra of investigated glass-ceramics are shown in Figure 4.21. Changes in the glass structure with heat treatment are clearly evident in the figure. The base glass has a broad peak over the region of 800-1100 cm^{-1}. As described earlier Raman spectrum of the SZS-1 glass has intense bands at ~860, 940 and 1040 cm^{-1} and a medium intense asymmetric band at ~620 cm^{-1} and a weak band at around 360 cm^{-1}. Bands at ~940 cm^{-1} and ~860 cm^{-1} are assigned to

Si-O$^-$ stretching vibrations of NBO in Q^2 and Q^1 structural units. Another band at around 1040 cm^{-1} is attributed to Si-O^0 vibrations of BO (Si-O-Si) in different Q^n silicate structural units. The concentration of Q^3 units in glasses is very low as the band around 1100 cm^{-1}, characteristic of stretching vibrations of Q^3 units, appears to have very weak intensity. Raman spectra of glass-ceramics SZS9-GC-2 and SZS9-GC-6 are exactly similar while that of SZS9-GC-4 and SZS9-GC-7 glass-ceramics are quite similar. The intensity of bands is higher for glass-ceramics which were heat treated for a longer time, which reflect the higher crystallinity of these glass-ceramics. With the heat treatment of the base glass at 950^{0}C the Raman spectra for glass-ceramic dominated by a very intense and sharp band at 860 cm^{-1} along with less intense broad bands at around 786 and 900 cm^{-1}. The spectrum also indicates the presence of a weak but sharp band at 882 cm^{-1}, which is superimposed on a lesser intense broad band at around 900 cm^{-1}. There are also other sharp but weak or lesser intense bands at around 354, 400, 565, 647 and 971 cm^{-1}. These sharp and intense bands correspond to crystalline phase having Q^1 structural units. The XRD studies revealed that these glass-ceramics have mainly $Sr_2ZnSi_2O_7$ phase along with $Sr_3Si_3O_9$ phase. It is reported that Raman spectra of melilites are dominated by the vibrational modes of pyrosilicate (T_2O_7) units (T = Si/Al) [221]. Therefore, these sharp Raman bands are assigned to the vibration of Si-O$^-$ units in $Sr_2ZnSi_2O_7$ crystalline phase, and broad bands are assigned to the residual glass. Raman spectra for glass-ceramics formed by heat treatment of the base glass at 1100°C are dominated by a broad and intense band at 776 cm^{-1} along with and sharp bands at around 312, 362, 562, 645, 852, 896, 971 and 1045 cm^{-1}. Based on the reported Raman spectrum of silicate crystals and minerals [222], these sharp bands are assigned to stretching and bending vibration of Si-O- units in $Sr_3Si_3O_9$ crystalline phase. It is observed that with the heat treatment for a longer time the intensity of the sharp band increases while that of the broad band remains almost the same. Based on reported the Raman spectra of silicate glasses having $B_2O_3/Al_2O_3/TiO_2$, this broad band is attributed to vibration of Al-O^-, B-O^- and Ti-O^- bands in tetrahedral units. As silicate phases crystallize with heat treatments, the residual glass in the glass-ceramics becomes richer in other network former. With the crystallization the spectra also show weak and broad bands at ~1300 cm^{-1} and ~1550 cm^{-1} which are attributed to vibrations of B-O^- bond in triangular (BO_3) borate units in the residual glass. Band appeared at ~780 cm^{-1} in spectra is assigned to vibrations of B-O^- bond in tetragonal (BO_4) borate units. This indicates that initially B_2O_3 is incorporated into the network as triangular (BO_3) borate units.

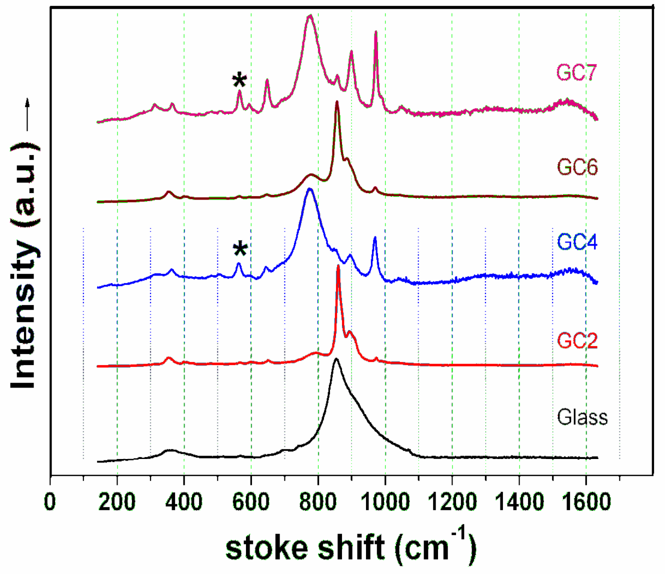

Figure 4.21: Raman spectra of SZS-9 glass-ceramics.

4.3.7.3 FTIR studies

The FTIR spectra of SZS-9 glass and glass-ceramic are shown in Figure 4.22. Broad bands in the spectrum of glass indicate the amorphous nature of the sample. A broad band centered at 950 cm^{-1} in the 1200-800 cm^{-1} region is characteristic of asymmetric vibrations of Si-O^-

within different Q^n (mainly Q^1 and Q^2) Si structural units. Intense broad band in the 300-600 cm^{-1} region is assigned to bending vibration of Si-O-Si linkages in different Q^n structural units. A less intense band in the region of 600-800 cm^{-1} is due to the symmetric stretching of Si-O^- and Si-O-Si units.

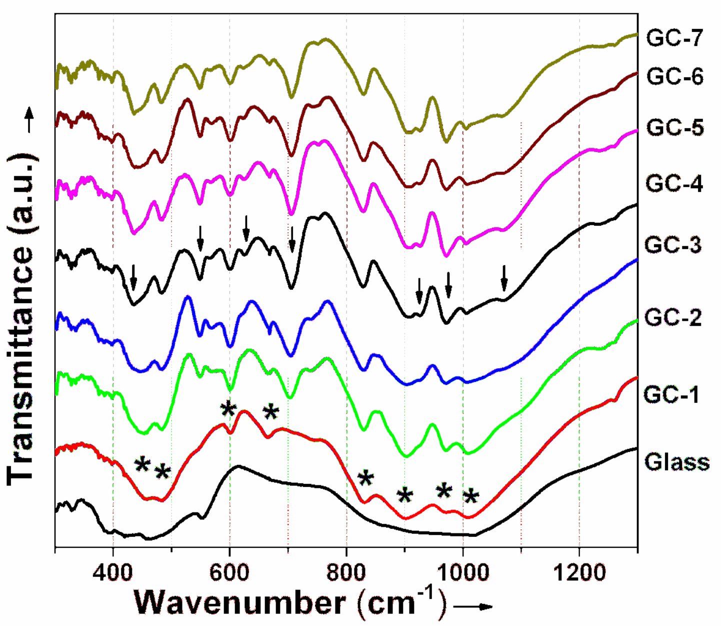

Figure 4.22: FTIR spectra of SZS-9 glass-ceramics.

For SZS9-GC-1 glass-ceramic, the presence of crystalline phases is depicted by splitting of the broad bands into number of sharp bands at around 1010, 970, 900, 830, 662, 600, 482 and 452 cm^{-1}. As reported in the literature these sharp bands are exactly matching with the vibration of crystalline $Sr_2ZnSi_2O_7$ phase [223]. Thus in accordance with XRD, FTIR also indicates the starting of the crystallization of $Sr_2ZnSi_2O_7$ phase. With the increase in temperature and dwell time these vibration bands become more sharp and intense for SZS9-GC-2 and SZS9-GC-3 glass-ceramics, thus reflecting the increase in the amount of $Sr_2ZnSi_2O_7$ crystalline phase in the glass-ceramics. Some additional bands also start appearing at around 1060, 930, 706, 625, 550 cm^{-1}, which become more intense with increase in dwell time and temperature. According to the literature these vibrational bands are characteristics of $Sr_3Si_3O_9$ crystalline phase [104]. With a further increase in the dwell time at higher temperature these bands become more sharp and intense, thus suggesting an increase in the amount of $Sr_3Si_3O_9$ crystalline phase in the glass-ceramics. For SZS9-GC-6 and SZS9-GC-7 glass-ceramics that were crystallized for 50 h at 950°C and 1100°C, respectively, number of sharp and intense vibrational bands, corresponding to both the crystalline phases is present. This indicates the higher crystalline nature of these glass-ceramics.

4.3.7.4 MAS-NMR studies

Figure 4.23 shows the ^{29}Si MAS-NMR spectra of SZS-9 glass-ceramics. The spectrum of SZS9-GC-1 shows two narrow resonances in the close proximity superimposed on a broad resonance. Narrow resonances at -77 and -79.75 ppm indicate the crystallization of silicate phase having mainly Q^1 structural units of 'Si'. The sharp resonance at -77 ppm is assigned to the Sr-hardystonite silicate phase ($Sr_2ZnSi_2O_7$) in accordance with XRD and chemical shift values of silicate minerals [224]. A weak but sharp resonance at around -80 ppm indicates another slightly more shielded Si structural units. A solid solution of Al/B in melilite family of Silicate minerals is quite common. These minerals have chemical formula $X_2YT_2O_7$ where Y, T are in tetrahedral coordination and B/Al can substitute these tetrahedral sites in the crystal structure. Substitution of Zn with Al/B is expected to change the chemical environment around Si. A significantly high intensity of a broad resonance characteristic of the glass indicates the higher amount of residual glass compared to the crystalline fraction in the SZS9-GC-1 glass-ceramic. With increasing temperature for SZS9-GC-3 glass-ceramic, two sharp and intense resonances corresponding to two different silicate crystalline phases appeared. The resonance at -77 ppm becomes more intense and sharp which reflects the higher amount of $Sr_2ZnSi_2O_7$ crystalline phase in the SZS9-GC. Based on the chemical shift value of cyclosilicate minerals another intense and sharp resonance at -88 ppm is attributed to the $Sr_3Si_3O_9$ phase having Q^2 structural units [224].

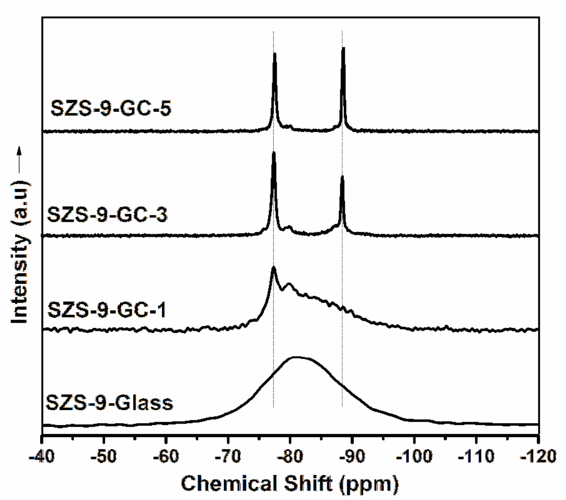

Figure 4.23: ^{29}Si MAS-NMR spectra of SZS-9 glass and glass-ceramics.

Figure 4.23 shows higher intensity of -77 ppm resonance compared to -88 ppm resonance for SZS9-GC-3 and very weak broad resonance at the bottom of both the sharp resonances. This indicates the high crystallinity of the glass-ceramics and higher amount of $Sr_2ZnSi_2O_7$ phase compared to $Sr_3Si_3O_9$ phase in the crystalline part of the glass-ceramics. With an increase in the temperature for SZS9-GC-5 glass-ceramic, the intensity of the peak at -88 ppm becomes more compared to the peak at -77 ppm that shows the higher crystallization of $Sr_3Si_3O_9$ phase at higher temperatures. The near weak peak appearing at -79 ppm may be due to the $Sr_2ZnSi_2O_7$ phase with Zn/Si sites substituted with Al/B atoms. Raman studies described subsequently also support this interpretation. Crystallization for SZS9-GC-5 glass-ceramic might have reached to its maximum possible extent as no broad resonance could be observed.

Further, assuming all the ZnO in the glass participate in the formation of $Sr_2ZnSi_2O_7$ and all the SrO participate in the formation of $Sr_2ZnSi_2O_7$ and $Sr_3Si_3O_9$, we can estimate that the glass can reach at most ~89 % crystallization. However, we are pursuing long term heat treatment studies to verify that there is no further crystallization.

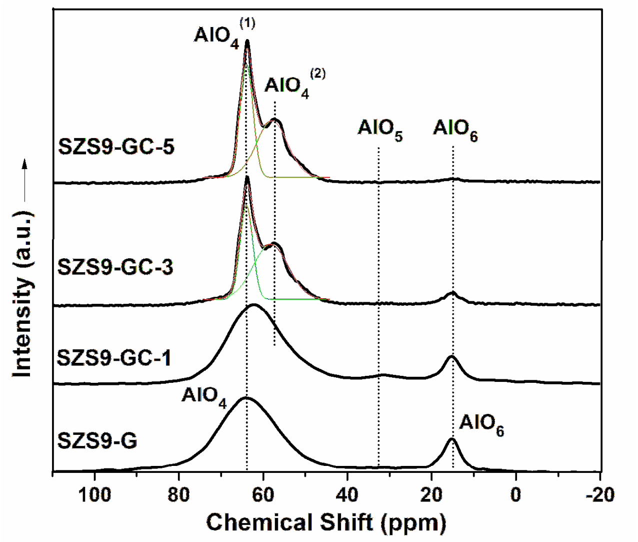

Figure 4.24: ^{27}Al MAS-NMR spectra of SZS-9 glass and glass-ceramics.

The ^{27}Al MAS-NMR spectra of SZS-9 glass and glass-ceramics are presented in Figure 4.24. At high magnetic fields (18.8T) the effects of quadrupolar broadening are significantly reduced leading to nearly Gaussian line shapes. The NMR spectrum of glass shows two resonance peaks around 15 ppm and 64 ppm, characteristic of AlO_6 and AlO_4 units, respectively [224]. Remarkable structural changes in the Al polyhedral units with the crystallization of the glass can be seen from NMR spectra of SZS-9 glass-ceramics (Figure 4.24)**.** With the crystallization intensity of a peak corresponding to AlO_6 units decreases progressively and finally reached to zero. During the crystallization at around 800°C for 2 h, a weak resonance at around 32 ppm is observed for the SZS9-GC-1 glass-ceramic, which is attributed to AlO_5 units. And this peak also vanishes with further crystallization. Resonance corresponding to AlO_4 units becomes narrower and shifts towards more negative chemical shift values. With crystallization an overlapped sharp resonance peak appeared on a comparatively broad resonance. This sharp resonance at 64 ppm indicates the development of a crystalline phase containing Al in tetrahedral coordination and broad resonance at around 58 ppm is due to the tetrahedral Al structural units existing in the residual glass.

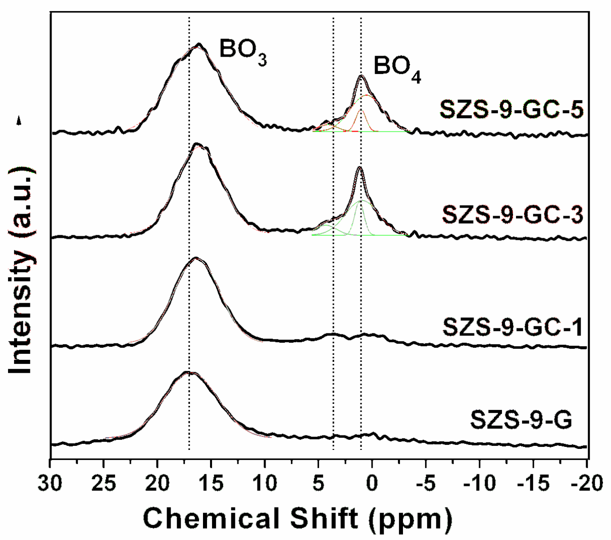

Figure 4.25: ^{11}B MAS-NMR spectra of SZS-9 glass and glass-ceramics.

The ^{11}B MAS-NMR spectra of SZS-9 glass-ceramics are shown in Figure 4.25. For the base glass the spectra consist of one broad resonance centered at ~17 ppm. The resonance is assigned to BO_3 structural unit [28, 48]. In the glass-ceramics (for example SZS9-GC-3), the shapes of the resonances change significantly compared to the parent glass. With the crystallization, in addition to the broad peak ~17 ppm, an additional sharp peak (~3 ppm) started appearing. The sharp peak can be attributed to ‘B’ in tetrahedral configurations existing in a crystalline material.

MAS-NMR spectra of the glass-ceramics generally confirm the phase emergence observed by the XRD. In accordance with the XRD, ^{29}Si MAS-NMR spectra show the crystallization of Sr-hardystonite ($Sr_2ZnSi_2O_7$) and strontium silicate ($Sr_3Si_3O_9$) phase and high crystallinity of the SZS-9 glass-ceramics. The NMR spectra of glass-ceramics confirm that the glass-ceramics reached to its maximum possible extent of crystallinity which reflects a high rate of crystallization for the SZS-9 glass. X-ray diffraction studies revealed that $Sr_2ZnSi_2O_7$ and $Sr_3Si_3O_9$ phases crystallize in SZS glass-ceramics and $Sr_2ZnSi_2O_7$ solid-solution phase formed in compositions having B_2O_3 and/or Al_2O_3. $Sr_2ZnSi_2O_7$ (Sr-hardystonite) is a one of the members of melilite group of minerals having a general formula $X_2Y(T_2O_7)$. It is reported that solid solution formation is quite common in members of melilite family of silicate minerals. Al/B may occupy the position of Y and T sites in the tetrahedral coordination. ^{27}Al and ^{11}B MAS-NMR spectra show the crystallization of B and Al in tetrahedral coordination. MAS-NMR studies along with XRD suggest the formation of $Sr_2ZnSi_2O_7$ solid-solution by incorporation of B and Al atoms in tetrahedral coordiantion in the $Sr_2ZnSi_2O_7$ crystalline phase.

4.3.8 Bonding properties and interface studies

Adhesion behaviour of a few representative SZS glasses to YSZ and Crofer-22-APU was investigated. Glasses were selected on the basis of TEC, viscosity and crystallization kinetics. SEM image of the interface between YSZ and SZS-4 glass after heat treatment at 900°C for 1 h in air ambient is shown in Figure 4.26(a). A continuous interface shows good bonding between the glass and YSZ. At the interface an elongated crystalline microstructure is also observed. Elemental line scans across the interface [Figure 4.26(b)] indicate the inter-diffusion of Sr, Si from glass to YSZ and Y, Zr from YSZ to glass. This inter-diffusion is responsible for good bonding of glass to YSZ and interfacial zone is found to be ~3-4 µm. SEM image of the interface between Crofer and SZS-4 glass after heat treatment at 1000°C for 1 h in air ambient is shown in Figure 4.26(c). Continuous interface shows good bonding between glass and Crofer. This good bonding is attributed to the inter-diffusion of Fe, Cr and Si across the interface [Figure 4.26(d)].

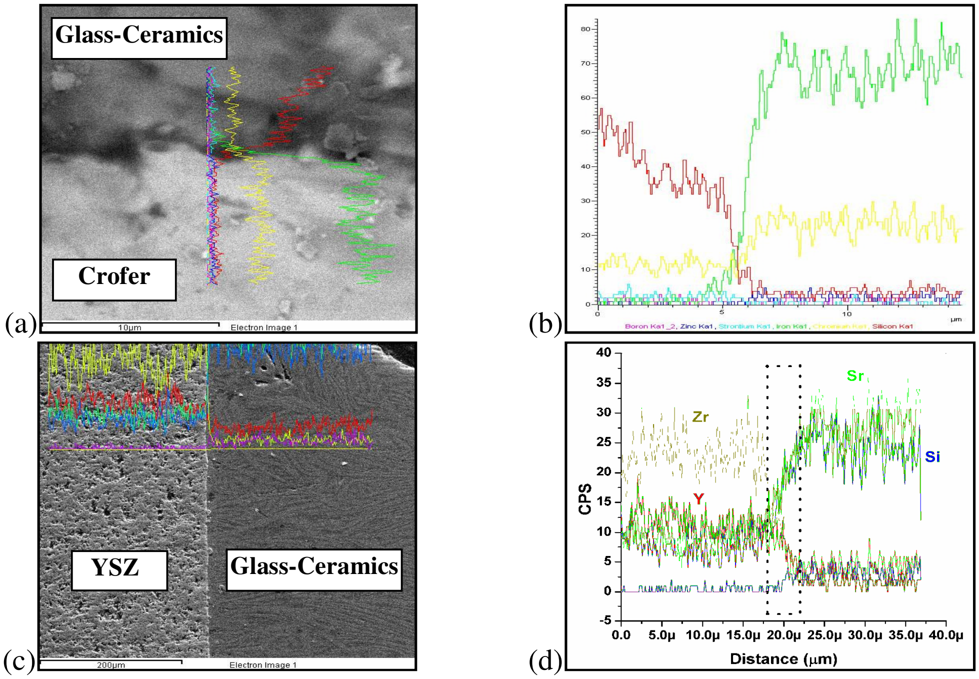

Figure 4.26: (a) SEM micrographs of the SZS-4 glass-ceramic to Crofer-22-APU interface after sealing at 950°C, (b) EDS line scans across the interface showing the inter-diffusion of Si, Sr, Fe and Cr, (c) SEM micrographs of the SZS-4 glass-ceramic to YSZ interface after sealing at 950°C, (d) EDS line scans across the interface showing the inter-diffusion of Si, Sr, Zr and Y.

Other SZS glasses namely SZS-6 and SZS-8 have also shown good bonding with the YSZ. The bonding behaviour of SZS-6 and SZS-8 glasses with Crofer-22-APU was also investigated.

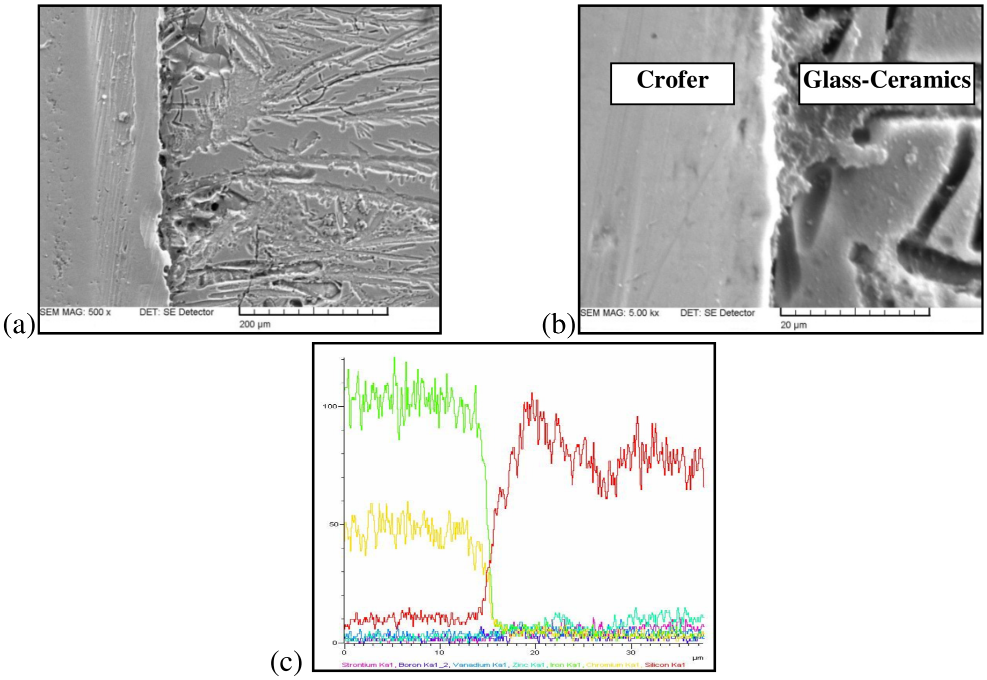

Figure 4.27: SEM micrographs of the SZS-6 glass-ceramic to Crofer-22-APU interface after sealing at 900°C, at different magnification (a) 0.5kx, (b) 5kx, (c) EDS line scans across the interface showing the inter-diffusion of Fe, Cr and Si.

Figure 4.27(a) and (b) show the SEM micrograph of the interface between Crofer and SZS-6 glass after a heat treatment at 950°C for 1 h in the air ambient. A smooth interface shows the good bonding between glass and Crofer resulting from good wetting. Prismatic crystalline microstructure is observed at the interface. Inter-diffusion of elements across the interface was observed through elemental line scans as presented in Figure 4.27(c). Inter-diffusion of Cr, Fe from metal to glass and Si from glass to metal takes place which is considered to be responsible for good bonding with Crofer. Interfacial zone was found to be ~

4 µm. Seals of SZS-6 glass with Crofer were leak tested at different elevated temperatures up to 950°C in the steps of 100°C, for 30 min at each temperature. Seals were found to withstand a vacuum of 10^{-6} mbar in the whole temperature range. This indicates the leak tightness of the seal at high temperatures. Seals of SZS-6 glass with Crofer were also found hermetic even after exposure at 850°C for 800 h, this reflect the long-term thermal and chemical stabilities of this glass-ceramic sealant. However, thermal stability studies are being continued for the long-term exposure (more than 1000 h) at elevated temperatures.

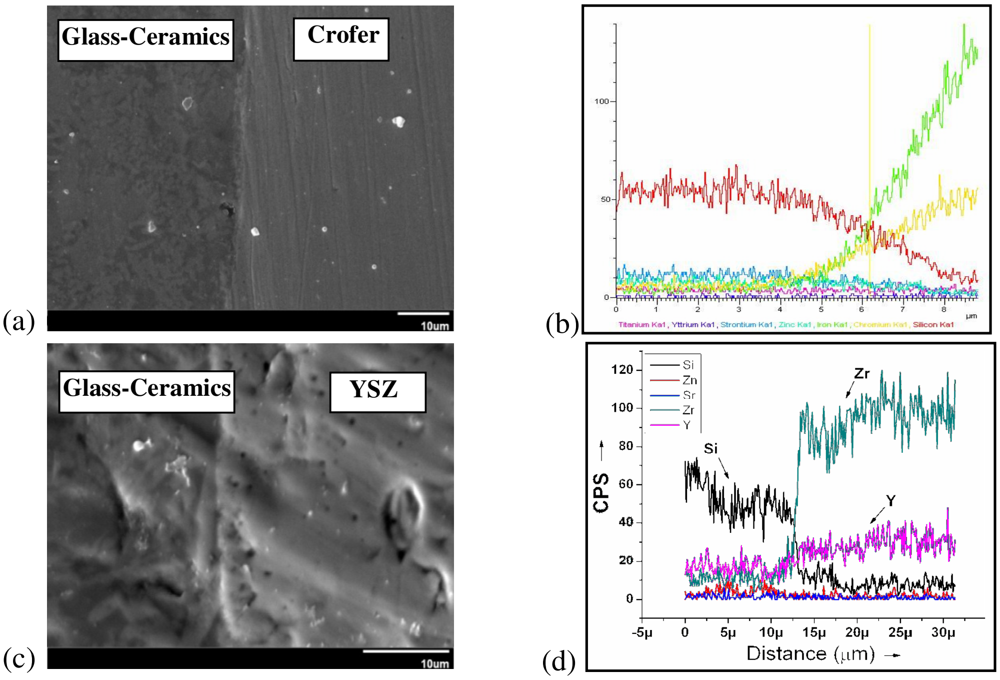

Figure 4.28: (a) SEM micrographs of the SZS-8 glass-ceramic to Crofer-22-APU interface after sealing at 950°C, (b) EDS line scans across the interface showing the inter-diffusion of Si, Sr, Fe and Cr, (c) SEM micrographs of the SZS-8 glass-ceramic to YSZ interface after sealing at 950°C, (d) EDS line scans across the interface showing the inter-diffusion of Si, Sr, Zr and Y.

SEM micrographs of interface of SZS-8 glass-ceramics with YSZ and Crofer, after sealing at 950°C, are shown in Figure 4.28(a) and (c), respectively. A smooth interface shows the good bonding of glass with YSZ and Crofer. Elemental line scans are presented in Figure 4.28(b) and (d), respectively. Thickness of interfacial zone is found to be ~3μm. Thus, the present study revealed that glasses having B_2O_3 are suitable for achieving good bonding with SOFC cell components. B_2O_3 reduces the viscosity of glass and rate of crystallization thereby at the sealing temperature sufficient amount of residual glass is available to make good bonding with the cell components. Further addition of small amount of V_2O_5 is beneficial for better flowability thereby lowering the sealing temperature.

4.4 Conclusions

New glass-ceramics in the SrO-Zn-O-SiO_2 system were investigated for the high temperature sealant application. The compositions of SZS glasses have shown requisite thermo-physical properties (TEC, T_g, T_{ds} and viscosity) for their use as a high temperature sealant for SOFC application. It is inferred from microstructural and crystallization kinetics studies that for SZS-1 glass (base composition) diffusion controlled bulk crystallization occurs with two and three dimensional growth. Liquid-in-liquid phase separation in SiO_2 and ZnO rich regions by spinodal decomposition mechanism has been observed prior to crystallization in this glass. $Sr_3Si_3O_9$ and $Sr_2ZnSi_2O_7$ phases crystallized in these regions upon further heat treatment, respectively. It is also found that with the addition of additives, surface crystallization mechanism start dominating over bulk crystallization and activation energy decreases. A composition (SZS-6 glass) having B_2O_3 and V_2O_5 additives shows the lowest activation energy for crystallization thereby a better control over the crystallization during the sealing process. The bonding behaviour also indicates that B_2O_3 and V_2O_5 are useful constituents for increasing the flow of glass at sealing temperature. Crystallized phases ($Sr_3Si_3O_9$ and $Sr_2ZnSi_2O_7$) in SZS glass-ceramics have matched high TEC, higher mechanical strength, chemical durability and dielectric properties therefore, advantageous in resultant glass-ceramic sealants. Raman and XRD studies together confirm that in early stage of crystallization, $Sr_2ZnSi_2O_7$ phase and later $Sr_3Si_3O_9$ phase formed in the SZS glass-ceramics. XRD and NMR studies confirm the formation of solid solution of $Sr_2ZnSi_2O_7$ phase in the SZS glass-ceramics containing B_2O_3 and/or Al_2O_3 additives. It is suggested that B and Al make solid solution by substituting Zn/Si at tetrahedral sites in $Sr_2ZnSi_2O_7$ phase.

Structural studies of SZS glasses and glass-ceramics indicate the depolymerization of silicate network with the incorporation of different additives. This is associated with the modification of thermo-physical properties of glasses. Raman and FTIR studies show the decisive role of structural units on formation of crystalline phases during the heat treatment.

On the basis of thermo-physical and bonding properties, SZS-6 glass having B_2O_3 and V_2O_5 additives seems to be more suitable for SOFC sealants. Seals of this composition with Crofer-22-APU were found vacuum compatible at high temperatures even after long-term (800 h) exposure at those temperatures. Thus, studies carried out so far demonstrate the potential of SZS glass-ceramics as high temperature sealants for SOFC application.

Chapter 5

Studies on Barium Zinc Silicate Glasses/Glass-ceramics

5.1 Introduction

Glasses and glass-ceramics in RO-BaO-SiO_2 (R=Mg, Zn) system have also been reported as candidate materials for the solid oxide fuel cell (SOFC) sealing application [157,171]. However, issues concerning long-term thermal and chemical stabilities arise for barium based silicate glasses for use as a sealant in the SOFC [162,163]. Recently, Zhang et al [170] have reported the role of the ZnO in the reduction of chromate phase formation at the interface. In the previous chapter, the thermo-physical properties of SZS glasses and glass-ceramics have been discussed in detail, with respect to their application as sealant materials for SOFC. Further, as the charge to radius ratio of Ba^{2+} is smaller compared to Sr^{2+} and the Ba-O bond is more ionic compared to Sr-O bond, it is expected that the thermo-physical properties, chemical reactivity etc would be quite different when Ba replaces Sr in the SrO-ZnO-SiO_2 glass system. Hence, for a comparative evaluation of the thermo-physical properties of these two glass systems, studies were carried out on BZS glass/glass-ceramics and described in the present chapter.

Preparation, thermo-physical properties, crystallization kinetics and microstructural aspects of a few glasses and glass-ceramics in BaO-ZnO-SiO_2 system with different additive have been discussed in this chapter. To demonstrate the suitability of materials for their use as a high temperature sealant for SOFCs, formation and testing of seals with cell components have also been described here. However, a comparative study of glasses in both the system will be done in the near future.

5.2 Experimental

5.2.1 Synthesis of glass/glass-ceramics samples

Table 5.1: Chemical compositions (in wt.% and mol%) of investigated BZS glasses.

Glass ID	Composition	BaO	ZnO	SiO_2	Nd_2O_3	B_2O_3	V_2O_5	TiO_2
BZS-1	(wt.%)	51	9	40	-	-	-	-
	(mol%)	30	10	60	-	-	-	-
BZS-2	(wt.%)	50.4	13.4	36.2	-	-	-	-
	(mol%)	30	15	55	-	-	-	-
BZS-3	(wt.%)	49.8	17.6	32.5	-	-	-	-
	(mol%)	30	20	50	-	-	-	-
BZS-4	(wt.%)	51	9	39	1	-	-	-
	(mol%)	30.4	10.1	59.3	0.3	-	-	-
BZS-6	(wt.%)	50	9	39	1	1	-	-
	(mol%)	29.6	10	58.8	0.3	1.3	-	-
BZS-7	(wt.%)	51	9	35	5	-	-	-
	(mol%)	32	10.6	56	1.4	-	-	-
BZS-8	(wt.%)	46	9	39	1	5	-	-
	(mol%)	26.4	9.7	57.2	0.3	6.3	-	-
BZS-9	(wt.%)	51	9	32	5	-	1	2
	(mol%)	32.6	10.8	52.2	1.5	-	0.5	2.5
BZS-10	(wt.%)	51	9	30	2	5	1	2
	(mol%)	40.7	41.3	9.1	0.5	5.9	0.5	2.1

Glasses of different composition in the BaO-ZnO-SiO_2 (BZS) system with different additives including Nd_2O_3, V_2O_5, TiO_2 and B_2O_3 (Table 5.1) were prepared by a melt-quench method following the procedure as described in chapter 2. Analytical grade $Ba(NO_3)_2$ (MERCK, India), B_2O_3 (MERCK, Germany), SiO_2 (Loba Chemie, India), and ZnO, V_2O_5, TiO_2 and

Nd_2O_3 (all from S. D. Fine Chem Ltd., India) were used as starting precursors. Depending on the composition, glass charges were melted in the temperature range 1450-1550°C in the air ambient. The glass was then annealed in the temperature range of 620-650°C for 4 h. Discs of bulk glasses were used for crystallization and other measurements. For the formation of glass-ceramics, parent glass discs were crystallized at 925°C for 2 h.

5.2.2 DTA

The crystallization temperature of glasses was determined from DTA experiments, as mentioned in chapter 2. The non-isothermal experiments were performed on approx 50 mg powdered samples, using a heating rate of 10°C/min. Glass samples in the powder form were obtained by ball milling of the crushed bulk glass. The particle size distribution of granulated glass powder was in the range 75-210 μm. To study the crystallization kinetics of a few representative BZS glasses the DTA scans were also recorded from room temperature to 1050°C in an air atmosphere with heating rates of 5, 10, 15 and 20°C/min.

5.2.3 Thermo-physical characterization

T_g, T_{ds} and TEC of the glass samples were determined using a dilatometer according to the methodology described in chapter 2. Flat circular discs of diameter 10 mm and thickness 3-4 mm were used for these measurements. The TEC being reported here is the average in the temperature range of 30-600°C for glasses and average in the range of 30-800°C for glass-ceramics. The density was measured at room temperature by Archimedes principle using DM water as an immersion liquid with an accuracy of ±0.03 g/cm^3. The MH of glass samples was measured by the Vickers indentation technique. Indentation was obtained by applying a 50 g load for 5 s.

5.2.4 XRD

Amorphous nature of glasses and various crystalline phases in glass–ceramics samples were identified using powder XRD technique with Cu K_α as an X-ray source. Diffractograms were recorded in the 2θ range of 10-70° with a speed of 2°/min (steps of 0.02°).

5.2.5 Microstructural characterization

Microstructural studies were carried out using SEM as described in chapter 2. Microstructure at the interface of a seal between glass-ceramics and SOFC components were also investigated by the SEM. Elemental line scanning was performed across the interface of seals using EDS.

5.2.6 Bonding properties and interface studies

The adhesion/bonding property of a few glasses with YSZ and Crofer-22-APU was investigated according to the method described in chapter 2. This was done by placing a glass disc on a sintered YSZ pellet and heated in a controlled manner in air at 1000°C for 1 h. In order to assess the adhesion property and chemical compatibility of a few representative BZS glasses with Crofer-22-APU, seals in a sandwich geometry (Crofer/glass/Crofer) were prepared by heating the assembly in a controlled manner at 1000°C in air for 1 h. Seals were fabricated and tested for vacuum integrity following the process described in chapter 2.

5.3 Results and Discussion

Clear, transparent and inclusion/bubble-free, BZS glasses were obtained for all the compositions. The glasses were colourless except those having Nd_2O_3 and/or V_2O_5. The glasses containing Nd_2O_3 having a tint of blue or purple colour, might be due to the presence of Nd^{3+} ions and glasses containing V_2O_5 and Nd_2O_3 were light greenish and bluish in colour due to the presence of V^{3+} and Nd^{3+} ions in the glass [177].

5.3.1 Thermo-physical properties

The thermo-physical properties measured for the BZS glasses are listed in Table 5.2. The viscosity of BZS glasses was also calculated from dilatometric data using VFT equation as described in chapter 4 and listed in Table 5.2.

Table 5.2: Thermo-physical properties of investigated BZS glasses.

Glass ID	$T_g \pm 2$ °C	$T_{ds} \pm 2$ °C	TEC ± 5% (10^{-7}/°C) (30-600°C)	$T_P \pm 2$ °C	η (at 1000°C) (dPa s)	$\rho \pm 0.03$ (10^3 kg/m^3)	MH ± 10% GPa
BZS-1	694	719	95	918	6.53	3.82	-
BZS-2	701	727	94	928	6.55	-	-
BZS-3	698	722	94	-	6.52	-	-
BZS-4	697	729	108	920	-	3.84	3.23
BZS-6	679	710	95	862	6.55	3.87	4.72
BZS-7	702	733	95	882	6.66	4.07	5.06
BZS-8	671	697	93	856	6.42	3.68	4.86
BZS-9	701	736	91	-	-	4.17	4.82
BZS-10	638	680	92	-	-	4.04	

It is clear that investigated glasses have density in the range of 3.68-4.07 x 10^3 kg/m^3 and MH in the range of 3.23-5.06 GPa. MH values of BZS glasses are found to be lower than that of the SZS glasses. This is attributed to lower field strength of Ba ions compared to Sr ions. The density of BZS glasses increases with Nd_2O_3 concentration and decreases with B_2O_3 concentration. This is understood, on the basis of molecular weight of Nd_2O_3 (high compared to that of SiO_2) and B_2O_3 (lower compared to that of BaO). Increased content of Nd_2O_3 causes high T_g and high MH of glass and consequently decreased TEC. This may be attributed to the formation of Si-O-Nd type cross linking which increase the connectivity of the network and results in the observed changes in the T_g, MH and TEC. The B_2O_3 having lower melting point reduces T_g and T_{ds} but as B_2O_3 replaces BaO, the glass former content increases in the glass resulting in a more connected glass network. Due to this increased connectivity the MH increases and consequently TEC decreases. The TEC for the investigated glasses are in the range of 91-108 x 10^{-7}/°C (30-600°C), which is closely matched with the TEC of other SOFC components like interconnect, electrodes and electrolytes [179,168]. TEC, MH, and ρ for the glass-ceramic samples are given in Table 5.3.

Table 5.3: Thermo-physical properties of a few representative BZS glass-ceramics.

Glass-ceramic ID	ρ ± 0.03 (10^3 kg/m^3)	MH ± 10% (GPa)	TEC ± 5% (10^{-7}/°C) (30-800°C)
BZS-4-GC	4.07	4.53	130
BZS-6-GC	3.88	4.93	124
BZS-7-GC	4.03	5.18	118
BZS-8-GC	3.72	-	126

For all the glass-ceramics, softening point was not observed up to 1000°C which is advantageous for their use for high temperature sealing application. The MH was found to be more after conversion into glass-ceramics which is also advantageous for better mechanical strength of the seal. All the studied BZS glass-ceramics have TEC in the range 118-130 x 10^{-7}/°C which is higher than TEC of corresponding BZS base glasses and are matching to the TEC of other components of SOFC within acceptable limits [179]. The DTA plots of the investigated glasses are shown in Figure 5.1. It is observed that substitution of ZnO for SiO_2 in BZS glass does not affect the TEC however, slightly increase the T_g and T_{ds}. Therefore, for all other compositions ZnO was kept constant at 9 wt.%.

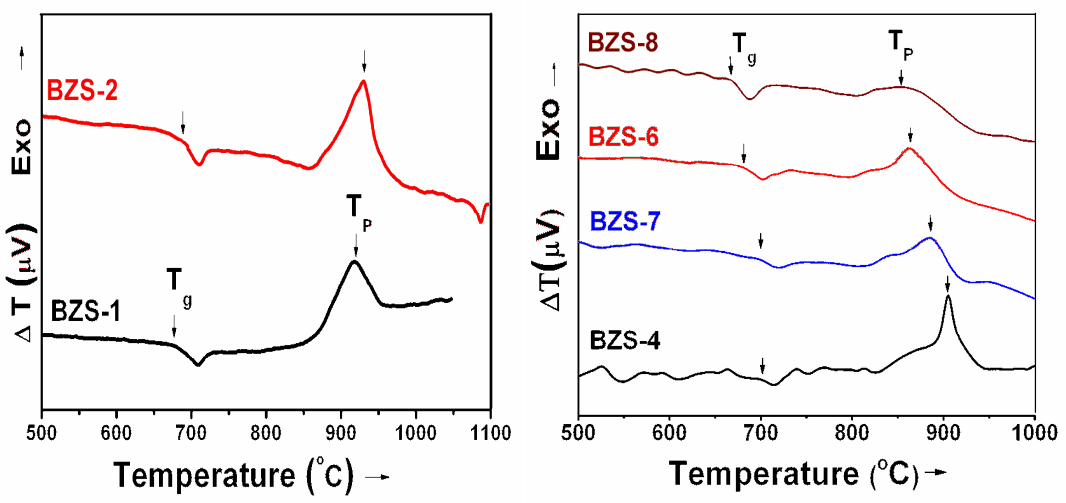

Figure 5.1: DTA curves of investigated BZS glasses.

5.3.2 XRD

A characteristic broad hump in the powder XRD pattern of BZS glasses confirmed the amorphous nature of the prepared glasses. Figure 5.2 shows the X-ray diffractograms of BZS glass-ceramics heat treated at 925°C for 2h. Different crystalline phases formed in the BZS glass-ceramics are summarized in Table 5.4. From XRD patterns of the glass-ceramics it is observed that mainly $BaSi_2O_5$ (sanbornite) phase crystallizes in all the glasses, except BZS-2, BZS-3 and BZS-7 glasses as listed in Table 5.4. For BZS-2 and BZS-3 glasses, $Ba_2Si_3O_8$ phase crystallized as a major component along with $Ba_5Si_8O_{21}$ and $BaSi_2O_5$ phases in minor amounts. For the BZS-7 glass, $Ba_5Si_8O_{21}$ phase crystallized in major amount and $BaSi_2O_5$ phase in a minor amount. Crystallization of different barium silicate phases in the BZS glass-ceramics are attributed to different BaO to SiO_2 wt. ratio in the parent glass. It can be seen from Table 5.4 that when a weight ratio of BaO to SiO_2 in BZS glass is close to 1.28 like BZS-1,4,6, and BZS-8, mainly $BaSi_2O_5$ (wt. ratio 1.28) phase crystallized in glass-ceramic. And when the weight ratio of BaO to SiO_2 in BZS glass is higher than 1.28 like BZS-2,3 and BZS-7, mainly other barium silicate phases with higher BaO to SiO_2 wt. ratio e. g. $Ba_2Si_3O_8$ (wt. ratio 1.70) and $Ba_5Si_8O_{21}$ (wt. ratio 1.59) are crystallized in the glass-ceramics. Thus, the nature of the crystalline phase and its composition depend on the relative ratios of BaO to SiO_2. It is reported that all these barium silicate crystalline phases have high TEC [225] and therefore, glass-ceramics having these phases are compatible for use as a sealants for SOFC.

Table 5.4: Crystalline phases in BZS glass-ceramics.

Glass-ceramic ID	**BaO/SiO_2 (wt. ratio) in Parent glass**	**Crystalline phases**
BZS-1-GC	1.27	$BaSi_2O_5$
BZS-2-GC	1.39	$BaSi_2O_5$, $Ba_5Si_8O_{21}$, $Ba_2Si_3O_8$
BZS-3-GC	1.53	$BaSi_2O_5$, $Ba_5Si_8O_{21}$, $Ba_2Si_3O_8$
BZS-4-GC	1.31	$BaSi_2O_5$
BZS-6-GC	1.28	$BaSi_2O_5$,
BZS-7-GC	1.45	$BaSi_2O_5$, $Ba_5Si_8O_{21}$
BZS-8-GC	1.18	$BaSi_2O_5$

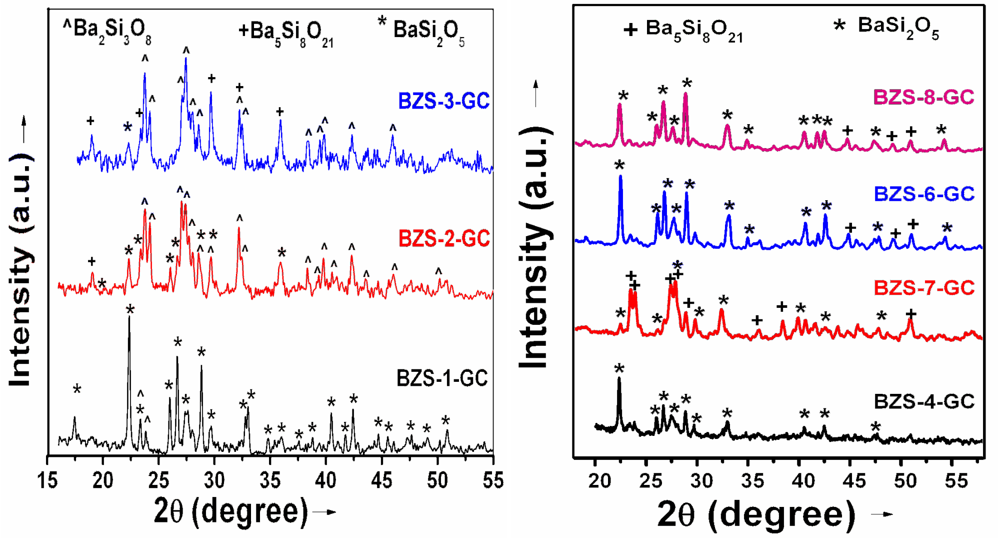

Figure 5.2: X-ray diffractograms of BZS glass-ceramics.

5.3.3 SEM analysis

SEM micrographs of BZS-1 glass-ceramic (Figure 5.3) show a very fine mixed plate like and granular type crystallites (size ~500 nm) of the BaSi$_2$O$_5$ phase. Crystallization kinetics study (described later) also confirms the bulk crystallization with two dimensional growths of crystals.

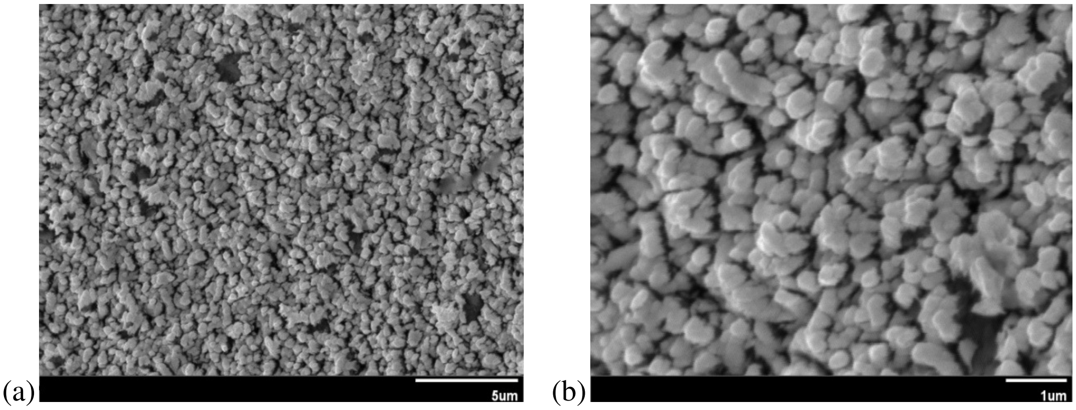

Figure 5.3: SEM micrographs of the BZS-1 glass-ceramic at different magnification (a) 10kx (b) 30kx

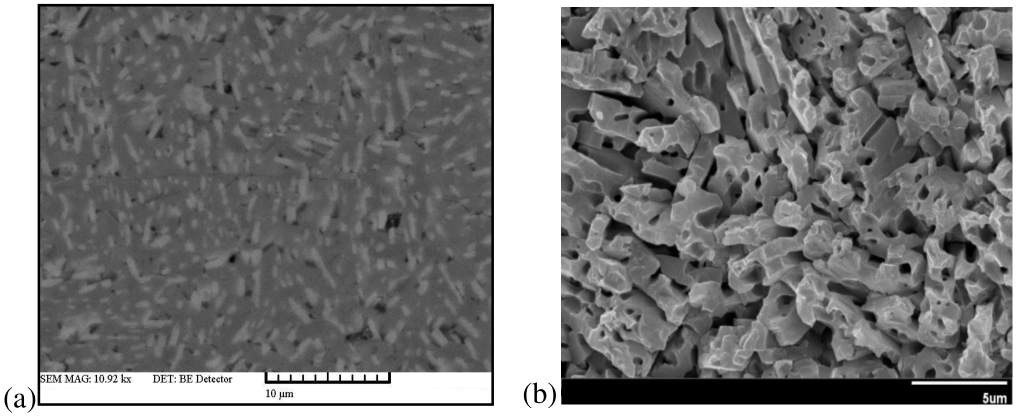

Figure 5.4: SEM micrographs of the BZS-6 glass-ceramic (a) BSE mode (b) SE mode

For BZS-6 glass-ceramic the micrograph (Figure 5.4) shows elongated crystals (2-4 µm in size) of the $BaSi_2O_5$ phase dispersed in a glassy matrix. For BZS-7 glass-ceramic, the SEM micrograph (Figure 5.5) shows granular crystals (4-5 µm in size) of $BaSi_2O_5$, $Ba_5Si_8O_{21}$ phases dispersed in a glassy matrix. At a higher magnification the micrograph shows a very fine, mixed plate like and granule type morphology of crystallites.

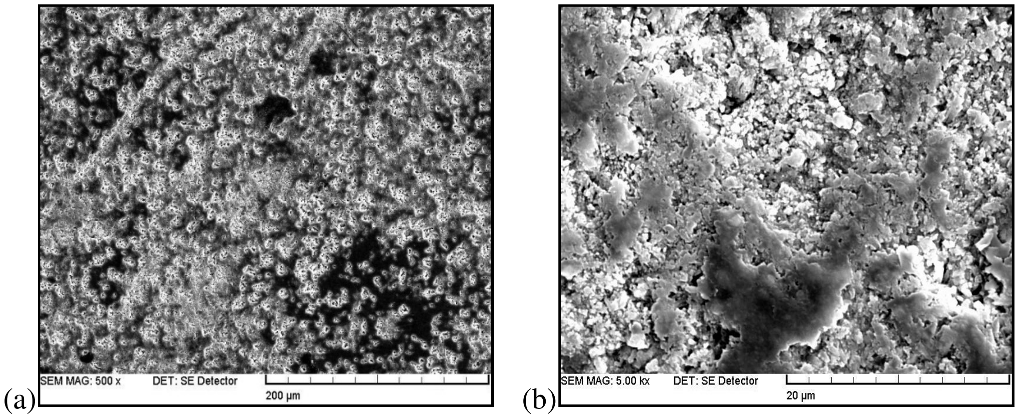

Figure 5.5: SEM micrographs of the BZS-7 glass-ceramic at different magnification (a) 0.5kx (b) 5kx.

5.3.4 Crystallization kinetics and mechanism of BZS glasses

The Non-isothermal crystallization kinetics of a few BZS glasses was investigated using Ozawa and Matusita-Sakka method as described in chapter 4. The Avrami parameter '*n*' was determined through Ozawa method from the crystallized fraction '*x*' obtained at different temperatures for different heating rates. The Ozawa plots of BZS-1 and BZS-8 glasses are shown in Figure 5.6 (a) and (b). Fitting of the data to straight lines ($R^2 \geq 0.98$) gives values of Avrami parameter '*n*' which increased gradually when temperature changes from higher to lower side. The average value of '*n*' is 1.9 for BZS-1 glass and 1.2 for BZS-8.

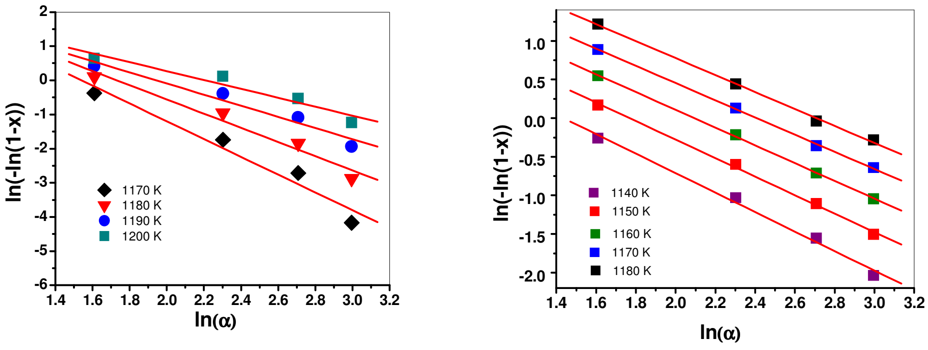

(a) (b)

Figure 5.6: Ozawa plots of (a) BZS-1 and (b) BZS-8 glasses.

Figure 5.7 (a) and (b) show the Marseglia plots of both the glasses. Using the value of *n*, the activation energy E_a (Marseglia) for both the peaks were calculated from the slope of these straight lines and tabulated in Table 5.5. The values of growth morphology parameters '*n*' and '*m*' for BZS-1 glass (Table 5.5) indicate a diffusion controlled bulk crystallization for this glass with varying number of nuclei. This bulk crystallization occurs via two dimensional growth of the crystal. The microstructure of the crystallized glass also conform the two to three dimensional growth of crystals. These results are consistent with the reported one for BZS glasses [171]. The values of growth morphology parameters '*n*' and '*m*' for BZS-8 glass (Table 5.5) indicate a diffusion controlled surface crystallization for this glass with varying number of nuclei.

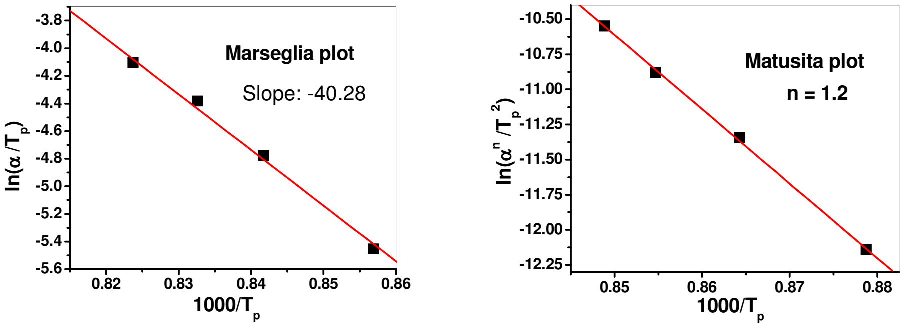

(a) (b)

Figure 5.7: Marseglia plots of (a) BZS-1 and (b) BZS-8 glasses.

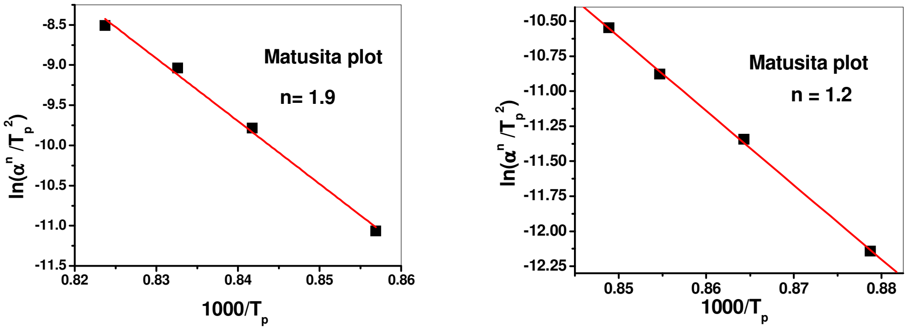

(a) (b)

Figure 5.8: Matusita plots of (a) BZS-1 and (b) BZS-8 glasses.

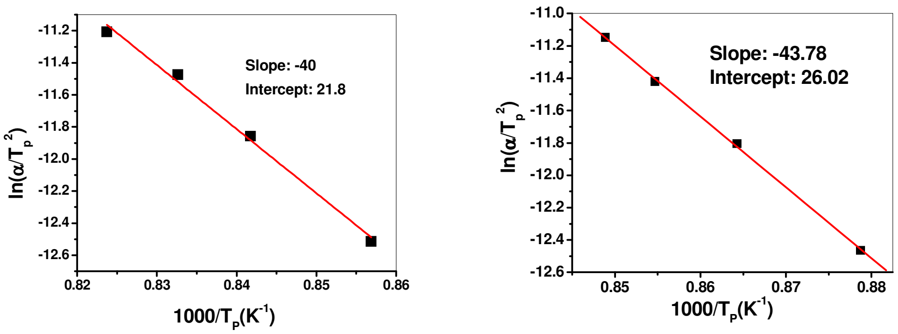

(a) (b)

Figure 5.9: Kissinger plots of (a) BZS-1 and (b) BZS-8 glasses.

Table 5.5: Activation energies and growth morphology parameters for crystallization of a few representative BZS glasses.

Sample	Average 'n' (Ozawa)	*m* (Matusita)	E_{ak} (kJ/mol) (Kissinger)	E_a (kJ/mol) (Marseglia)	E_a (kJ/mol) (Matusita)
BZS-1	1.9	1	333	636	648
BZS-8	1.2	1	364	448	441

Figure 5.8 (a) and (b) show the Matusita-Sakka plots of BZS-1 and BZS-8 glasses, respectively. Data were fitted to straight lines with simple least squares method with $R^2 \geq 0.99$. The value of 'mE_a' was calculated from the slope of these straight lines and found to be 648 kJ/mol for the BZS-1 glass and 441 kJ/mol for the BZS-8 glass as summarized in Table 5.5. It can be seen from Table 5.5, that the activation energy 'E_a' is quite high compared to 'E_{ak}' for the BZS-1 glass and this value is comparable to 'E_{ak}' for the BZS-8 glass. Relatively higher activation energy for the BZS-1 glass compare to the BZS-8 glass suggests that the kinetics is more activated with the temperature for this composition. Lower activation energy for the BZS-8 glass indicates that this composition has a better control over the crystallization

during the sealing process. The Kissinger plots of both the BZS glasses are shown in Figure 5.9 (a) and (b). Data were fitted to straight lines with simple least squares method, obtaining $R^2 \geq 0.99$. The Kissinger activation energy 'E_{ak}' was calculated from the slope of these plots and given in Table 5.5.

5.3.5 Bonding properties and interface studies

The adhesion behaviour of a few glasses to YSZ was investigated. The SEM image of the interface between YSZ and BZS-8 glass after a heat treatment at 900°C for 1 h in air ambient is shown in Figure 5.10(a) and (b).

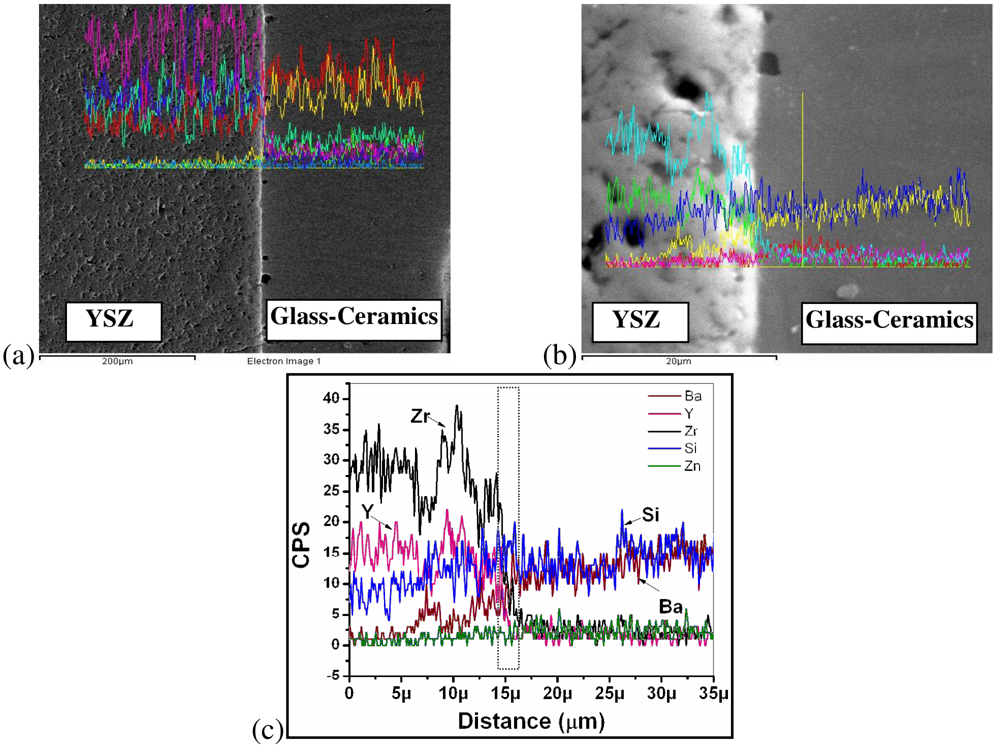

Figure 5.10: SEM micrographs of the BZS-8 glass-ceramic to YSZ interface after sealing at 900°C at different magnification (a) 1kx, (b) 10kx, (c) EDS line scans across the interface showing the inter-diffusion of Si, Ba, Zr and Y.

A continuous interface shows good bonding between glass and YSZ. Elemental line scans across the interface [Figure 5.10(c)] indicate that the inter-diffusion of Ba, Si from glass side to YSZ side and inter-diffusion of Y, Zr from YSZ side to glass side is responsible for a good bonding with YSZ. It is found that the interfacial zone is around 3-4 µm. The SEM image of the interface between Crofer-22-APU and BZS-8 glass after a heat treatment at 1000°C for 1 h in air ambient is shown in Figure 5.11(a). Continuous interface shows good bonding between glass and Crofer. This bonding is attributed to the inter-diffusion of Fe, Cr and Si across the interface [Figure 5.11(b)].

Testing for vacuum integrity of seal between BZS-8 glass-ceramic and Crofer-22-APU revealed the hermeticity of the seal up to 800 h at 800°C. This indicates the long-term stability of the BZS-8 glass-ceramic for use as a high temperature sealant.

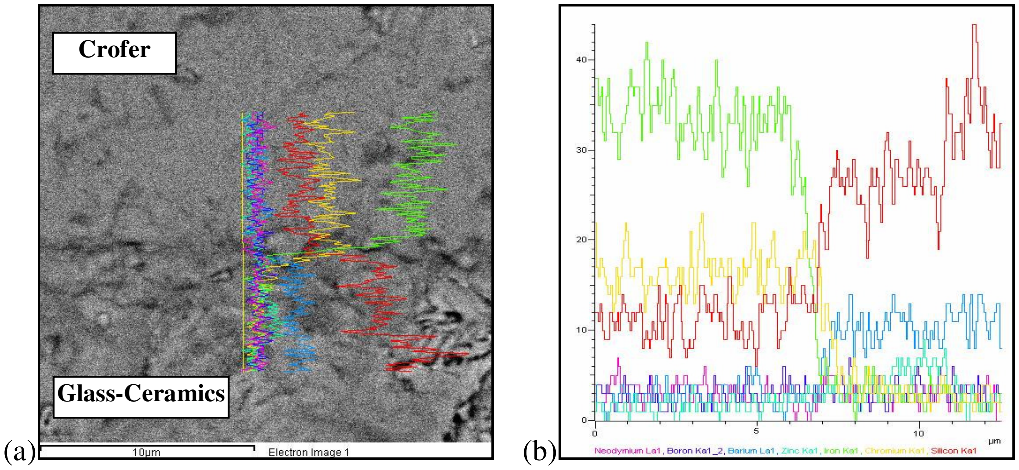

Figure 5.11: (a) SEM micrographs of the BZS-8 glass-ceramic to Crofer-22-APU interface after sealing at 1000°C (b) EDS line scans across the interface showing the inter-diffusion of Si, Fe and Cr.

5.4 Conclusion

Barium zinc silicate based glasses/glass-ceramics have been prepared and characterized. Investigated barium zinc silicate based glasses/glass-ceramics have requisite dilatometric and viscosity properties for their application as a sealant for SOFC. It is found that addition of Nd_2O_3 increases the MH, T_g and T_{ds} but reduces the TEC due to an increased cross-linking. Addition of B_2O_3 is useful for improving the flow property and suppressing the crystallization tendency, that are beneficial for sealing applications. From the crystallization studies, it is concluded that the weight ratio of BaO to SiO_2 decides the formation of different barium silicate crystalline phases in the glass upon heat treatment. In all BZS glasses, the crystallization of barium silicate phases having high TEC is advantageous for good thermal and mechanical stabilities of the glass-ceramic sealants. The base glass (BZS-1) shows the bulk crystallization and with the additives, the surface crystallization mechanism starts dominating. On the basis of thermo-physical and bonding properties, the BZS-8 composition seems to be more suitable as high temperature sealant for SOFC.

Chapter 6

Summary and Future Scope

Recently, alkaline earth based silicate glasses and glass-ceramics got renewed interest for their use as high temperature sealants for p-SOFCs. Similarly, phosphate glasses have attracted much interest in various scientific and technological fields, after the development of novel compositions of superior chemical and physical properties in the recent past. Therefore, in this dissertation we have investigated some technologically important phosphate and silicate based glasses and glass-ceramics. Present investigations are mainly focused on preparation, thermo-physical properties and structural/microstructural aspects of sodium aluminium titano-phosphate (NATP) glasses, strontium zinc silicate (SZS) and barium zinc silicate (BZS) based glasses/glass-ceramics. Investigations carried out on NATP glasses, SZS and BZS glasses/glass-ceramics are discussed in Chapters 3, 4 and 5, respectively in this dissertation. This chapter summarizes the work carried out in the thesis and presents the important finding along with future scope of the work.

The primary aim of investing NATP glasses was to study the effect of TiO_2 addition on various thermo-physical and optical properties of sodium alumino-phosphate (NAP) glasses, as these glasses have potential application in low temperature hermetic seals and optoelectronic devices. It is found that T_g, ρ and MH increase while TEC and V_m decrease up to 10 mol% TiO_2 and beyond 10 mol% these properties show the reverse trend when P_2O_5 is replaced by TiO_2. An attempt has been made to correlate the observed thermo-physical properties with structural aspects of the NATP glasses. Raman, FTIR and ^{31}P MAS-NMR studies confirm that addition of TiO_2 in the NAP glass results in a progressive depolymerization of the glass with the formation of P-O-Ti linkages at the expense of P-O-P linkages. Raman spectra revealed that TiO_2 enters in the glass network in the form of octahedral and tetrahedral units and at a higher concentration of TiO_2, tetrahedral structural units are more favourable. Interestingly a significant change in the Al coordination from octahedral to tetrahedral was observed through ^{27}Al MAS-NMR for glass samples containing more than 10 mol% TiO_2. Based on optical studies, the observed luminescence (broad emission peak at ~435 nm) has been attributed to different types of luminescent centers present in the glass. The variation in $E_{optical}$ values and emission maxima for these glasses are also in accordance with the structural changes in the glass. From structure-property correlation it is inferred that the role of TiO_2 and Al_2O_3 changes from network modifier to network former in NATP glasses around 10 mol% TiO_2. A decrease in the extent of degradation of the glass surface in humid environment was observed with the TiO_2 incorporation in the NAP glasses, which reflect the higher chemical durability of NATP glasses. The development of phosphate glass composition with a higher chemical durability is beneficial to make use of the unique properties of phosphate glasses in various technologies. The NATP glass having TiO_2 content around 10 mol%, have a TEC around 160 x 10^{-7}/°C, which is closely matched with the thermal expansion of Cu and Cu-Be alloy. Therefore, this composition is suitable for making matched type hermetic glass-to-metal seals with these metals and alloys. Further, investigation on effect of two intermediate oxides (mixed intermediate effect) as a function of the $TiO_2/(Al_2O_3+TiO_2)$ ratio with fixed amount of Na_2O and P_2O_5, will be useful to get deeper understanding about the role of Al_2O_3 and TiO_2 in NATP glasses.

Strontium zinc silicate glasses and glass-ceramics have been investigated as potential high temperature sealants for SOFCs. Main aim to investigate the SZS system is to develop a suitable composition for SOFC sealant applications. Studied compositions of SZS glasses fulfill the most important criteria (TEC, T_g, T_{ds} and viscosity) of thermo-physical properties for use as a high temperature sealants for the SOFCs. Upon further optimizing the composition of SZS glasses using various additives, it is found that B_2O_3 and V_2O_5 allow a better bonding of glasses with SOFC components. The XRD and microstructural studies revealed that the parent SZS glass phase separated into SiO_2 and ZnO rich regions prior to crystallization and $Sr_3Si_3O_9$ and $Sr_2ZnSi_2O_7$ phases crystallized in these regions upon further heat treatment, respectively. The microstructural evolution with heat treatment depicts the spinodal decomposition mechanism for liquid in liquid phase separation in this glass. Based on the crystallization kinetics using Ozawa and Matusita-Sakka methods it is inferred that a diffusion controlled bulk crystallization with 2-3 dimensional growth occurs for the SZS glass. With the addition of additives a surface crystallization mechanism starts dominating over the bulk crystallization and the activation energy decreases. Lower activation energy indicates a better control over crystallization process during sealing. This information is useful to develop and optimize suitable glass-ceramic sealants and sealing procedure. Both the crystallized phase ($Sr_3Si_3O_9$ and $Sr_2ZnSi_2O_7$) in SZS glass-ceramics have high thermal expansion therefore, advantageous for the glass-ceramics based sealants for the SOFC. The desirable crystalline phases having a matched TEC, higher mechanical strength, chemical durability and dielectric properties are formed in the SZS glass-ceramics, which indicate long term stability for their use as a sealant for SOFC.

The structural studies of SZS glasses and glass-ceramics indicate the depolymerization of silicate network with the incorporation of different additives. This is associated with the modification of thermo-physical properties of glasses. In an interesting result, the Raman spectroscopy revealed a three member ring type structure for the $SrSiO_3/Sr_3Si_3O_9$ phase. Raman and FTIR studies show the decisive role of structural units on the formation of crystalline phases during heat treatment of the glass. Raman and XRD studies together confirm that in early stage of crystallization, $Sr_2ZnSi_2O_7$ phase and later $Sr_3Si_3O_9$ phase formed in the SZS glass-ceramics. The XRD studies suggested the formation of a solid-solution of $Sr_2ZnSi_2O_7$ phase in SZS glass-ceramics containing B_2O_3 and/or Al_2O_3, but it is difficult to identify the nature and composition of the solid-solution. ^{27}Al and ^{11}B MAS-NMR spectra confirmed the crystallization of B and Al in the tetrahedral coordination. Thus, on the basis of combined studies of NMR and XRD it is inferred that a solid-solution of $Sr_2ZnSi_2O_7$ phase is formed in the SZS glass-ceramics with the substitution of B/Al at Si or Al tetrahedral sites. Information about crystallization kinetics and mechanism is important to develop suitable glass-ceramic sealants and sealing procedure. Crystallization kinetics studies indicated that, with the incorporation of additives in the glass, a surface crystallization mechanism starts dominating over the bulk crystallization and the activation energy decreases. Based upon these studies, a composition (SZS-6 glass) with B_2O_3 and V_2O_5 additives has been found most suitable and seals were fabricated with Crofer-22-APU. These seals were vacuum compatible at elevated temperatures, even after 800 h exposure at 850°C and further studies regarding long-term use are underway.

BZS glasses and glass-ceramics have also been prepared as a potential sealant for the SOFC. The BZS glasses and glass-ceramics have shown adequate thermo-physical properties like TEC, T_g, T_{ds}, MH etc, for their application as SOFC sealants. Crystallization kinetics of BZS glasses also revealed a diffusion controlled bulk crystallization with two dimensional growth of crystals from a varying number of nuclei. With the addition of additives a surface crystallization mechanism starts dominating over the bulk crystallization and the activation energy decreases. This information is useful to develop and optimize suitable glass-ceramics sealants and sealing procedure. BZS glass-ceramics have desirable high TEC due to the formation of various compatible barium silicate crystalline phases having high TEC. Seals with Crofer-22-APU were prepared using the BZS-8 glass (most suitable composition) and vacuum tested at high temperatures successfully. The main aim to investigate the BZS glass-ceramics is to compare the long term chemical and thermal stabilities, especially interfacial reaction with Crofer-22-APU, of these sealants with SZS glass-ceramics sealants, in near future.

In the thesis efforts have been made to show that the thermo-physical properties of the investigated glasses are a sensitive function of structural configurations present in these glasses and can be modified by incorporating suitable additives. Studies also demonstrate the utility of structural/microstructural and thermo-physical characterization in optimization of composition of glasses/glass-ceramics for novel applications like high temperature sealing. However, there is a need to augment this information about the structure of glasses with a variety of other structure sensitive techniques like high resolution EXAFS, XPS, as well as small angle X-ray and neutron scattering. It is proposed to carry out these studies in near future. MAS-NMR experiments like spin echo double resonance (SEDOR) and rotational echo double resonance (REDOR) are being proposed to investigate the structure and environment around the next nearest neighbour of Si atom. Further, such experiments can also give information regarding cation distribution in the glass. The ^{17}O MQ-MAS is planned to understand the environment around the oxygen atom as well as to estimate different types of oxygen atoms in the glasses and glass-ceramics. The ^{51}V MAS-NMR is also proposed to investigate the effect of V_2O_5 on the structure and therefore on properties of the glass. ZnO can behave as a glass modifier or glass former depending on the composition of the glass. It will be interesting to study the structural surrounding of Zn atom in investigated SZS/BZS glasses by means of EXAFS. To show the insulating properties of studied glasses and glass-ceramics, measurements of electrical conductivity with temperature are planned in the near future. The phase quantification may be initiated for these systems using MAS-NMR and XRD. Chemical durability of the prepared glasses in different media (acidic, alkaline and neutral) and at different temperatures is also worth to investigate. Detailed electron probe microanalysis (EPMA) and electron backscattered diffraction (EBSD) studies to investigate the morphology and relative concentration of different crystalline and glassy phases will be helpful for getting deep insights to the crystallization behaviour. Synchrotron radiation based X-ray diffraction experiments are proposed for understanding the solid-solution formation in the glass-ceramics. In-situ HTXRD (high temperature XRD) will also be useful to understand the phase evolution mechanism in the glass-ceramics. It is also proposed to carryout TEM (transmission electron microscopy) and SAED (small angle electron diffraction) studies on these glasses to understand the phase separation and nucleation mechanism of the crystallization. Studies related to isothermal crystallization kinetics are also proposed in the future.

Studies carried out so far demonstrated the potentiality of SZS and BZS glass-ceramics for high temperature sealant applications for SOFC. Therefore, it will be useful to study the wetting behaviour of glasses on different cell components using the high temperature microscopy. Such experiments are planned in the near future. Other studies include long-term phase stability by a combination of XRD and MAS-NMR in wet oxidizing and reducing environments that mimic the operational conditions of fuel cells. Further scope also exists in terms of reaction studies with other fuel cell components, especially over long term use. Effect of ZnO and other additives on the formation of $BaCrO_4$/$SrCrO_4$ needs to be investigated further.

Bibliography

[1] P. Boolchand, Series on Directions in Condensed Matter Physics, Vol. 17, “Insulating and Semiconducting glasses” World Scientific, Singapore (2000).

[2] K. Richardson, D. Krol, K. Hirao, Int. J. Appl. Glass Sci. 1 (2010) 74.

[3] E.E. Stroganova, N.Y. Mikhailenko, O.A. Moroz, Glass Ceram. 60 (2003) 315.

[4] I.W. Donald, B.L. Metcalfe, R.N.J. Taylor, J. Mater. Sci. 32 (1997) 5851.

[5] S.R. Ovshinsky, J. Non-Cryst. Solids 73 (1985) 395.

[6] S.W. Martin, “Glass”, World book online America, Eds. (2000).

[7] J.E. Hammesfahr and C.L. Strong, “Creative Glass Blowing”, W.H. Freeman and Co. Ltd., San Francisco (1968).

[8] C162-Compilation of ASTM Standard Definitions. The American Society for Testing Materials, Philadelphia PA (1945).

[9] S.R. Elliott, “Physics of Amorphous Materials”, Longman, London (1984).

[10] J.E. Shelby, “Introduction to Glass Science and Technology”, RSC (1997).

[11] M. Arbab, L.J. Shelestak, C.S. Harris, Am. Ceram. Soc. Bull. 84 (2005) 30.

[12] I. Prigogine and R. Defay "Chemical Thermodynamics" Longman (1954) ISBN 0582462835.

[13] Walter Kauzmann, Chem. Rev. 43 (1948) 219.

[14] A. Hruby, Czech. J. Phys. B 23 (1973) 1623.

[15] G. Adam and J.H. Gibbs, J. Chem. Phys. 43 (1965) 139.

[16] D. Turnbull and M.H. Cohen, J. Chem. Phys. 34 (1961) 120.

[17] M. H. Cohen and D. Turnbull, J. Chem. Phys. 52 (1970) 3038.

[18] C.A. Angell and L.M. Torell, J. Chem. Phys. 78 (1983) 937.

[19] M.H. Cohen and G.S. Grest, Phys. Rev. B 20 (1979) 1077.

[20] A.C. Wright, C.A. Yarker, P.A.V Johnson, R.N. Sinclair, J. Non-Cryst. Solids 76 (1985) 333.

[21] S.R. Elliott, J. Phys. Condens. Matter 4 (1992) 7661.

[22] H. Bach and D. Krause, “Analysis of the Composition and Structure of Glass and Glass Ceramics”, Springer (1999).

[23] S.R. Elliott, Phys. Rev. Lett. 67 (1991) 711.

[24] W.H. Zachariasen, J. Am. Ceram. Soc. 54 (1932) 3841.

[25] B.E. Warren, J. Am. Ceram. Soc. 24 (1941) 256.

[26] G.N. Greaves, J. Non-Cryst. Solids 71 (1985) 203.

[27] J.D. Bernal, Nature 183 (1959) 141.

[28] A.L. Greer, T. Egami, A. Inoue, S. Ranganathan, (Eds), “Supercooled Liquids, Glass Transition and Bulk Metallic Glasses”, Materials Research Society, Boston, (2003).

[29] D. Sprenger, H. Bach, W. Meisel, P. Gutlich, J. Non-Cryst. Solids 159 (1993) 187.

[30] K.J. Rao, Structural Chemistry of Glasses, Elsevier (2002), ISBN 0080439586.

[31] S.R. Elliot, “Glass 99”, XVth Int. Congr. on Glass, Leningrad (1989) pp. 65.

[32] A.C. Wright, “Glass 99”, XVth Int. Congr. on Glass, Leningrad (1989) pp. 30.

[33] R. Dupree, D. Holland, D. S. Willliams, J. Non-Cryst. Solids 81 (1986) 185.

[34] R. Dupree, N. Ford, D. Holland, Phys. Chem. Glasses 28 (1987) 78.

[35] P.W. Wang and L. Zhang, J. Non-Cryst. Solids 194 (1996) 129.

[36] H.S. Liu, P.Y. Shih, T.S. Chin, Phys. Chem. Glasses 37 (1996) 227.

[37] E. Kordes, W. Vogel, R. Feterowsky, Z. Elektrochem. 57 (1953) 282.

[38] R.K. Brow, J. Non-Cryst. Solids 263 & 264 (2000) 1.

[39] F.F. Sene, J.R. Martinelli, L. Gomes, J. Non-Cryst. Solids 348 (2004) 63.

[40] J.H. Campbell and T.I. Suratwala, J. Non-Cryst. Solids 263 & 264 (2000) 318.

[41] M.J. Weber, J. Non-Cryst. Solids 123 (1990) 208.

[42] P. S. Anantha and K. Hariharan, Mater. Chem. Phys. 89 (2005) 428.

[43] J.J. Hudgens and S.W. Martin, J. Am. Ceram. Soc. 76 (1993) 1691.

[44] F.L. Galeener and J.C. Mikkelsen, Solid State Commun. 30 (1979) 505.

[45] G. Guo, Glass Technol. 39 (1998) 138.

[46] G. Guo, Mater. Res. Bull. 34 (1999) 621.

[47] A. Ghosh and B. K. Chaudhuri, J. Non-Cryst. Solids 103 (1988) 83.

[48] D.E. Day, Z. Wu, C.S. Ray, P. Hrma, J. Non-Cryst. Solids 241 (1998) 1.

[49] W. Poch, Glastech. Ber. 37 (1964) 533.

[50] J. Krogh-Moe, J. Non-Cryst. Solids 1 (1969) 269.

[51] M. Imaoka, "Advances in Glass Technology", Plenum Press, New York (1962) pp.149-164.

[52] C.G. Bergeron "Borate Glasses" L.D. Pye, V.D. Frechette, N.J. Kreidl (Eds), Plenum Press, New York (1978) pp. 445-362.

[53] S.W. Martin and C.A. Angell, J. Non-Cryst. Solids 66 (1984) 429.

[54] G.E. Jellison and P.J. Bray "Borate Glasses", L.D. Pye, V.D. Frechette, N.J. Kreidl (Eds), Plenum Press, New York (1978) pp. 353-367.

[55] V. Uitert, L.G., and S.H. Wemple, Appl. Phys. Lett. 32 (1978) 403.

[56] M.J. Weber, "Critical Materials Problems in Energy Production", Academic Press, New York (1986) pp. 261.

[57] J. Lucas, "Materials Science and Technology: A Comprehensive Treatment", Vol. 9, R.W. Cahn, P. Haasen and E.J. Kramer (Eds), VCH, Weinheim (1991) pp. 455.

[58] A.J. Leadbetter and A.C. Wright, J. Non-Cryst. Solids 7 (1972) 156.

[59] D.L. Price, M.L. Saboungi, S. Susman, K.J. Volin, A.C. Wright, J. Non-Cryst. Solids 150 (1992) 287.

[60] Yamane, M., H. Kawazoe, S. Inoue, K. Maeda, Mat. Res. Bull. 20 (1985) 905.

[61] J. Zarzycki, “Materials Science and Technology”, Vol. 9, R.W. Cahn, P. Haasen and E.J. Kramer (Eds) VCH, Weinheim (1991).

[62] P. Duwez, R.H. Villain, W. Clement Jr., J. Appl. Phys. 31 (1960) 36.

[63] W. Klement, R.H. Willens, P. Duwez, Nature 187 (1960) 869.

[64] W.L. Johnson, Mater. Sci. Forum 225-227 (1996) 35.

[65] A. Inoue, Acta Mater. 48 (2000) 279.

[66] R. Schulz, N. Chretien, N. Alexandrov, J. Aubin, R. Roberge, Mater. Sci. Eng. 99 (1988) 19.

[67] W.V. Titow, “PVC Technology”, Elsevier, 1984.

[68] European Commission Report on Best Available Techniques in the Glass Making Industry, 2001.

[69] D.M. Mattox, Handbook of physical vapour deposition processing (PVD): “Film formation, adhesion, surface preparation and contamination control”, Noyes Publications (1998) pp. 29-54.

[70] W. Primak, Phys. Rev.110 (1958) 1240.

[71] M. Atzmon, K.M. Unruh, W.L. Johnson, J. Appl. Phys. 22 (1985) 707.

[72] T. Masumoto, “Current Topics in Non-Crystalline Solids”: M.D. Baro, N. Clavaguera (Eds.), World Scientific, Singapore, 1985.

[73] D. Stoffler, Fortschr. Mineral. 51 (1974) 256.

[74] L. Young, “Anodic Oxide films”, Academic Press, New York 1961.

[75] C.J. Brinker and G.W. Scherer, “Sol-Gel Science”, Academic Press, San Deigo, 1990.

[76] P.W. Macmillan, “Glass-Ceramics”, Academic Press, 1977, pp. 176.

[77] S.D. Stookey and G.H. Beall "Explorations in Glass: An Autobiography", Wiley Blackwell, 2001.

[78] R. Becker and W. Doring, Ann. Phys. 24 (1935) 719.

[79] R.D. Maurer, J. Appl. Phys. 33 (1962) 2132.

[80] N. Volmer and A. Weber, Z. Phys. Chem. 119 (1925) 277.

[81] K.A. Jackson, "Crystal Growth", N.H. Publishing Co., 1997.

[82] P.F. James, in "Glass and Glass-Ceramics", ed. M. H. Lewis, Chapman and Hall, London, 1989, Ch. 3, pp. 59.

[83] B. Vonnegut, J. Appl. Phys. 18 (1947) 593.

[84] B. Vonnegut, J. Colloid. Sci. 3 (1948) 563.

[85] A. Paul, "Chemistry of Glasse", Champman and Hall, London & New York, 1985.

[86] D. R. Uhlmann, J. Am. Ceram. Soc. 66 (1983) 95.

[87] M. Yamane and J. D. Mackenzie, J. Non-Cryst. Solids 15 (1974) 153

[88] D.M. Sclapp, Phys. Chem. Glasses 6 (1965) 168.

[89] K.W. Peter, J. Non-Cryst. Solids 5 (1970) 103.

[90] T. Ozawa, J. Therm. Anal. 9 (1976) 369.

[91] H.E. Kissinger, J. Res. Nat. Bur. Stand. (US) 57 (1956) 217.

[92] K. Matusita, T. Komatsu, R. Yokota, J. Mater. Sci. 19 (1984) 291.

[93] B.D. Cullity, "Elements of X-ray Diffraction", Addison-Wilson Publishing Comp. Inc., U.S.A, 1959.

[94] H.P. Klug and L.E. Alexander, "X-ray Diffraction Procedures", Wiley-Interscience Publication, New York, 1974.

[95] R. Guinibuitere, "X-Ray Diffraction by Polycrystalline Materials", ISTE Ltd., 2007.

[96] Y. Waseda, "The Structure of Non-crystalline Materials: Liquids and Amorphous Solids", McGraw Hill publishers, 1980.

[97] R.W. Cahn, P. Haasen, E.J. Kramer, "Material Science and Engineering: Characterization of Materials", VCH Publisher Inc., New York, 1991.

[98] R. Wiesendanger, "Scanning Probe Microscopy and Spectroscopy: Methods and Applications", Cambridge University Press, Cambridge; New York (1994).

[99] C. N. Banwell and E. M. McCash, "Fundamentals of Molecular Spectroscopy", 4th Edition, Tata McGraw-Hill publishers Ltd, New Delhi, 2000.

[100] A.P. Roy, S.K. Deb, M.A. Rekha, A.K. Sinha, Indian J. Pure Appl. Phys. 30 (1992) 724.

[101] B.O. Mysen, L.W. Finger, D. Virgo, F.A. Seifert, Am. Mineral. 67 (1982) 686.

[102] E.R. Andrew, A. Bradbury, R.G. Eades, Nature, 183 (1959) 1802.

[103] I.W. Donald, B.L. Metcalfe, S.K. Fong, L.A. Gerrard, J. Non-Cryst. Solids 352 (2006) 2293.

[104] T. Okura, T. Miyachi, H. Monma, J. Eur. Ceram. Soc. 26 (2006) 831.

[105] P. Bergo, S.T. Reis, W.M. Pontuschka, J.M. Prison, C.C. Motta, J. Non-Cryst. Solids 336 (2004) 159.

[106] S. Kumar, P. Vinatier, A. Levasseur, K.J. Rao, J. Solid State Chem. 177 (2004) 1723.

[107] J.Y. Wei, Y. Hu, L.G. Hwa, J. Non-Cryst. Solids 288 (2001) 140.

[108] A.G. Dias, J.M.S. Skakle, I.R. Gibson, M.A. Lopes, J.D. Santos, J. Non-Cryst. Solids 351 (2005) 810.

[109] S.J. Kalita, A. Bhardwaj, H.A. Bhatt, Mater. Sci. Eng. C 27 (2007) 441.

[110] R.K. Brow, J. Am. Ceram. Soc. 76 (1993) 913.

[111] R.K. Brow, R.J. Kirkpatrick, G.L. Turner, J. Am. Ceram. Soc. 76 (1993) 919 and the references there in.

[112] S. Mamedov, D. Stachal, M. Stowistch, D. Quitmann, J. Chem. Phys 123(12) (2005) 1.

[113] J. Schneider, S.L. Oliveira, L.A.O. Nunes, H. Panepucci, J. Am. Ceram. Soc. 86 (2003) 317.

[114] H. Inoue, A. Makshima, T. Kanazawa, T. Nanba, I. Yasui, Phys. Chem. Glasses 36 (1995) 37.

[115] K.V. Shah, M. Goswami, R. Kumar, S. Manikandan, V.K. Shrikhande, G.P. Kothiyal, Phys. Chem. Glasses 46 (2005) 274.

[116] S. Krimi, A. El Jazouli, L. Rabardel, M. Couzi, I. Mansouri, G. Le Flem, J. Solid State Chem. 102 (1993) 400.

[117] L. Montagne, G. Palavit, A. Shaim, M. Et-tabirou, P. Hartmann, C. Jager, J. Non-Cryst. Solids 293-295 (2001) 719.

[118] R.K. Brow, D.R. Tallant, W.L. Warren, A. McIntyre, D.E. Day, Phys. Chem. Glasses 38 (1997) 300.

[119] E. Fergin, C. Duchesne, R. Olazcuaga, G. Flem Le, C. Cartier, L. Canioni, P. Segonds, L. Sarger, A. Ducasse, J. Non-Cryst. Solids 168 (1994) 132.

[120] E.M. Vogel, M.J. Weber, D.M. Krol, Phys. Chem. Glasses 32 (1991) 231.

[121] J. Tauc, “Amorphous and Liquid Semiconductors”, Plenum press, London and New York (1974) pp. 159-220.

[122] N.F. Mott and E.A. Davis, “Electronic Process in the Non-crystalline Materials”, 2nd Edition, Clarendon press, Oxford University, New York (1979).

[123] V.K. Shrikhande, V. Sudarsan, G.P. Kothiyal, S.K. Kulshreshtha, J. Non-Cryst. Solids 353 (2007) 1341.

[124] X. Liu, D.B. Hollis, J. McDougall, Phys. Chem. Glasses 37(4) (1996) 160.

[125] N.F. Mott and E.A. Davis, “Electronic Process in the Non-crystalline Materials”, 2nd Edition, Clarendon press, New York (1979) pp. 272-300.

[126] D. Banerjee, V.K. Sudarsan, A. Joseph, R.K. Mishra, I. Singh, P.K. Wattal, D. Das, J. Am. Ceram. Soc. 93(10) (2010) 3252.

[127] C. Dayanand, R.V.G.K. Sarma, G. Bhikshamaiah, M. Salagram, J. Non-Cryst. Solids 167 (1994) 122.

[128] L.E. Bausa, F. Jaque, J.G. Sole, A. Duran, J. Mater. Sci. 23(6) (1988) 1921.

[129] L.E. Bausa, J.G. Sole, A. Duran, J.M.F. Navarro, J. Non-Cryst. Solids 127 (1991) 267.

[130] I.M. Batyaev and Y.G. Kobezhikov, Tech. Phys. 48(7) (2003) 889.

[131] I.M. Batyaev and A. V. Leonov, Glass Phys. Chem. 30 (2004) 425.

[132] A.N. Trukhin, J. Non-Cryst. Solids 189(1-2) (1995) 1.

[133] Dheeraj Jain, V. Sudarsan, R.K. Vatsa, C.G.S. Pillai, J. Lumin. 129 (2009) 439.

[134] S.W. Martin, Eur. J. Solid State Inorg. Chem. 28 (1991) 163.

[135] R.K. Brow, R.J. Kirkpatric, G.L. Turner, J. Am. Ceram. Soc. 73(8) (1990) 2293.

[136] W.F. Bleam and S.F. Dec, J.S. Frye, Phys. Chem. Miner. 16 (1989) 817.

[137] B.N. Nelson and G.J. Exarhos, J. Chem. Phys. 71 (1979) 2739.

[138] P. Tarte, A. Rulmont, C.M. Ansay, Spectrochim. Acta A 42 (1986) 1006.

[139] T. Kasuga and Y. Abe, J. Non-Cryst. Solids 243 (1999) 70.

[140] C. Nelson and D.R. Tallant, Phys. Chem. Glasses 27 (1986) 75.

[141] J. Yifen, J. Dehua, C. Xiangsheng, B. Behya, H. Xihuai, J. Non-Cryst. Solids 80 (1986) 147.

[142] S. Sakka, F. Miyaji, K. Fukumi, J. Non-Cryst. Solids 112 (1989) 64.

[143] J.J. Hudgens, R.K. Brow, D.R. Tallant, S.W. Martin, J. Non-Cryst. Solids 223 (1998) 21.

[144] T. Uchino and T. Yoko, J. Non-Cryst. Solids 263 & 264 (2000) 180.

[145] Y.M. Moustafa, K. El-Egili, J. Non-Cryst. Solids 240 (1998) 144 and references there in.

[146] L. Montagne, G. Palavit, G. Mairesse, M. Draoui, K. Aomari, M.S. Idrissi, Phys. Chem. Glasses 38(1) (1997) 15.

[147] C. Dayanand, G. Bhikshamaiah, V. J. Tyagraju, M. Salagram, A.S.R. Krishna Murthy, J. Mater. Sci. 31 (1996) 1945.

[148] A. Shaim and M. Et-tabirou, Mater. Chem. Phys. 80 (2003) 63.

[149] S. Elangovan, J.J. Hartvigsen, L.J. Frost, Int. J. Appl. Ceram. Technol. 4 (2007) 109.

[150] C. Story, K. Lu, W.T. Reynold Jr., D. Brown, Int. J. Hydrogen Energy 33 (2008) 3970.

[151] R.N. Singh, J. Mater. Eng. Perform. 15 (2006) 422.

[152] J.W. Fergus, J. Power Sources 147 (2005) 46.

[153] S.C. Singhal, Solid State Ionics 152-153 (2003) 405.

[154] B.C.H. Badwal, Solid State Ionics 143 (2001) 39.

[155] R.N. Singh, Int. J. Appl. Ceram. Technol. 4 (2007) 134.

[156] N.Q. Minh, Solid State Ionics 174 (2004) 271.

[157] C. Lara, M.J. Pascual, A. Duran, J. Non-Cryst. Solids 348 (2004) 149.

[158] S.M. Gross, T. Koppitz, J. Remmel,U. Reisgen, Ceram. Eng. Sci. Proc. 26 (2005) 239.

[159] S. Ghosh, A.D. Sharma, P. Kundu, S. Mahanty, R.N. Basu, J. Non-Cryst. Solids 354 (2008) 4081.

[160] M.J. Pascual, A. Guillet, A. Duran, J. Power Sources 169 (2007) 40.

[161] S.B. Sohn, S.Y. Choi, G.H. Kim, H.S. Song, G.D. Kim, J. Non-Cryst. Solids 297 (2002) 103.

[162] P. Batfalsky, A. C. Haanappel, J. Malzbender, N. H. Menzler, V. Shemel, I. C. Vinke, R. W. Steinbrech, J. Power Sources 155 (2006) 128.

[163] Z. Yang, G. Xia, K.D. Meinhardt, K.S. Weil, J.W. Stevenson, J. Mater. Eng. Perform. 13 (2004) 327.

[164] M. Brochu, B.D. Gauntt, R. Shah, G. Miyake, R.E. Loehman, J. Eur. Ceram. Soc. 26 (2006) 3307.

[165] K. Eichler, G. Solow, P. Otschic, W. Schaffrath, J. Eur. Ceram. Soc. 19 (1999) 1101.

[166] K.L. Ley, M. Krumplet, R. Kumar, J.H. Meiser, I. Bloom, J. Mater. Res. 11 (1996) 1489.

[167] S.T. Reis and R.K. Brow, J. Mater. Eng. Perform. 15 (2006) 410.

[168] S. Ghosh, A.D. Sharma, A.K. Mukhopadhyay, P. Khundu, R.N. Basu, Int. J. Hydrogen Energy 35 (2010) 272.

[169] A. Goel, M.J. Pascual, J.M.F. Ferreira, Int. J. Hydrogen Energy 35 (2010) 6911.

[170] T. Zhang, H. Zhang, G. Li, H. Yung, J. Power Sources 195 (2010) 6795.

[171] M.J. Pascual, C. Lara, A. Duran, Phys. Chem. Glasses: Eur. J. Glass Sci. Technol. B 47(5) (2006) 572.

[172] P.W. McMillan and G. Partridge, J. Mater. Sci. 7 (1972) 847.

[173] Z. X. Chen and P. W. McMillan, J. Mater. Sci. 20 (1985) 3428.

[174] P. W. McMillan, G. Partridge, F. R. Ward, J. Mater. Sci. 4 (1969) 634.

[175] Y. Kim, M. R. Towler, A. Wren, C. Ohtsuki, J. Mater. Sci.: Mater. Med., 20 (2009) 2267.

[176] D. Boyd, G. Carroll, M. R. Towler, C. Freeman, P. Farthing, I. M. Brook, J. Mater. Sci.: Mater. Med., 20 (2009) 413.

[177] M. Yamane and Y. Asahara, "Glasses for photonics", Cambridge University Press, 2004, ISBN 0-511-03862-3 ebook, pp.45.

[178] K. J. Rao, "Structural chemistry of glasses", Elsevier Science and technology, (2002) 401.

[179] F. Tietz, Ionics 5 (1999) 129.

[180] R. Wang, Z. Lu, C. Liu, R. Zhu, X. Huang, B. Wei, N. Ai, W. Su. J. Alloy. Compd. 432(1-2) (2007) 189.

[181] R.G. Beaman, J. Polym. Sci. 9 (1952) 470.

[182] S. Sakka and J.D. Mackenzie, J. Non-Cryst. Solids 6 (1971) 145.

[183] W. Vogel, Glass Chemistry. Springer-Verlag, 1992.

[184] M.B. Volf, "Chemical Approach to Glass", Series on Glass Science and Technology, Vol. 7. Elsevier, New York, 1984.

[185] M.A. Matveev, G.M. Matveev and B.N. Frenkel, "Calculation and Control of Chemical, Optical and Thermal Properties of Glass", Holon, Israel, 1975.

[186] M.R. Reddy, M.S. Reddy and N. Veeraiah, Indian J. Pure Appl. Phys. 44 (2006) 446.

[187] V.S. Costa, F.S. Lameiras and K.L. Bray, J. Non-Cryst. Solids 273 (2000) 209.

[188] M.E. Huntelaar, E.H.P. Cordfunke, A. Scheele, J. Alloy. Compd. 19(1) (1993) 87.

[189] M. Ardit, G. Cruciani, M. Dondi, Z. Kristallogr. 225(7) (2010) 298.

[190] N. Morimoto, Y. Nakajima, Acta. Crystallogr. Sect. B: Struct. Sci. 31 (1975) 1041.

[191] B. Tiwari, A. Dixit, C.G.S. Pillai, S.C. Gadkari, G.P. Kothiyal, J Am. Ceram. Soc. 95(4) (2012) 1290.

[192] T. Joseph and M.T. Sebastian, J Am. Ceram. Soc. 93(1) (2010) 1470.

[193] G. Ervin Jr. and E.F. Osborn, Am. Miner. 34(9-10) (1949) 717

[194] K.S. Weil, J.E. Deibler, J.S. Hardy, D.S.Kim, G.G. Xia, L.A. Chick, C.A. Coyle, J. Mater. Eng. Perform. 13 (2004) 316.

[195] M. Kerstan, M. Muller and C. Russel, Mater. Res. Bull. 46 (2011) 2456.

[196] D.U. Tulyaganov, S. Agathopoulos, H.R. Fernandes, J.M.F. Ferreira, Ceram. International 32 (2006) 195.

[197] W. Holand, G. Beall, "Glass-ceramic Technology", The American Ceramic Society, Westerville, Ohio, 2002.

[198] L. R. Pinckney, S. A. Tietje, U.S. Patent 7,378,361 May 27, 2008.

[199] J.D. Frantz and B.O. Mysen, Chem. Geol. 121 (1995) 55.

[200] B.N. Roy, J. Am. Ceram. Soc. 70 (1987) 183.

[201] E.I. Kamitsos, J.A. Kapoutsis, H. Jain, C.H. Hsieh, J. Non-Cryst. Solids 171 (1994) 31.

[202] S. L. Lin, C.S. Hawang, J. Non-Cryst. Solids 202 (1996) 61.

[203] D.U. Tulyaganov, S. Agathopoulos, J.M. Ventura, M.A. Karakassides, O Fabrichnaya, J.M.F. Ferreira, J. Eur. Cerm. Soc. 26 (2006) 1463.

[204] B. Tiwari, M. Pandey, V. Sudarsan, S.K. Deb, G. P. Kothiyal, Physica B 404 (2008) 47.

[205] E.I. Kamitsos, M.A. Karakassides, G.D. Chryssikos, Phys. Chem. Glasses 30 (1989) 229.

[206] G.D. Chryssikos, J. Raman Spectrosc. 22 (1991) 645.

[207] C.L. Raluca and A. Ioan, J. Non-Cryst. Solids 353 (2007) 2020.

[208] S. D. Ross, "Inorganic Infrared and Raman Spectra", McGraw-Hill, New York, 1972.

[209] A. Goel, D.U. Tulyaganov, M.J. Pascaul, E.R. Shaaban, F. Munoz, Z. Lu, J.M.F. Ferreira, J. Non-Cryst. Solids 356 (2010) 1070.

[210] R. Martens and W.M. Warmuth, J. Non-Cryst. Solids, 265 (2000) 167.

[211] J.G.Wood, S. Prabhakar, K.T. Mueller, C.G. Pantano, J. Non-Cryst. Solids 349 (2004) 276.

[212] L.S. Du and J. F. Stebbins, J. Non-Cryst. Solids 315 (2003) 239.

[213] M. Kord, V.K. Marghussian, B.E. Yekta, A. Bahrami, J. Non-Cryst. Solids 355 (2009) 141.

[214] T. Ohgaki, Y. Nagumao, K. Soga, A. Yasumori, J. Ceram. Soc. Jap. 115(3) (2007) 201.

[215] O.V. Mazurin and E.A. Porai-Koshits, "Phase Separation in Glass", North-Holland Physics Publisher, Amsterdam, Netherland, 1984.

[216] E.R. Segnit, J. Am. Ceram. Soc. 37 (1954) 273.

[217] A. Goel, D.U. Tulyaganov, V.V. Kharton, A. A. Yaremchenko, S. Eeiksson, J.M.F. Ferreira, J. Power Sources 189 (2009) 1032.

[218] K. Matusita and S. Sakka, J. Non-Cryst. Solids 38-39 (1980) 741.

[219] E.A. Marseglia, J. Non-Cryst. Solids 41 (1980) 31.

[220] K. Matusita, K. Miura, T. Komatsu, Thermochim. Acta 88 (1985) 283.

[221] E. Dowty, Phys. Chem. Minerals 14 (1987) 122.

[222] M. Handke, M. Sitarz, W. Mozgawa, J. Mol. Struc. 450 (1998) 229.

[223] Z, Zhang, Y. Wang, H. Wang, Z. Sun, L. Jia, J. Phys. Conf. Series 152 (2009) 12050.

[224] K.J.D. Mackenzie and M.E. Smith, "Multinuclear Solid-state NMR of Inorganic Materials", Pergamon material series, 2002.

[225] M. Kerstan and C. Russel, J. Power Sources, 196 (2011) 7578.